THE REACTION OF DICYANOACETYLANE WITH ATOMIC OXYGEN AND ACTIVE ...
OBENAUF, RALPH HARRY, JR.
ProQuest Dissertations and Theses; 1972; ProQuest Dissertations & Theses Global

INFORMATION TO USERS

This dissertation was produced from a microfilm copy of the original document. While the most advanced technological means to photograph and reproduce this document have been used, the quality is heavily dependent upon the quality of the original submitted.

The following explanation of techniques is provided to help you understand markings or patterns which may appear on this reproduction.

1. The sign or "target" for pages apparently lacking from the document photographed is "Missing Page(s)". If it was possible to obtain the missing page(s) or section, they are spliced into the film along with adjacent pages. This may have necessitated cutting thru an image and duplicating adjacent pages to insure you complete continuity.

2. When an image on the film is obliterated with a large round black mark, it is an indication that the photographer suspected that the copy may have moved during exposure and thus cause a blurred image. You will find a good image of the page in the adjacent frame.

3. When a map, drawing or chart, etc., was part of the material being photographed the photographer followed a definite method in "sectioning" the material. It is customary to begin photoing at the upper left hand corner of a large sheet and to continue photoing from left to right in equal sections with a small overlap. If necessary, sectioning is continued again — beginning below the first row and continuing on until complete.

4. The majority of users indicate that the textual content is of greatest value, however, a somewhat higher quality reproduction could be made from "photographs" if essential to the understanding of the dissertation. Silver prints of "photographs" may be ordered at additional charge by writing the Order Department, giving the catalog number, title, author and specific pages you wish reproduced.

University Microfilms

300 North Zeeb Road
Ann Arbor, Michigan 48106

A Xerox Education Company

Reproduced with permission of the copyright owner. Further reproduction prohibited without permission.

72-23,213

OBENAUF, Jr., Ralph Harry, 1945-
THE REACTION OF DICYANOACETYLENE WITH ATOMIC OXYGEN AND ACTIVE NITROGEN STUDIED IN A FLOW SYSTEM WITH MASS SPECTROMETRIC DETECTION.

Carnegie-Mellon University, Ph.D., 1972
Chemistry, physical

University Microfilms, A XEROX Company, Ann Arbor, Michigan

THIS DISSERTATION HAS BEEN MICROFILMED EXACTLY AS RECEIVED.

Reproduced with permission of the copyright owner. Further reproduction prohibited without permission.

Carnegie-Mellon University

CARNEGIE INSTITUTE OF TECHNOLOGY

AND

MELLON INSTITUTE OF SCIENCE

THESIS

SUBMITTED IN PARTIAL FULFILLMENT OF THE REQUIREMENTS

FOR THE DEGREE OF DOCTOR OF PHILOSOPHY

TITLE THE REACTION OF DICYANOACETYLENE WITH ATOMIC OXYGEN AND ACTIVE NITROGEN STUDIED IN A FLOW SYSTEM WITH MASS SPECTROMETRIC DETECTION.

PRESENTED BY RALPH H. OBENAUF

ACCEPTED BY THE DEPARTMENT OF CHEMISTRY

C W Hand — MAJOR PROFESSOR — April 8, 1972 — DATE

A. A. Coretto, Jr. — DEPARTMENT HEAD — April 8, 1972 — DATE

APPROVED BY THE COLLEGE COUNCIL

DEAN — April 27, 1972 — DATE

Reproduced with permission of the copyright owner. Further reproduction prohibited without permission.

PLEASE NOTE:

Some pages may have

indistinct print.

Filmed as received.

University Microfilms, A Xerox Education Company

Reproduced with permission of the copyright owner. Further reproduction prohibited without permission.

Abstract

The reaction of dicyanoacetylene with oxygen atoms and active nitrogen has been studied in a fast-flow system with time-of-flight mass spectrometric detection to determine the relative susceptibilities of the cyano and acetylene functions to atom attack. Design considerations and construction parameters of the instrument are given in detail.

For reaction with oxygen atoms the second order rate constant at room temperature is 1.1×10^{-15} cm^3/molecule sec (standard deviation 0.3×10^{-15}), invariant over the pressure range 0.75 - 5.0 torr. In the presence of molecular oxygen the stoichiometric factor is 1.2, increasing to 5.5 oxygen atoms consumed per dicyanoacetylene molecule in the absence of molecular oxygen. Initial attack is at the acetylenic bond, and stable end products are CO, NO, CO_2 and C_2N_2. CN, OC_3N, OC_2N and C_2N are observed as important intermediates, and the presence of the intermediate C_2O is inferred. First mass spectrometric evidence of the species OC_2N_2 has been obtained.

The reaction between active nitrogen and dicyanoacetylene was studied over the pressure range 0.7 - 8.0 torr and from room temperature up to 200°C. The reaction bears great similarity to the equally complex reaction of active nitrogen with acetylene, which supports the hypothesis that the site of initial N-atom attack is on an acetylenic rather than a terminal carbon. Three distinct reaction zones are identified, the slow region, the flame region, and the post-flame region. The reaction rate is about the same in the slow and post-flame

Reproduced with permission of the copyright owner. Further reproduction prohibited without permission.

regions, and at least an order of magnitude faster in the flame region. The flame zone, characterized by intense CN emission, is a chain recombination of N atoms mediated by CN and NCN radicals and initiated by small quantities of C_4N_2. In the slow region at low pressures the initial steps are

$$N + C_4N_2 \underset{k_{-1}}{\overset{k_1}{\rightleftharpoons}} NC_4N_2^* \qquad (1)$$

$$NC_4N_2^* + N_2 \xrightarrow{k_2} NCN + C_3N + N_2 \qquad (2)$$

Kinetic data provide the rate constant estimates

$$k_1 = 5.3 \pm 4.3 \times 10^{-15} \text{ cm}^3/\text{molecule sec}$$
$$k_{-1} \leqslant 1.4 \pm 1.1 \times 10^{8} \text{ sec}^{-1}$$
$$k_2 \leqslant 7.2 \times 10^{-10} \text{ cm}^3/\text{molecule sec}$$

At higher pressures the slow region is governed by a more complex chain mechanism, different from that in the flame region. There is a small but significant temperature dependence of the rate constant in the high-pressure region ($E_a = 700 \pm 450$ cal/mole), but there is no significant temperature dependence in the low pressure region.

Major products are C_2N_2 and C_6N_2, and CN and C_2N are observed as intermediates.

Reproduced with permission of the copyright owner. Further reproduction prohibited without permission.

To Joanne

Reproduced with permission of the copyright owner. Further reproduction prohibited without permission.

ACKNOWLEDGMENTS

I am forever indebted to my advisor, Professor Clifford W. Hand who has taught me everything from plumbing to electronics and all the chemistry in between. To me Dr. Hand is more than an excellent teacher, he is a friend as well.

I am grateful to the many professors and fellow graduate students, in particular Denis J. Bogan and Professor Joe V. Michael for our many discussions and helpful suggestions.

I gratefully acknowledge financial support by the Air Force and the University of Alabama.

Lastly, I would like to apologize to all those who operate the flow system at the University of Alabama for my construction of a left-handed instrument; unless, of course, said operator is fortunate enough to be a fellow southpaw.

Reproduced with permission of the copyright owner. Further reproduction prohibited without permission.

TABLE OF CONTENTS

		Page
	Abstract	ii
	Acknowledgments	v
	List Of Tables	viii
	List Of Figures	x
I	Introduction	1
II	Design and Construction Of the Flow Reactor	6
	General Considerations	6
	The Flow Reactor	7
	Pinhole Inlet System	15
	Flow Metering Systems	17
	Ancillary Equipment	30
	Evaluation Of Capabilities and Limitations	32
	Production Of Atoms and Measurement Of Atom Concentration	44
	Wall Poisoning	53
III	Preparation and Purification Of Reagents	59
IV	Methods Of Rate Constant Determination	64
V	The Reaction Of Acetylene With Oxygen Atoms	70
VI	The Reaction Of Dicyanoacetylene With Oxygen Atoms	72
	Introduction	72
	Results	74
	Identification Of Products and Intermediates	81
	Discussion	84

Reproduced with permission of the copyright owner. Further reproduction prohibited without permission.

Page

VI The Reaction Of Dicyanoacetylene With Oxygen Atoms (Contd.). 72

Mechanism 86

Conclusion. 91

VII The Reaction Of Dicyanoacetylene With Active Nitrogen. . . . 92

Introduction. 92

General Features Of the Reaction. 93

The Slow Reaction Zone. 95

Nitrogen Atom Consumption In the Flame Zone 104

The Post Flame Zone 111

Mechanism Of the Flame Zone 113

Mechanism In the Slow Reaction Zone 117

The Low Pressure Region. 118

The High Pressure Region 122

Appendix A The Heat Equation; Application To the Fast Flow Reactor 128

Appendix B Correction Of Rate Constants For Axial Diffusion. 147

Appendix C Species Present In Active Nitrogen. 151

Appendix D Production Of $N_2(^3\Sigma_u^+)$ In the Absence Of Nitrogen Atoms 153

Appendix E Third Body Effects. 159

Appendix F Selected Heats Of Formation 167

References 168

Reproduced with permission of the copyright owner. Further reproduction prohibited without permission.

LIST OF TABLES

	Title	Page
1.	Average Cross Sectional Area Determined For the Flow Reactor	8
2.	Values Of Standard Volumes For Reactant Flow Metering Systems	21
3.	Calculated Flow Ranges For Selected Lengths Of Capillaries	26
4.	Correction Factors For Change In Gas Viscosity Due To Change In Temperature	28
5.	Linear Regression Fit Of Capillary Flow Meter Calibration	29
6.	Pressure Drop Along the Flow Reactor At One Torr	35
7.	Equilibrium Constants For $2NO_2 \rightleftharpoons N_2O_4$	45
8.	Correction Factors For NO_2 Flows At Various Pressures	47
9.	O-Atom Wall Recombination For Different Poisoning Techniques	57
10.	Gas Analysis Of Matheson Ultrapure Oxygen	60
11.	Instrumental Background At Different Titanium Sponge Furnace Temperatures	61
12.	Literature Values For the Reaction Of O Atoms With Acetylene	71
13.	Second Order Rate Constants For the Reaction Of Dicyanoacetylene With O Atoms	77
14.	Second Order Rate Constants For the Reaction Of Dicyanoacetylene With Active Nitrogen	96
15.	Rate Constants For the Reaction Of Dicyanoacetylene With Active Nitrogen At Elevated Temperatures	103
16.	Initial Reactant Ratios For Maximum N-Atom Consumption By Dicyanoacetylene	107
A1.	Values Of the Independent Variable At the Zeros Of the the Zeroth Order Bessel Function	134
A2.	Temperature At the Center Of the Gaseous Plate At 1.0 Torr.	139

Reproduced with permission of the copyright owner. Further reproduction prohibited without permission.

	Title	Page
A3.	Temperature At the Center Of the Gaseous Plate At 10.0 Torr.	140
A4.	Values Of the Fourier Modulus.	142
A5.	Central Temperatures For the Infinite Gaseous Cylinder and Gaseous Plate	144
B1.	Contribution To the Measured Rate Constant From Axial Diffusion	150
D1.	Quenching Rate Constants For the Reaction Of $N_2(A)$ With Small Molecules	154
E1.	Best Values Of the Observed Rate Constant For the Reaction Of Dicyanoacetylene With Active Nitrogen.	162
E2.	Polynomial Fit Of the Rate Constant For the Reaction Of Dicyanoacetylene With Active Nitrogen	164

Reproduced with permission of the copyright owner. Further reproduction prohibited without permission.

LIST OF FIGURES

	Title	Page
1.	Final Design, Fast Flow Reactor	10
2.	Average Reactor Temperature At Various Applied Voltages	11
3.	Schematic Diagram: Flow System Interconnections	13
4.	Working Diagram: O-Ring Seal Of Flow Reactor To T.O.F.	14
5.	Pinhole Inlet To T.O.F. Ion Source	16
6.	Reactant Flow Metering System	18
7.	Linearity Of Pressure Transducer Response	19
8.	Carrier Gas Capillary Flow Meter	24
9.	Maximum Linear Flow Velocities At Low Pressure	33
10.	Probe Effect At 299°K Without Flushing Line	37
11.	Probe Effect At 458°K Without Flushing Line	39
12.	Residual Probe Effect In Determination of k_w At 300°K With Flushing Line	43
13.	Apparent Percent Dissociation Of Molecular Oxygen Measured At Various Ionizing Voltages	49
14.	Relative Oxygen and Nitrogen Atom Concentrations During the Nitric Oxide Titration Of Active Nitrogen	51
15.	Determination Of Rate Of Heterogeneous Removal Of Oxygen Atoms	55
16.	Rate Of Removal Of DCA By O Atoms At 4.95 Torr	75
17.	Rate Of Removal Of DCA By O Atoms At 2.97 Torr	76
18.	Fixed Probe Method: The Rate Of Removal Of O Atoms By DCA At 5.05 Torr	78
19.	Fixed Probe Method: The Rate Of Removal Of O Atoms By DCA At 2.93 Torr	79
20.	Appearance Potential Determination Of the m/e = 28 Product From Reaction Of O Atoms With DCA	82

Reproduced with permission of the copyright owner. Further reproduction prohibited without permission.

	Title	Page
21.	Effect Of Total Pressure On the Observed Second Order Rate Constant For N + DCA	99
22.	Rate Of Removal Of DCA By N Atoms At 5.20 Torr	100
23.	Rate Of Removal Of DCA By N Atoms At 2.54 Torr	101
24.	Nitrogen Atom Concentration Versus Initial DCA Concentration At 3.00 Torr	106
25.	Unfiltered Emission From N + DCA Flame	110
26.	Rate Of Removal Of DCA By N Atoms In Flame and Post-Flame Zones; Unfiltered Emission Intensity	112
27.	Reciprocal Plot Of Low Pressure Data From Table 14	121
A1.	Δ Temperature Versus Time For Gaseous Plate At 1.0 Torr	145
A2.	Δ Temperature Versus Time For Gaseous Plate At 10.0 Torr	146
D1.	Final Design: Argon Discharge Flow Reactor	157
E1.	Polynomial Fit Of the Observed Rate Constant For N + DCA In the Slow Reaction Region	165

Reproduced with permission of the copyright owner. Further reproduction prohibited without permission.

I Introduction

The study of elementary processes is of great theoretical and practical importance in reaction kinetics. With the knowledge of these processes it is conceivable that far more complex mechanisms may be constructed and perhaps the major reaction pathway directed or altered. Since 1950 an enormous amount of work has been done on one of the simplest of chemical processes, the reactions of atoms. Techniques such as photolysis and electrical discharges have been available for a long time for the production of atoms in the laboratory; however, the classical methods of analysis of stable reactants and products left much to be desired, resulting in very little information concerning the elementary and intermediate steps of the reaction.

In recent years sensitive analytical tools have been developed such as mass spectroscopy, electron spin resonance, spectroscopic observation of chemiluminescence and fluorescence and ion cyclotron resonance, which permit the quantitative determination of atom and radical concentrations. This has made possible the study of many elementary processes which have found important application in the fields of combustion, upper atmosphere chemistry and more recently in air polution research.

The reactions of oxygen and hydrogen atoms and active nitrogen have received most attention; however, studies have also been carried out with carbon atoms, halogen atoms, and alkali metal atoms as well as reactions of atoms in excited states, principally the noble gas metastables. Comprehensive reviews[1-4] are available which cover the

Reproduced with permission of the copyright owner. Further reproduction prohibited without permission.

history of the work which has been done on these systems and need not be discussed here.

One of the most versatile instruments used in these studies was the fast flow reactor, in which dilute concentrations of reactants in an inert carrier are pumped through a cylindrical tube. Knowledge of the total flow of gas, pressure, temperature and dimensions of the tube make possible the calculation of an average linear flow velocity, LFV, along the reactor. The faster the speed at which a reaction takes place, then the higher the LFV used so that the course of the reaction may be viewed as a function of distance, d, along the tube which is related to the time of reaction t_r, by

$$t_r = d/LFV$$

In practice it is more convenient to hold the detector at a fixed position and vary t_r by changing the point at which reactant mixing occurs along the reactor.

Photometric, spectroscopic and mass spectrometric detection have been widely used in fast flow experiments yielding complementary results by providing information which could not be obtained exclusively by one technique. Spectroscopic detection furnishes excited state formation and distribution information while mass spectrometric detection has the unique advantage that it is not dependent on any specific property of the species to be observed and therefore monitors all species present in the system at high sensitivity with generally unambiguous identification.

The present work deals with the construction of a modified

Reproduced with permission of the copyright owner. Further reproduction prohibited without permission.

Wood-Bonhoeffer flow reactor with time-of-flight mass spectrometric detection and the study of the reactions of oxygen atoms and active nitrogen with dicyanoacetylene, DCA. While conceptually simple in theory and design numerous experimental difficulties were present. The large number of calibrations and standardizations necessitated maximum accuracy in the individual operations so that experimental errors would not be excessive. When the study of a new reaction was begun instrumental modifications were almost always necessary; therefore, flexibility was designed into the instrument to minimize the time spent in making these modifications while maximizing the types of reactions which could be studied. Constant surveillance was maintained to minimize systematic errors, and periodic comparisons of results of well known systems to the accepted values were most useful.

Several basic experimental limitations existed (vide infra) which govern the range of rate constants accessible by fast-flow techniques. Radial and axial diffusion of reactant at the point of mixing and viscous pressure drop along the flow tube, giving rise to a nonlinear flow velocity, affect the credibility of the measurement of t_r. Kaufman[1] establishes rough limits of $10^2 < \text{LFV} < 10^3$ cm/sec at one torr with respect to heterogeneous O-atom removal at room temperature for a 2 cm diameter flow tube. Since most reactions were observed under pseudo first-order conditions, then the concentration of excess reagent was adjusted until the pseudo first-order rate constant is of the order 0.1 - 10 sec^{-1}, magnitudes accessible in the "allowed" range of linear flow velocities. This permits measurement of bimolecular rate constants over a dynamic range of 10^6, say between 1×10^{-16} and 1×10^{-10} cm^3/molecule sec.

Reproduced with permission of the copyright owner. Further reproduction prohibited without permission.

Volume recombination of atoms is slow at pressures used in our studies and therefore was generally not a serious problem; however, this was not the case with surface recombination. With atoms in excess the observed second order rate constant, k_{obs} was extracted from the pseudo first order rate constant, k', by division by the atom concentration within the reactor.

$$k_{obs} = k'/[\text{Atoms}]$$

This procedure relied on the atom concentration remaining constant along the entire length of the flow tube. This was true, as will be discussed in Section IV, to a good approximation for a well poisoned reactor if t_r is short (i.e. $\lesssim$ 200 msec); therefore, the LFV selected for an experiment, while being slow enough to eliminate the aforementioned diffusion and pressure drop effects, could not be so slow as to cause marked depletion of atoms along the flow tube. With stable reactant in excess the observed first order rate constant contained the wall removal rate constant in addition to that arising from reaction with substrate molecules. Here again care was taken in the choice of experimental conditions so that the heterogeneous term was negligible.

Many[5-21] studies of the reactions of atomic oxygen and active nitrogen have been carried out with cyanogen and acetylene and its derivatives. We have extended this study to the reaction with dicyanoacetylene, a molecule which contains both the cyano and acetylene functions in an attempt to determine their relative susceptibility to atom attack. In studies with both active nitrogen and

Reproduced with permission of the copyright owner. Further reproduction prohibited without permission.

atomic oxygen the reaction was found to be similar in many respects to the corresponding reaction with acetylene. Results have indicated that initial atom attack is at the central carbons rather than at the cyano groups.

Reproduced with permission of the copyright owner. Further reproduction prohibited without permission.

II Design and construction of the Flow Reactor

General Considerations

There are numerous parameters to be considered when beginning construction of a fast flow system, many of which are interrelated. As a starting point it is necessary to study the various descriptions of other systems found in the literature (for example references 1, 4, 21-24). We also visited several laboratories to observe similar systems in operation.

A set of initial requirements was chosen, based on experience gained by other researchers, to give maximum flexibility to the various types of systems that may be studied while enabling a wide range of rate constants to be measured. They are as follows: 1) Approximately 20 mm diameter flow tube; 2) Axial variable position reactant inlet; 3) 0-50 msec reaction time at 10 m/sec flow velocity; 4) Operating pressures of 0-10 torr; 5) Operating temperatures of 300-500°K; 6) Provision for temperature measurement within the reactor; 7) Choice of reactant: hydrogen atoms, oxygen atoms, active nitrogen or stable gas.

Reproduced with permission of the copyright owner. Further reproduction prohibited without permission.

The Flow Reactor

The reactor was constructed of 22 mm Pyrex tubing, the cross sectional area being measured by the successive additions of 25 ml aliquots of water to the reactor while it was clamped in a vertical position and measurement of the height covered by the water. Table 1 shows the results of one such determination; the average cross sectional area was 2.80 cm^2 (standard deviation 0.02 cm^2). Accurate determination of this parameter is essential for the calculation of the linear flow velocity (vide infra).

Using general design consideration three, it is readily seen that in order to have a reaction time, i.e., time between mixing of reagents and their sampling at the downstream end of the flow reactor, of 0-50 msec at a linear flow velocity of 10^3 cm/sec required a 50 cm length of flow reactor over which the reactants may be introduced.

The problem arises, when we wish to heat the reactor, of obtaining a uniform temperature along this 50 cm length. In order to produce meaningful data at elevated temperatures a constant temperature length of reactor, long enough to permit rate determination, must be available. If for instance it requires 45 cm to raise the temperature of the flowing gas to the desired operating temperature, at a given pressure and linear flow velocity, then only the last 5 cm of the reactor will have a constant temperature and therefore a constant linear flow velocity.

In Appendix A we have carried out calculations of the time requirements for gas heating. For the worst case where a 200°K temperature increase is desired at 10 torr pressure the infinite uniform gaseous plate approximation predicts that 99% of the temperature increase will

Reproduced with permission of the copyright owner. Further reproduction prohibited without permission.

Table 1: Average Cross Sectional Area Determined For Fast Flow Reactor: 2.80 cm^2 (Standard Deviation 0.02 cm^2).

Total Volume of Water Added (cm^3)	Total Height Covered by Water (cm)	Cumulative Average Cross Sectional Area (cm^2)	Incremental Average Cross Sectional Area (cm^2)
0.0	0.00		
			2.84
25.0	8.80	2.84	
			2.78
50.0	17.80	2.81	
			2.81
75.0	26.70	2.81	
			2.79
100.0	35.65	2.80	
			2.78
125.0	44.65	2.80	

Reproduced with permission of the copyright owner. Further reproduction prohibited without permission.

be accomplished in 10 msec, corresponding to 10 cm at 10^3 cm/sec. The exact solution predicts that an even shorter length will be required. Thus there is no need for a pre-heat section for the flow-reactor; the 50 cm length is sufficient to heat the gas and have about 40 cm left for rate determination.

The final design is shown in figure 1. The 50 cm length of the reactor enclosed in the 32 mm outer tube was wrapped with 24 gauge nichrome wire in a spiral with the return lead enclosed in a 2 mm Pyrex tube; two electrical feed-throughs were located just behind the standard taper. Wrappings were at ca. 5 mm intervals, spaced further apart near the sampling end to avoid overheating of the portion enclosed by the mass spectrometer. The heater was powered by a standard 110 v variac.

Temperatures were measured with a chromel-alumel thermocouple enclosed in a 3 mm (O.D.) Pyrex tube which entered the reactor through an off-axis sliding seal at the rear. The probe was pre-stressed into a slight upward arc to counteract gravitational sag, and thus temperature could be measured on the axis of the reactor over its entire 50 cm length. Using this design a 30 cm length of reactor was obtained which could be heated to about 500°K with temperatures uniform within 5%. Figure 2 shows the average reactor temperature obtained at various applied voltages.

Reactant was introduced to the flow system by means of an axial probe (6 mm Pyrex tubing) which entered at the rear of the reactor through a sliding seal. A glass guy was provided at the standard taper to support the probe. Atoms were generated in the carrier stream which entered the reactor by a sidearm located directly behind the

Reproduced with permission of the copyright owner. Further reproduction prohibited without permission.

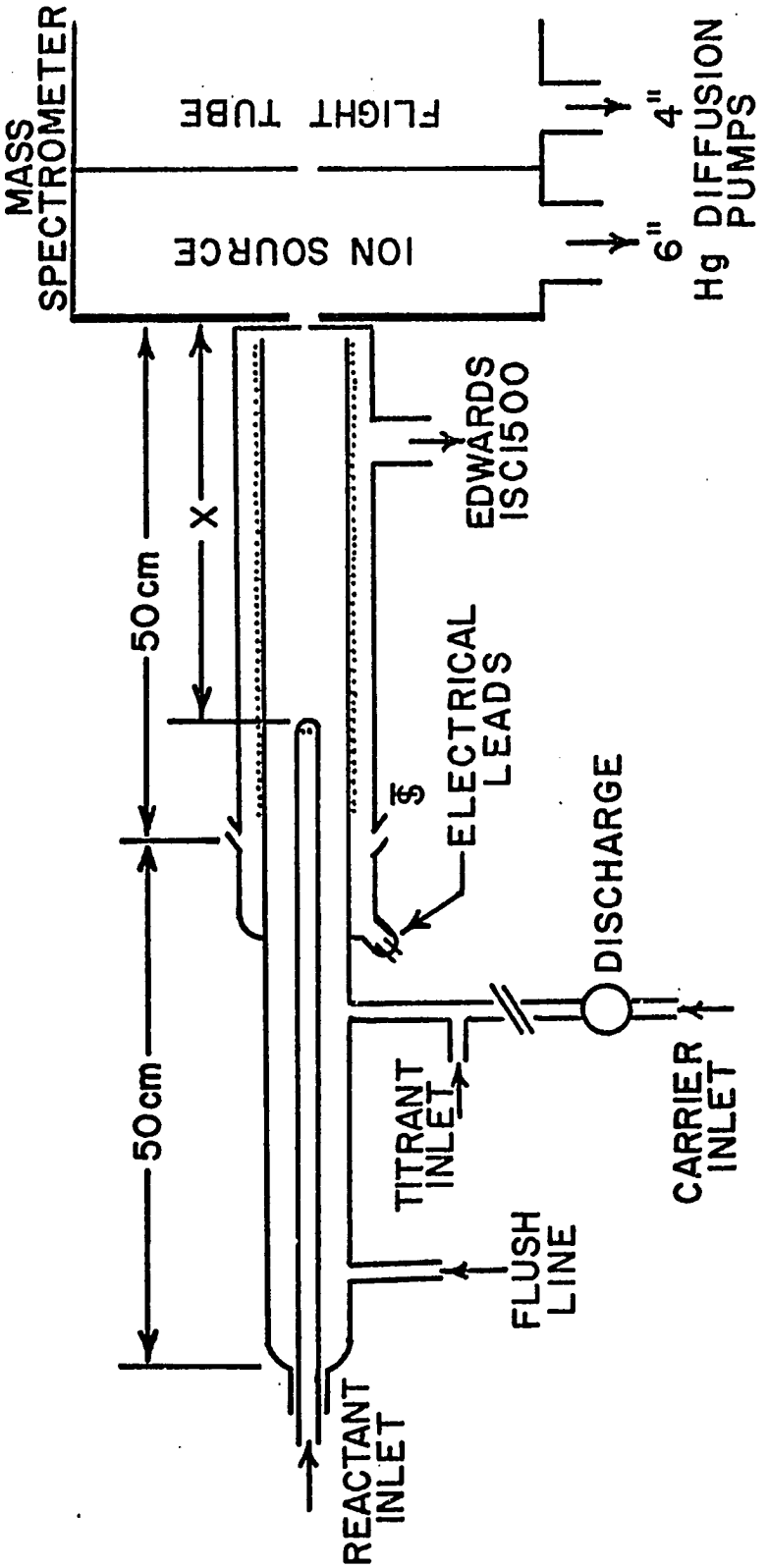

Figure 1: Discharge flow reactor: final design.

Reproduced with permission of the copyright owner. Further reproduction prohibited without permission.

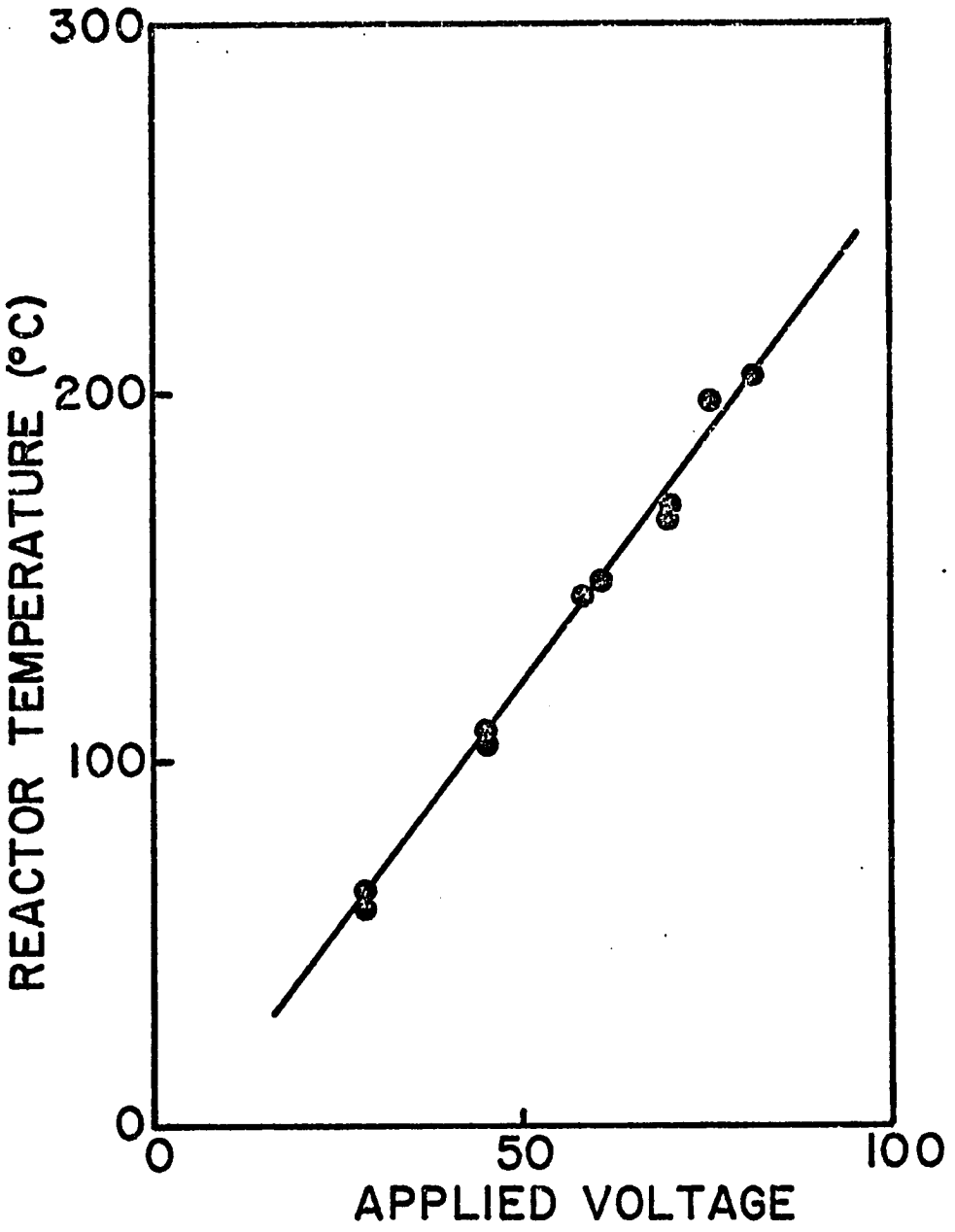

Figure 2: Average reactor temperature (± 5 percent) versus voltage applied to reactor heater.

Reproduced with permission of the copyright owner. Further reproduction prohibited without permission.

standard taper.

Both probes, reactant inlet and thermocouple, entered the reactor through an extension tube which was continuously flushed with undischarged carrier gas. This prevented atoms from contacting fresh, unpoisoned surfaces created when the probe position was changed. This modification, also used by Niki et al.,[22] has been found to greatly reduce nonreproducibility associated with what we have come to call "probe effects" and which will be discussed in detail later.

The flow system is shown schematically in figure 3. As can be seen provisions were made so that reactant (titrant) from either or both reactant flow metering systems could be directed to the reactant or carrier gas inputs prior to entry to the flow reactor. This is necessary as one reactant flow system is normally reserved for titrant (NO_2 for oxygen or hydrogen atom titrations, NO for nitrogen atom titrations), the other for stable reactant, and switching of the inputs, as will be shown later, is required for several operations.

The flow reactor was connected to the mass spectrometer by an O-ring seal around the outer flow tube (see figure 4). O-rings* were constructed of compound 994-75, a fluorocarbon elastomer which is stable to about 535°K. Operation of the reactor at temperatures somewhat above 500°K required the replacement of the O-ring after about 20 hours of operation. A jet of air was directed at the O-ring retaining flange to cool the O-ring and time-of-flight ion source.

---

* #PRP 568-218, purchased from PARCO, Ontario, California.

Reproduced with permission of the copyright owner. Further reproduction prohibited without permission.

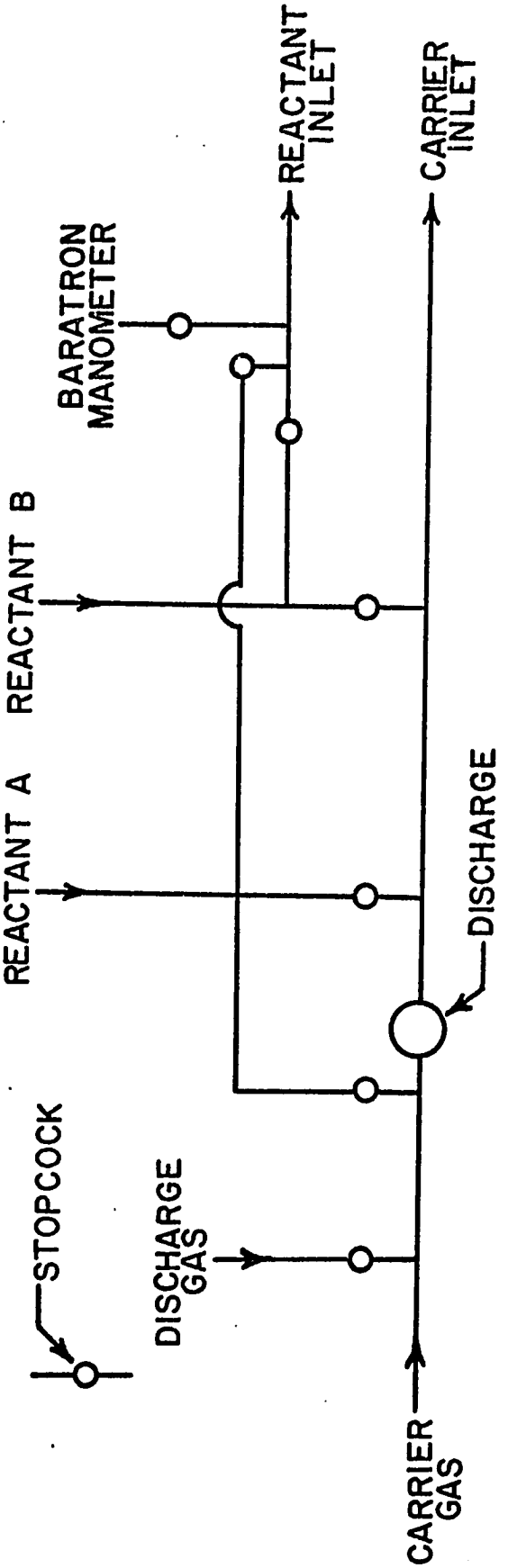

Figure 3: Schematic diagram of flow system interconnections.

Reproduced with permission of the copyright owner. Further reproduction prohibited without permission.

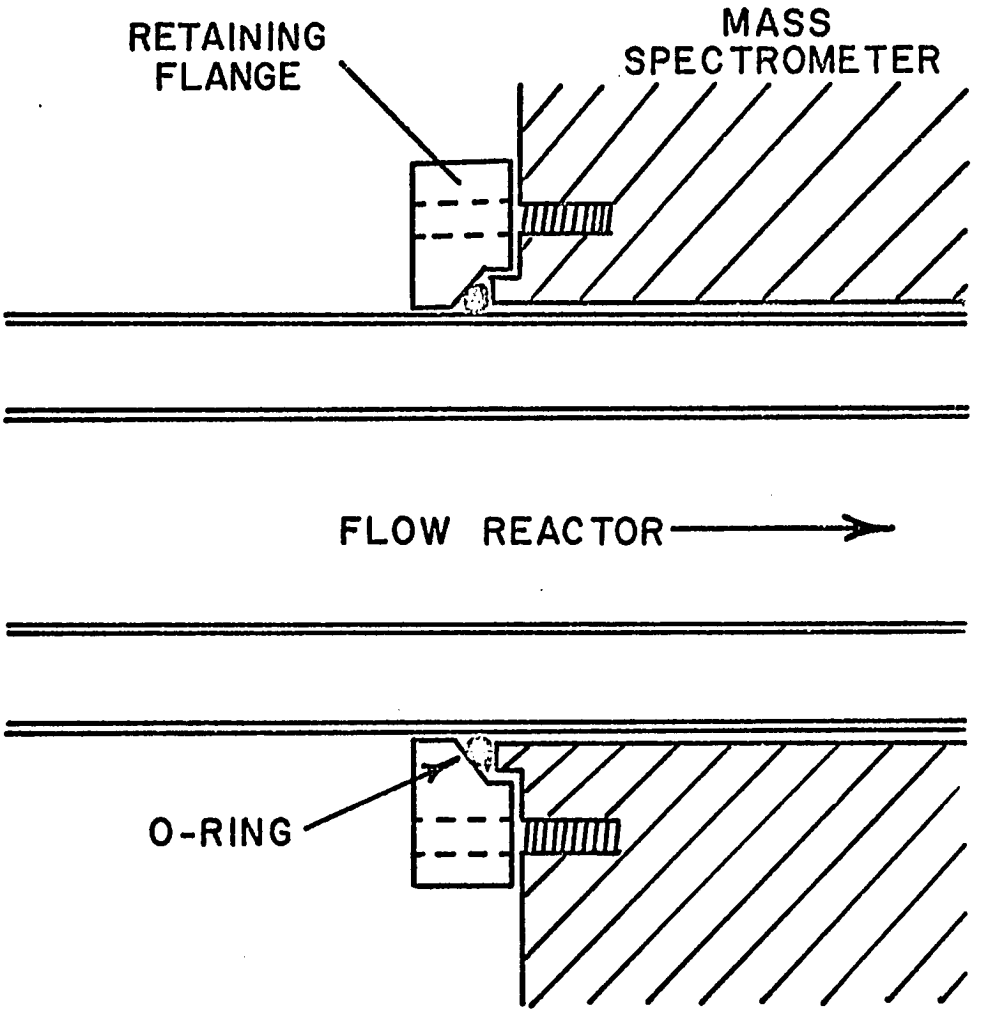

Figure 4: O-Ring seal of flow reactor to time-of-flight mass spectrometer.

Reproduced with permission of the copyright owner. Further reproduction prohibited without permission.

The Pinhole Inlet System

A pinhole inlet was designed to allow sampling from the flow reactor directly into the TOF ion source. Pinholes were constructed from microscope cover slips (Corning 25 mm diameter by 0.22 mm thick) so that discharged gas would contact only glass surfaces prior to sampling. The cover slip was masked by dipping in melted parafin and then scratching a small (ca. 0.5 mm) circular hole through the wax in the center of the plate. The coverslip was then etched five times, three minutes each, with 50% hydrofluoric acid and thoroughly cleaned.

This procedure will not etch a hole completely through the plate, however, the thickness will be reduced to the point at which a small (about .01 mm diameter) hole can be burned through with a tesla coil operated at medium power. The pinholes were then enlarged by careful grinding with a flame-sharpened tungsten needle. Pinholes were produced ranging from 0.05 to 0.5 mm diameter, measured under a microscope with a graduated ocular.

The pinholes were mounted with DeKhotinsky cement on a stainless steel backing plate which was in turn butted against the bottom of the TOF fast reaction chamber (see figure 5). In the original design the cover slip was held in place by an annular spacer bolted to the backing plate; however, this spacer was later eliminated so that the inner flow tube could extend closer to the face of the pinhole.

Reproduced with permission of the copyright owner. Further reproduction prohibited without permission.

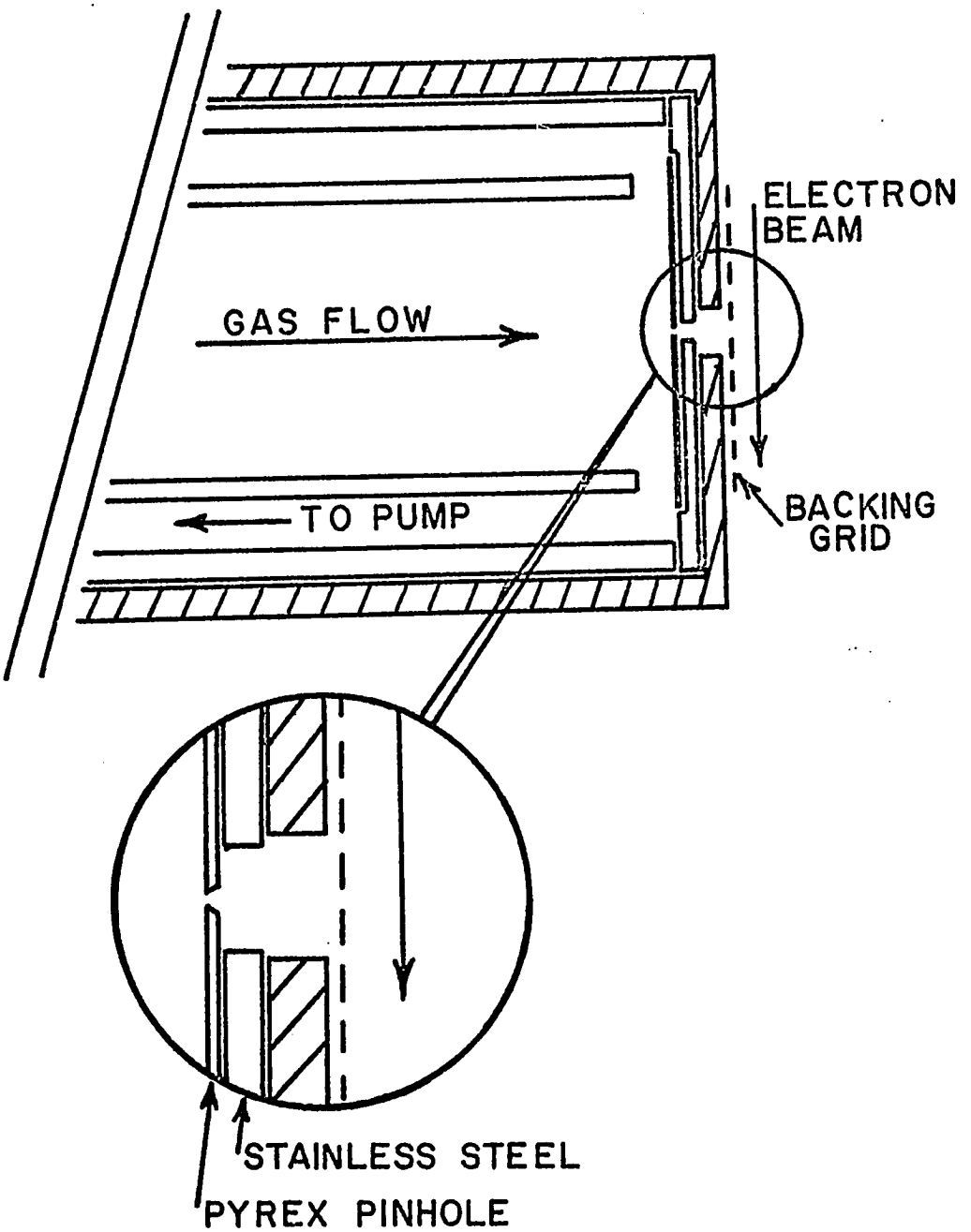

Figure 5: Pinhole inlet system to mass spectrometer ion source; insert drawn to 7:1 scale.

Reproduced with permission of the copyright owner. Further reproduction prohibited without permission.

Flow Metering Systems

Reactant and titrant gas flows were measured to an accuracy of 0.5 percent by monitoring the pressure drop from a known volume with Dynasciences Model P7D-0.1PSID differential pressure transducers (see figure 6). The transducers were calibrated against a MKS Baratron Type 144 capacitance manometer; for convenience the transducer output was set at 10 volts equal to 5 torr differential pressure. The linearity of response at several different reference pressures (i.e., the total pressure on the positive pressure arm of the transducer) is shown in figure 7, the slope of which is 2.01 $\pm$ 0.01 volts/torr. The output was read on a Leeds and Northrup Speedomax G strip chart recorder provided with a multiple scale attenuator so that differential pressures ranging from 5.0 to 0.05 torr (full scale reading) could be made.

Reactant flows were regulated with Edwards LB1B fine control needle valves equipped with viton O-rings. Although the valves could be opened up to 18 turns, in operation they rarely had to be opened more than two revolutions to obtain the desired flow.

A typical reactant flow under experimental conditions is 5×10^{-8} moles/sec. Since the duration of a run is about two hours, about 4×10^{-4} moles will be used, therefore a five liter ballast volume was provided (see figure 6) so that a negligible (ca. 2 torr) pressure drop would occur in the reactant system, holding the output flow constant while measurements are taken.

Two reactant flow metering systems were constructed, one used exclusively for stable reactant, the other for atom titrant. The system volume, defined from figure 6 as the portion within the dashed box minus the interchangeable volume attached at the standard taper,

Reproduced with permission of the copyright owner. Further reproduction prohibited without permission.

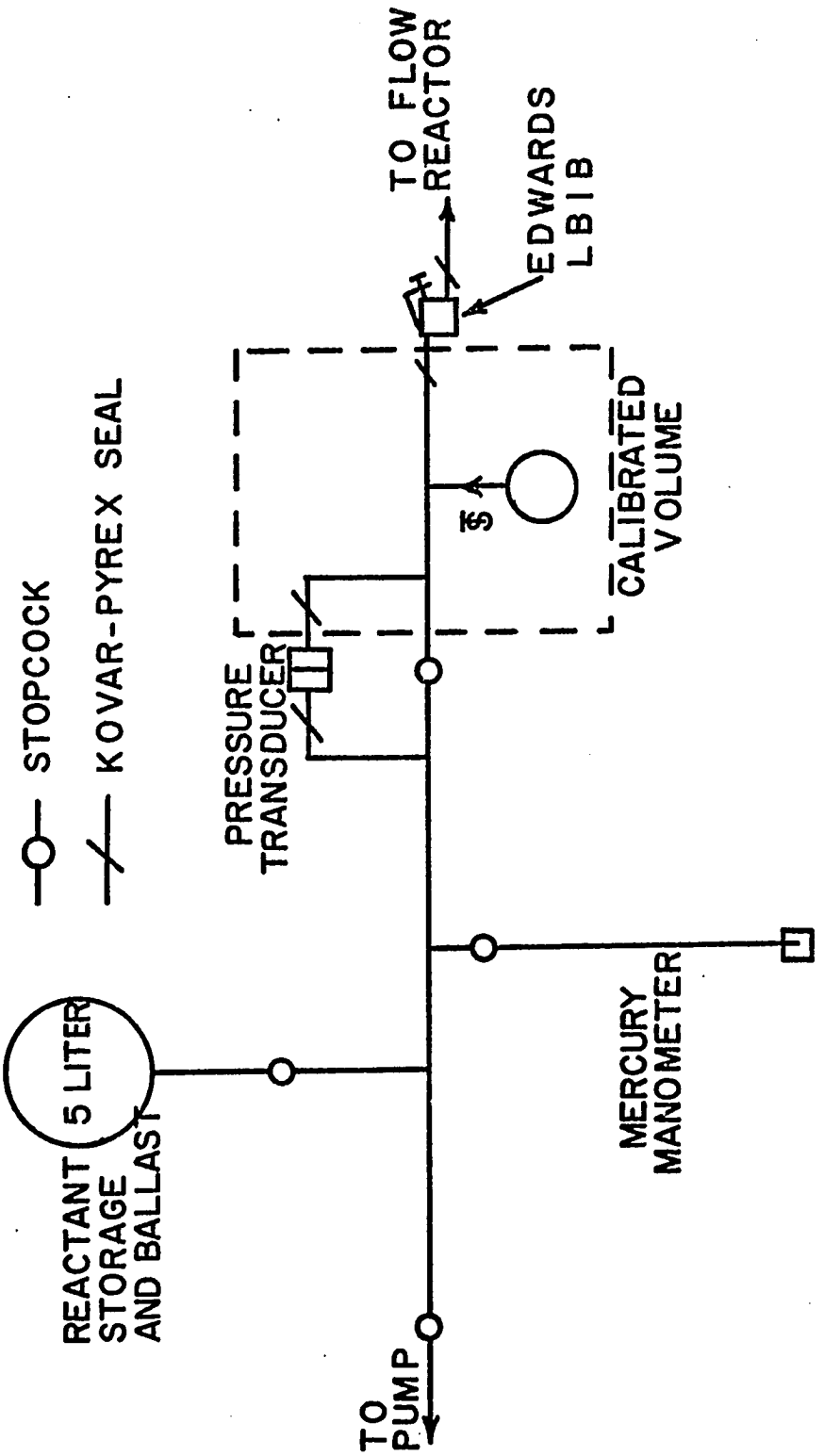

Figure 6: Reactant flow metering system; mercury in the manometer is protected from the gas being metered by a layer of Dow Corning QF-1-0065 fluoro-silicone fluid.

Reproduced with permission of the copyright owner. Further reproduction prohibited without permission.

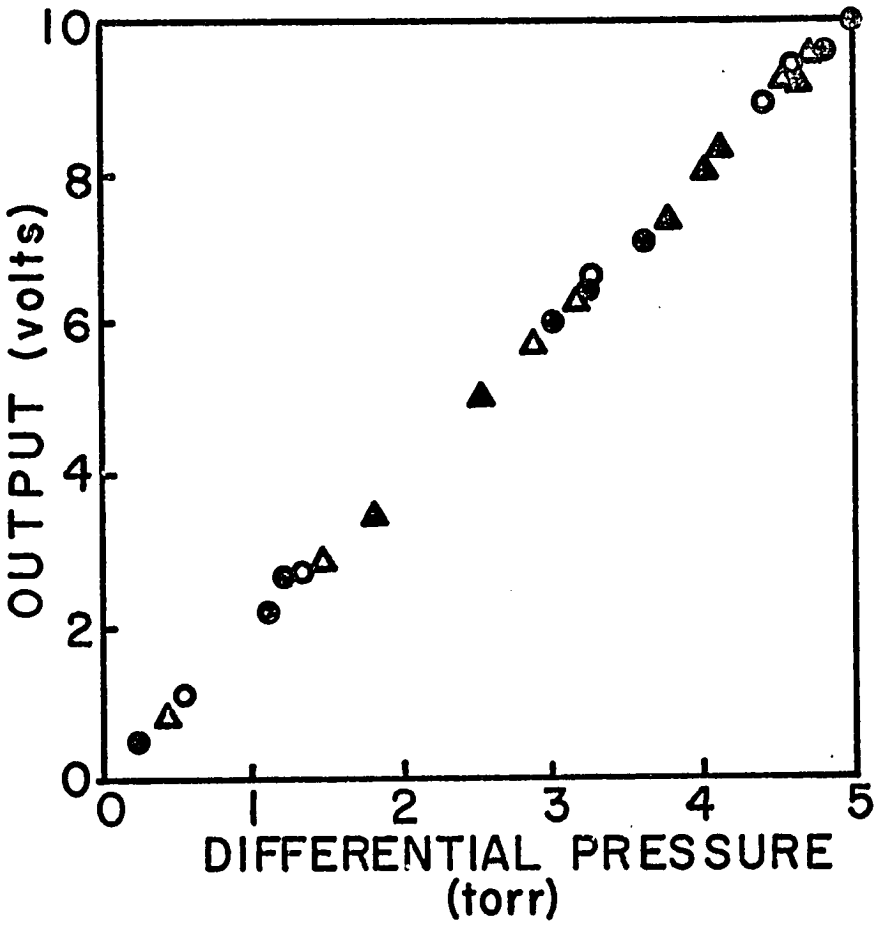

Figure 7: Linearity of pressure transducer response measured at selected reference pressures: ● = 0.0; ▲ = 90.0; O = 250; Δ = 500 torr. Differential pressure measured with MKS Baratron Type 144 capacitance manometer.

Reproduced with permission of the copyright owner. Further reproduction prohibited without permission.

was constructed as compactly as possible to allow maximum flexibility in the choice of volume from which to measure the pressure drop, the resulting volume being on the order of 25 cm^3 (see Table 2). This volume was measured to an accuracy of 0.1 percent with a gas burette, connected through a stopcock at the standard taper, by evacuating the system, then drawing water into the burette by opening the stopcock and equalizing pressures with a leveling bulb. Determinations were made at least four times, first with water, then with dibutyl-phthalate as a check.

Interchangeable volumes were made ranging in size from approximately 5 to 1000 cm^3 capacity (see Table 2), volumes determined to 0.1 percent accuracy by filling with water and weighing (the smaller volumes were determined by filling with mercury to increase the accuracy of the measurement). The maximum flow measurable can be figured considering a 5 torr pressure drop from a 1025 cm^3 volume in 10 seconds to be about 3×10^{-5} moles/sec. The minimum flow is calculated based on a 10 percent mixture of reactant in a suitable inert diluent flowing from a 30 cm^3 volume at 0.05 torr in 60 seconds as about 1×10^{-10} moles/sec.

The maximum carrier gas flow required will occur at 2,000 cm/sec linear flow velocity and 10 torr pressure, and may be calculated from the expression

$$F = \frac{LFV \times P_r \times A_r}{R \times T_r} \qquad (1)$$

where: T_r, P_r = temperature and pressure in the flow reactor

A_r = reactor cross sectional area

LFV = linear flow velocity

Reproduced with permission of the copyright owner. Further reproduction prohibited without permission.

Table 2: Values for Standard Volumes Used in Reactant and Titrant Flow Metering Systems.

Volume Calibrated	Volume (cm^3)	Method of Volume Determination
Reactant System	23.95 ± 0.03	gas burette
Titrant System	27.00 ± 0.03	gas burette
I	1095.0 ± 0.2	H_2O
II	1089.3 ± 0.2	H_2O
III	105.34 ± 0.02	H_2O
IV	122.35 ± 0.02	H_2O
V*	2068.2 ± 0.4	H_2O
VI*	509.7 ± 0.2	H_2O
VII*	3.863 ± 0.004	Hg
VIII*	102.34 ± 0.02	H_2O
IX	4.552 ± 0.002	Hg

* Calibration carried out by Leighton K. Derr, present address: Daren-Millican Company, LaGrange, Ga.

Reproduced with permission of the copyright owner. Further reproduction prohibited without permission.

R = gas constant; 6.24×10^4 torr $cm^3/^oMole$

$$F_{max} = \frac{(2000)(10)(2.80)}{(300)(6.24 \times 10^4)} = 3.0 \times 10^{-3} \text{ moles/sec}$$

The minimum carrier gas flow will occur at LFV = 100 cm/sec and 1 torr pressure:

$$F_{min} = \frac{(100)(1.0)(2.80)}{(300)(6.24 \times 10^4)} = 1.5 \times 10^{-5} \text{ moles/sec}$$

The maximum reactant or titrant flow is then found considering 1.0 percent reactant in carrier to be 3×10^{-5} moles/sec. The minimum reactant flow is more difficult to estimate since catalytic decomposition of the excess reactant may require a greater than 100 fold excess in a pseudo first-order experiment, as is discussed in Section VII; however, using a 100 fold excess of reactant which is 0.1 percent of the carrier flow at F_{min} gives a minimum reactant flow required of 1.5×10^{-10} moles/sec. Both of these extremes are within the reach of the reactant flow metering system capabilities.

A ball float type flowmeter (rotameter) was purchased (from Scientific Glass Apparatus Company, Bloomfield, New Jersey, 3/32 inch diameter floats) for the measurement of carrier gas flows. Flows were measured by operating the rotameter at a pressure in excess of one atmosphere (900 torr) and adjusting the flow with a needle valve downstream of the tube.

Although company literature indicates that readings are reproducible to one percent, which is sufficient for our purposes, it was found that only 5-10 percent reproducibility could be obtained in our system. The floats were subject to oscillations within the tube and would stick to the wall giving erroneous readings. Attempts to correct these problems

Reproduced with permission of the copyright owner. Further reproduction prohibited without permission.

by careful cleaning and degreasing were unsuccessful. A ballast volume was attached to the pressure regulator to eliminate any pressure fluctuations which might arise; however, no increase in reproducibility was obtained.

Capillary flow meters[23] were therefore constructed in order to obtain better measurement of carrier gas flows. Two such flow meters were made, one to measure the inert carrier flow, the other to permit introduction of 5-10 percent hydrogen, oxygen or nitrogen into a stream of inert carrier. The range of carrier gas flows required has been previously calculated to be 1.5×10^{-5} - 3.0×10^{-3} moles/sec; however, this must be extended downward to about 7.5×10^{-7} moles/sec when introduction of the gas to be discharged is considered.

The experimental arrangement is shown in figure 8. Dibutylphthalate, DBP, was chosen as the manometric fluid because of its low vapor pressure and density (1.0 torr = 12.97 mm DBP[25]), and relative inertness to chemical attack. Five capillaries were made with sufficient overlap of flow ranges so that most flows could be obtained on either of two tubes. The capillaries were all interchangeable and could be used on either flow meter. For simple Poiseuille flow:[1]

$$P_2^2 - P_1^2 = \frac{16Fl\eta RT}{r^4\pi} \qquad (2)$$

where l and r are the length and radius of the tube in cm, F the flow rate in moles/sec, η the gas viscosity in g/cm.sec, P_1 and P_2 are the pressures in dynes/cm^2 at the ends of the length l, and R = 8.31×10^7 erg/mole·°K.

Capillaries having nominal diameters of 0.5, 1.0 and 1.5 mm were available for use. Using the Poiseuille equation, lengths for the

Reproduced with permission of the copyright owner. Further reproduction prohibited without permission.

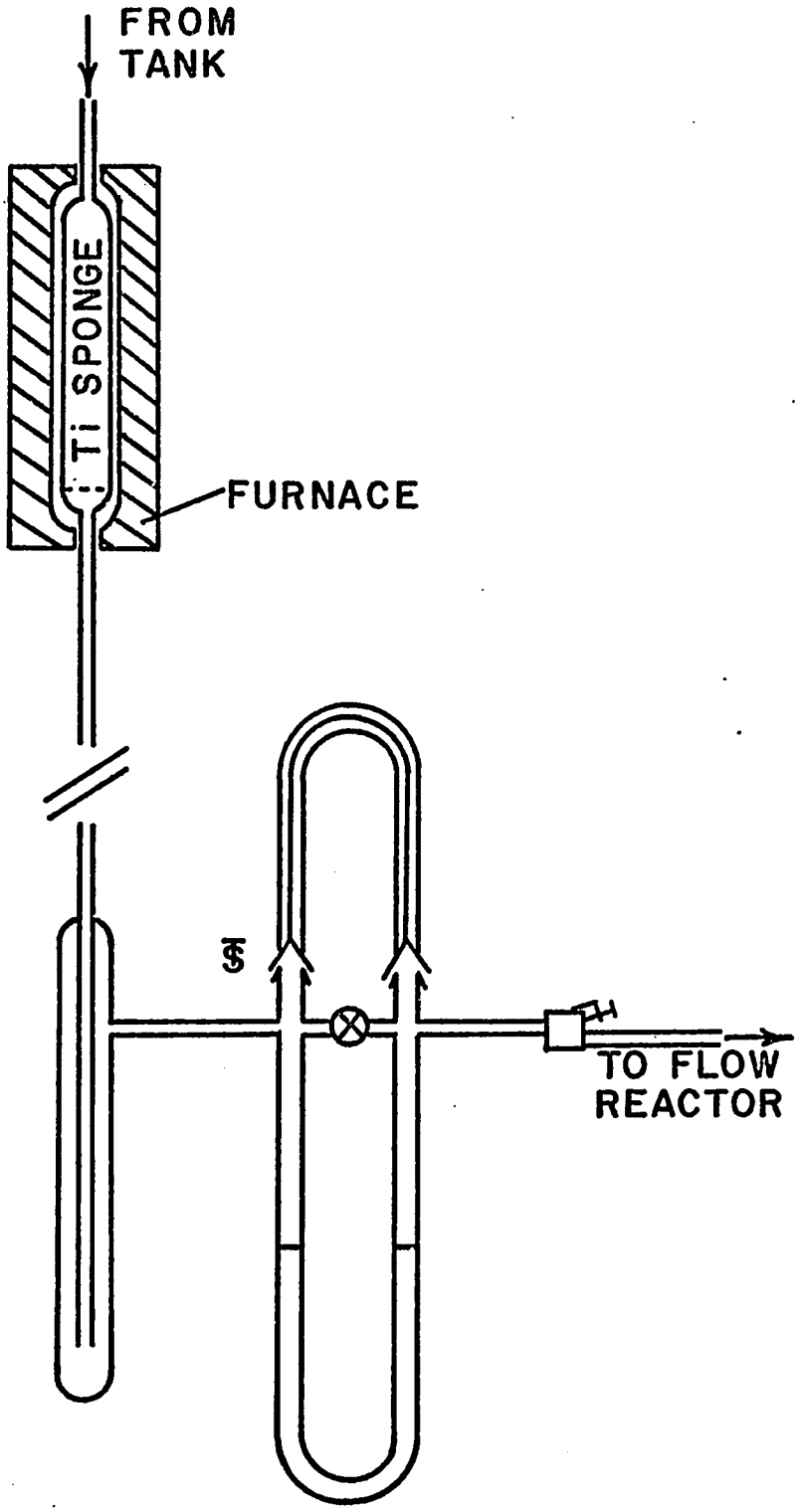

Figure 8: Capillary flow meter used for measurement of carrier gas flows.

Reproduced with permission of the copyright owner. Further reproduction prohibited without permission.

capillaries were calculated based on a convenient range of $P_2^2 - P_1^2$ from 10 to 200 mm DBP. The results are shown in Table 3 for helium at room temperature with $P_2 = 900$ torr.

The calculated ranges of flow are approximate, as the exact diameters of the capillaries are not known; also, the true ranges can be expected to be lower due to end effects and narrowing of the capillary at the 180° bend.

The flow meters were operated with $P_2 = 900$ torr. Making the substitution $P = P_2 - P_1$ into the equation for Poiseuille flow

$$F = CP(2P_2 - P) \qquad (3)$$

where $C = r4\pi/16l\eta RT$

Therefore since P is always less than 15 torr

$$F \approx 2CPP_2$$

$$dF = 2C[PdP_2 + P_2dP] \qquad (4)$$

Assuming reading errors of one torr in P_2 and 1 mm DBP (0.1 torr) in P, it is seen that the error in flow measurement will be predominantly in the dibutylphthalate reading.

Calibration was carried out with helium by venting the flow meter into an open end burette and timing the rate of climb of soap bubbles produced at the base. An open end manometer located at the bottom of the burette indicated that no pressure differential (less than 0.01 torr) existed across the length of the burette during this calibration.

In addition to the usual temperature and atmospheric pressure

Reproduced with permission of the copyright owner. Further reproduction prohibited without permission.

Table 3: Calculated Flow Ranges for Selected Lengths of Capillaries: Helium at 300 K; $\eta_{He} = 1.941 \times 10^{-4}$ Poise;[25] Input Pressure 900 Torr.

Capillary	Length (cm)	Diameter (mm)	F_{min} (10mm DBP) (moles/sec)	F_{max} (100mm DBP) (moles/sec)
A *	100	0.5	6.2×10^{-6}	1.2×10^{-4}
1	20	0.5	3.1×10^{-5}	6.2×10^{-4}
2	40	1.0	2.5×10^{-4}	5.0×10^{-3}
3	10	1.0	1.0×10^{-3}	2.0×10^{-2}
4	20	1.5	2.5×10^{-3}	5.1×10^{-2}

* Calibration carried out by Leighton K. Derr, present address: Daren-Millican Company, LaGrange, Ga.

Reproduced with permission of the copyright owner. Further reproduction prohibited without permission.

corrections applied to the measured flows, a correction factor defined as:

$$K(x, T) = \left(\frac{\eta_{He}298}{\eta_x T}\right) \cdot \left(\frac{298}{T}\right)^{\frac{1}{2}} \qquad (5)$$

where

x = gas flowing through capillary

T = temperature of gas (°K)

was applied to all data obtained.

The correction factors are listed in Table 4 for the several gases and temperatures pertinent to our system. Flows were referenced to helium at 298°K by

$$F = F_o K(x,T) \qquad (6)$$

where

F = true flow

F_o = flow corresponding to helium at 298°K for a given ΔP_{DBP}.

In Table 5 the results of the calibration are listed with and without the correction factor, K. The correction factor improved the linear regression fit in each case, the resulting values being accurate to better than 0.5 percent.

A set of constants, K(x, T), was calculated from known viscosity data[25] over the temperature range 20-30°C for helium, argon, nitrogen, oxygen and hydrogen. Thus the flow of any of these gases could be determined by multiplying the value of F_o from Table 3 times the appropriate value for K.

Reproduced with permission of the copyright owner. Further reproduction prohibited without permission.

Table 4: Correction Factors, K(x,T), Referenced to Helium at 25°C for Change in Gas Viscosity Due to Change in Temperature for Selected Gases.

Temperature (°C)	Helium	Argon	Nitrogen	Oxygen	Hydrogen
20	1.0278	0.8999	1.1412	0.9850	2.2810
21	1.0213	0.8960	1.1345	0.9776	2.2676
22	1.0162	0.8915	1.1280	0.9710	2.2548
23	1.0107	0.8860	1.1220	0.9630	2.2413
24	1.0057	0.8810	1.1150	0.9570	2.2287
25	1.0000	0.8766	1.1082	0.9495	2.2157
26	0.9948	0.8715	1.1025	0.9425	2.2022
27	0.9895	0.8660	1.0960	0.9355	2.1890
28	0.9842	0.8605	1.0895	0.9290	2.1764
29	0.9786	0.8545	1.0830	0.9225	2.1636
30	0.9737	0.8475	1.0763	0.9160	2.1529

Reproduced with permission of the copyright owner. Further reproduction prohibited without permission.

Table 5: Linear Regression Fit (95% Confidence Limit) of the Capillary Flow Meter Calibrations to the Equation $Y(x)=A+Bx$ Where $Y(x) = F$ (moles/sec), $x = \Delta P_{DBP}$(mm). Corrected Values Are Those Corrected for Change in Gas Viscosity Due to Change in Temperature.

	Uncorrected		Corrected	
Capillary	$Ax10^7$ (moles/sec)	$Bx10^7$ (moles/sec-mm)	$Ax10^7$ (moles/sec)	$Bx10^7$ (moles/sec-mm)
A*			0.85±.23	0.374±.001
1	3.87±1.00	2.296±.007	1.78±.60	2.307±.004
2	13.2±3.8	17.14±.04	12.2±3.7	17.12±.04
3	84±19	63.2±.4	79±18	63.6±.4
4	641±72	116.0±.8	643±70	115.3±.8

* Calibration carried out by Leighton K. Derr, present address: Daren-Millican Company, LaGrange,Ga.

Reproduced with permission of the copyright owner. Further reproduction prohibited without permission.

Ancillary Equipment

The mass spectrometer was a Bendix Model 12 Time-of-Flight modified by the substitution of a Model 14 ion source and John Fluke high voltage power supply. The Model 14 ion source was necessary to permit the use of the pinhole sampling system as the standard Model 12 source does not have a fast reaction chamber (i.e., that portion of the TOF which encloses the flow reactor, see figure 5). To increase sampling efficiency the inlet to the ion source from the flow reactor was enlarged to 0.1-inch diameter and the aperture in the backing plate was enlarged to 0.25-inch diameter and covered with molybdenum mesh (approximately 100 gauge). These modifications permitted a larger fraction of the particles which passed through the pinhole to enter the ionizing chamber without obstruction.

The TOF ion source and drift tube were differentially pumped with an Edwards 6M3A 6-inch mercury diffusion pump (backed by an ED660 forepump) on the ion source and a 4-inch mercury diffusion pump (backed by a Welch 1402 forepump) attached to the drift tube. The teflon baffle between the source and drift tube was removed to increase pumping efficiency.

Maximum sensitivity varied somewhat with experimental conditions, but for most of the work reported was about 10^{12} particles/cm^3 in the flow reactor.

High pumping speed was provided for the flow reactor by an Edwards EDISC1500 (1600 liter/min.) pump. The pumping speed, and therefore the reactor pressure, could be adjusted by either throttling with a Veeco SR100S O-ring seal valve (1-inch diameter port) or bleeding air into the throat of the pump via a small needle valve.

Reproduced with permission of the copyright owner. Further reproduction prohibited without permission.

Pressure in the reactor was monitored (through the reactant probe with no gas flowing through the probe) with a MKS Baratron Type 144 (Burlington, Massachusetts) capacitance manometer.

Oxygen atoms or active nitrogen were produced in a microwave discharge excited by a 125 W generator (2.45GHz, Kiva MPG-2 Kensington, MD.) with an Evenson type cavity. The generator was equipped with a SWR (standing wave ratio) meter:

$$SWR = \frac{V_{FWD} + V_{REF}}{V_{FWD} - V_{REF}}$$

where V_{FWD} and V_{REF} are the forward and reflected powers in the power output cable. In operation the generator was run at 40-50 watts forward power to prolong the life of the magnetron tube, and the cavity could generally be tuned for SWR $\leq$ 1.2. Molecular oxygen was discharged in about a 10% dilution in helium; however, nitrogen was discharged pure. The cavity was continuously cooled with compressed air.

In several experiments the chemiluminescence was measured with an unfiltered RCA 931A photomultiplier tube positioned 10 cm from the flow reactor behind two 3 x 8 mm slits. This arrangement permitted observation of emission integrated along a 0.5 cm length of the reactor. In one experiment a Heath EU-700-51 monochromator was used to obtain a spectrum of the emission.

Reproduced with permission of the copyright owner. Further reproduction prohibited without permission.

Evaluation of Capabilities and Limitations

The linear flow velocity, LFV, in the reactor is calculated by

$$\text{LFV (cm/sec)} = \frac{F \times R \times T_r}{P_r \times A_r} \qquad (7)$$

where: F = gas flow (moles/sec)

T_r, P_r = temperature and pressure in the flow reactor

A_r = reactor cross section (cm^2)

R = gas constant; 6.24×10^4 torr $cm^3/°mole$

The limiting factor in obtaining high LFV is the pumping speed of the reactor pump. We were quite fortunate in having a large (1600 liter/min) reactor pump; however, experimental limitations to the maximum linear flow velocities still exist at low pressures. This limitation was measured by admitting carrier gas to the reactor with the pump operating at full capacity and measuring the reactor pressure as a function of the flow rate of admitted gas. The results are shown in figure 9 for nitrogen carrier in terms of maximum LFV attainable as a function of reactor pressure.

Measurements were not taken at pressures greater than 1.5 torr as the flow velocities attainable are generally in excess of those required. The reactor and complementary systems were originally designed for a 2000 cm/sec LFV over the entire range of pressure 0-20 torr. The falloff below 1.5 torr is due to the constriction in the pumping line at the pinhole inlet to the TOF; however, no attempt was made to correct this problem as linear flow velocities in excess of 500 cm/sec were rarely required at low pressures, thus no difficulty arose.

Kaufman[1] reports that pressure drop along the reactor is negligible

Reproduced with permission of the copyright owner. Further reproduction prohibited without permission.

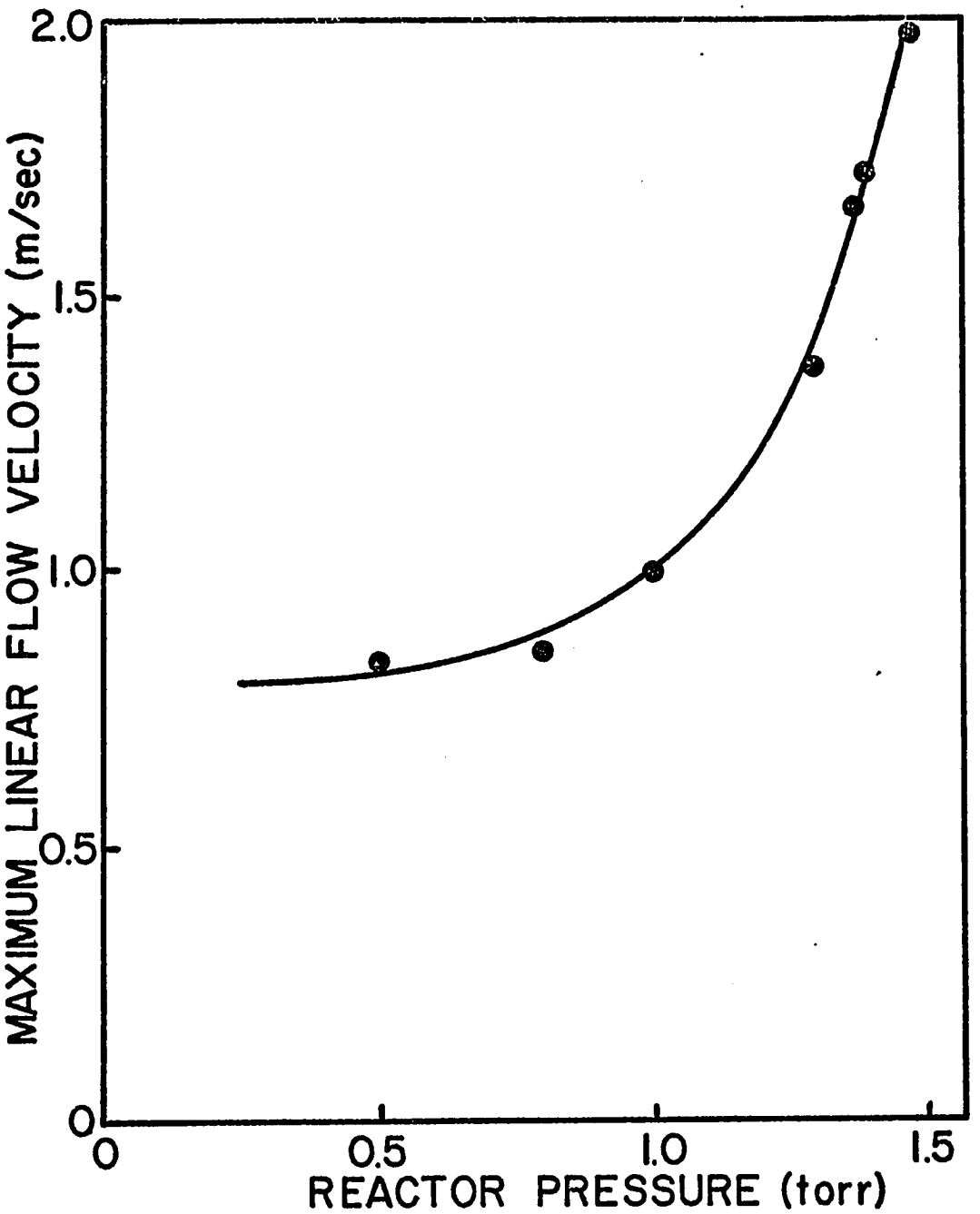

Figure 9: Maximum linear flow velocity at low reactor pressures. Data obtained with the Edwards 1SC1500 pump operating at full capacity.

Reproduced with permission of the copyright owner. Further reproduction prohibited without permission.

at LFV < 1000 cm/sec and one torr, but becomes important at lower pressures. This was verified for our system as reported in Table 6. The pressure was found to be constant within one percent for LFV = 100 cm/sec, typical of the flow velocities used at one torr.

In the original design of the flow reactor the probes entered the reactor directly behind the standard taper, that is, the 50 cm flushed extension tube did not exist. This original configuration gave rise to anomalous results associated with what we have come to call "probe effects".

The probe effect is illustrated in figures 10 and 11 in which the log of the oxygen atom concentration at the pinhole is plotted versus the position of the probe tip. Oxygen atoms were produced by the nitric oxide titration of active nitrogen[3] prior to entry to the flow reactor. The O-atom concentration was then monitored at the pinhole as the probe position was changed (with no flow of any gas through the probe) first by pushing the probe in by successive 5 cm intervals, then by probe withdrawal also in 5 cm increments, and allowing for equilibration (ca. 10-15 min.) each time the probe was moved. As the probe is moved in, atoms are consumed faster by recombination on the fresh, unpoisoned surface; however, as the probe is withdrawn the O atoms fail to return to their original value even though there is no flow of reactant through the probe. The same trends are observed for N-atom recombination; however, the magnitude of the effect is less than half that observed with oxygen.

The data presented in figures 10 and 11 of course bear no direct relationship to measured rate constants, but do demonstrate the non-reproducibility of results arising from the "probe effect". If the

Reproduced with permission of the copyright owner. Further reproduction prohibited without permission.

Table 6: Pressure Drop Along the Flow Reactor Measured at 298°K and 100 cm/sec Linear Flow Velocity, Nitrogen Carrier.

Distance From Pinhole (±0.1 cm)	Reactor Pressure (±0.002 Torr)
1.5	0.985
3.5	0.985
11.5	0.987
21.5	0.989
31.5	0.990
41.5	0.991
51.5	0.991
3.5	0.986
1.0	0.985

Reproduced with permission of the copyright owner. Further reproduction prohibited without permission.

Figure 10: The probe effect at 298 °K; reactor pressure 1.0 torr; 140 cm/sec linear flow velocity. Oxygen atoms were produced at the probe tip by the nitric oxide titration of active nitrogen. Data obtained by monitoring m/e = 16 peak height at different probe positions first moving the probe in by 5 cm intervals, ●, then moving the probe out by 5 cm intervals▲.

Reproduced with permission of the copyright owner. Further reproduction prohibited without permission.

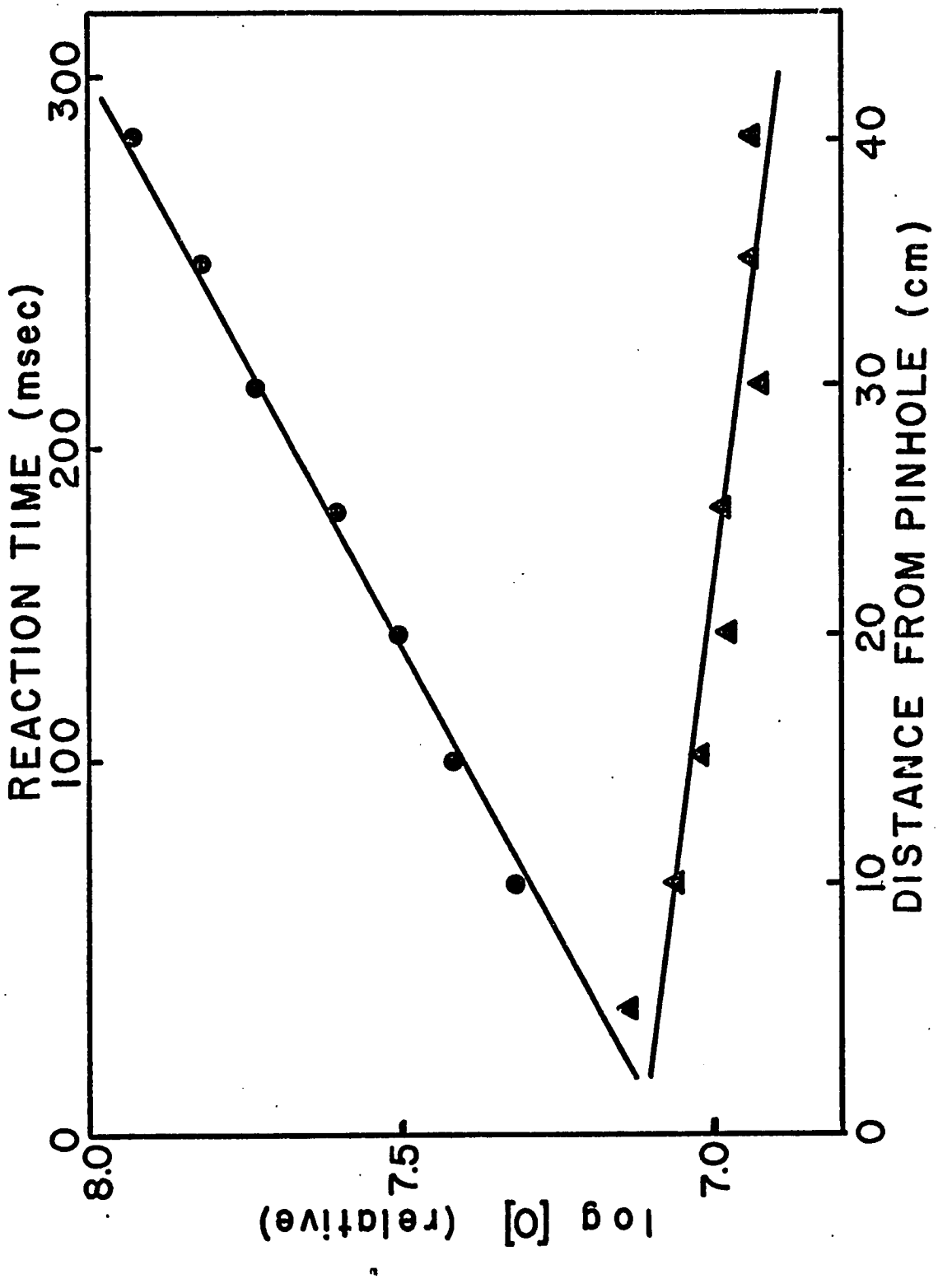

Reproduced with permission of the copyright owner. Further reproduction prohibited without permission.

Figure 11: The probe effect at 458°K; reactor pressure 1.0 torr; 214 cm/sec linear flow velocity. Oxygen atoms were produced at the probe tip by the nitric oxide titration of active nitrogen. Data obtained by monitoring m/e = 16 peak height at different probe positions first moving the probe in by 5 cm intervals, ● , then moving the probe out by 5 cm intervals▲.

Reproduced with permission of the copyright owner. Further reproduction prohibited without permission.

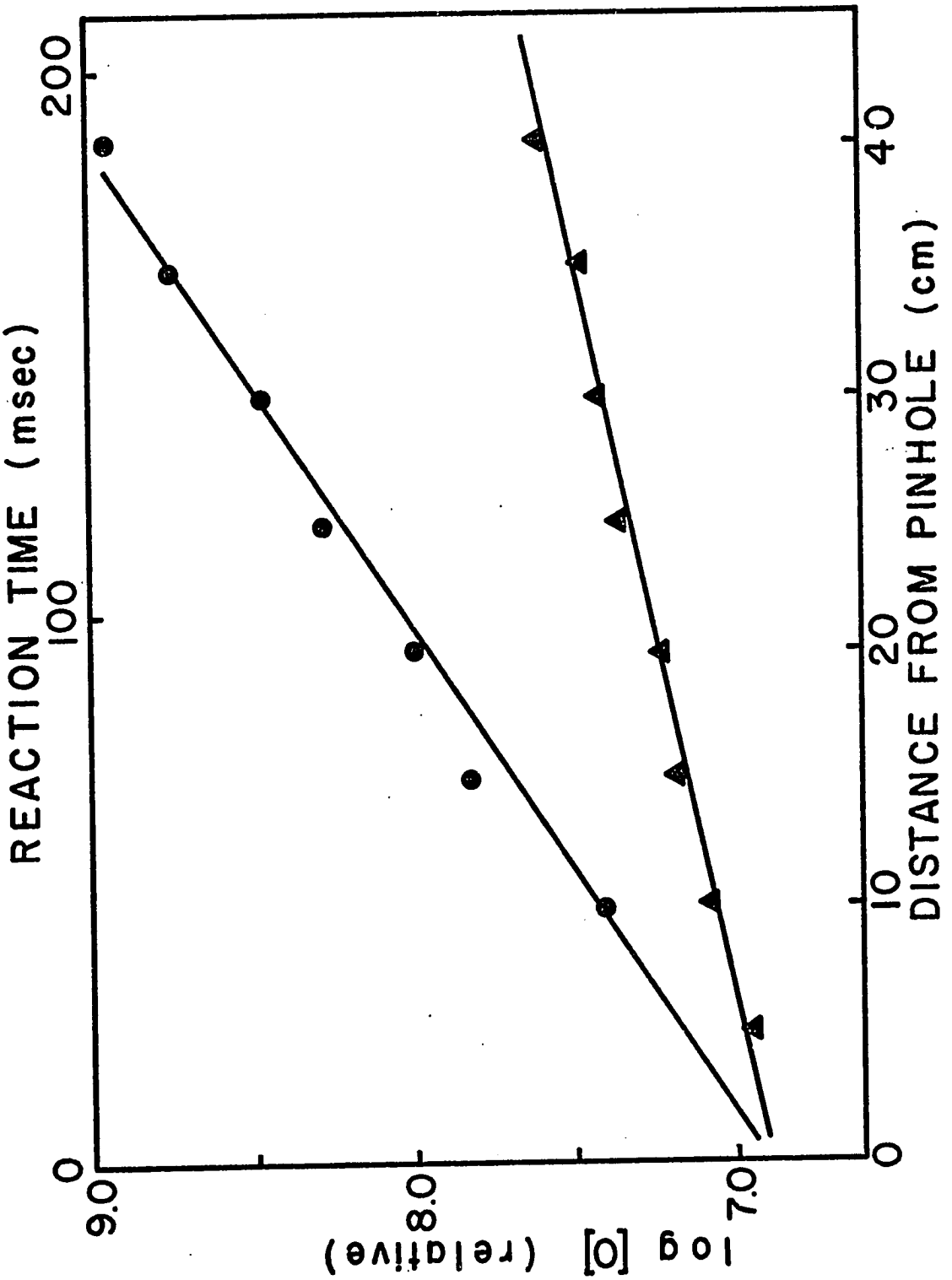

Reproduced with permission of the copyright owner. Further reproduction prohibited without permission.

atom concentration was so markedly affected by the presence or absence of the probe alone, with no flow through the probe, then there could be little confidence in the data obtained when the reactant was admitted to the flow reactor through the probe while the probe position was changed. The effect is undoubtedly very complex, related to the degree of surface poisoning and coverage, change in surface to volume ratio and change in linear flow velocity behind the probe tip; however, we were able to eliminate serious errors arising from the probe effect by incorporation of the flushing line.

With the flushing line plots similar to figures 10 and 11 show less than 5 percent change in atom concentration for corresponding "insertion" and "withdrawal" points. The effectiveness of the flushing is illustrated in figure 12 where the first order O-atom recombination rate constant, k_w, for

$$O \xrightarrow{k_w} \tfrac{1}{2}O_2$$

is determined by titrating active nitrogen at the probe tip with nitric oxide. Since the corresponding wall recombination for nitrogen atoms is much slower the heterogeneous recombination of N atoms is negligible, and [N] is virtually constant along the reactor: hence the reaction

$$N + NO \longrightarrow N_2 + O$$

generates a constant concentration of oxygen atoms at the probe tip, regardless of probe position. The integrated form of the rate expression for O-atom wall removal is then:

Reproduced with permission of the copyright owner. Further reproduction prohibited without permission.

$$\log [O] = -(k_w/2.303)t + \log [O]_o \qquad (8)$$

where

$$\log [O]_o = \text{constant}$$

The values for k_w determined from figure 12 for the successive insertion and withdrawal points are 3.0 and 3.1 sec^{-1}, respectively, which are easily within the limits of experimental error. In all data to follow points were taken in random order so that any residual effect will appear as a random rather than systematic error; in any case, the systematic error due to probe effects cannot exceed five percent, the limit shown in figure 12.

Reproduced with permission of the copyright owner. Further reproduction prohibited without permission.

Figure 12: The residual probe effect in the determination of k_{wall} for heterogeneous O-atom removal with the flushed extention tube: 298°K 1.01 torr, O atoms produced by nitric oxide titration of active nitrogen at the probe tip. Data obtained by monitoring m/e = 16 peak height at different probe positions first moving the probe in by 5 cm intervals, ●, $k_{wall}^{in} = 3.0$ sec^{-1} then moving the probe out by 5 cm intervals, ▲, $k_{wall}^{out} = 3.1$ sec^{-1}.

Reproduced with permission of the copyright owner. Further reproduction prohibited without permission.

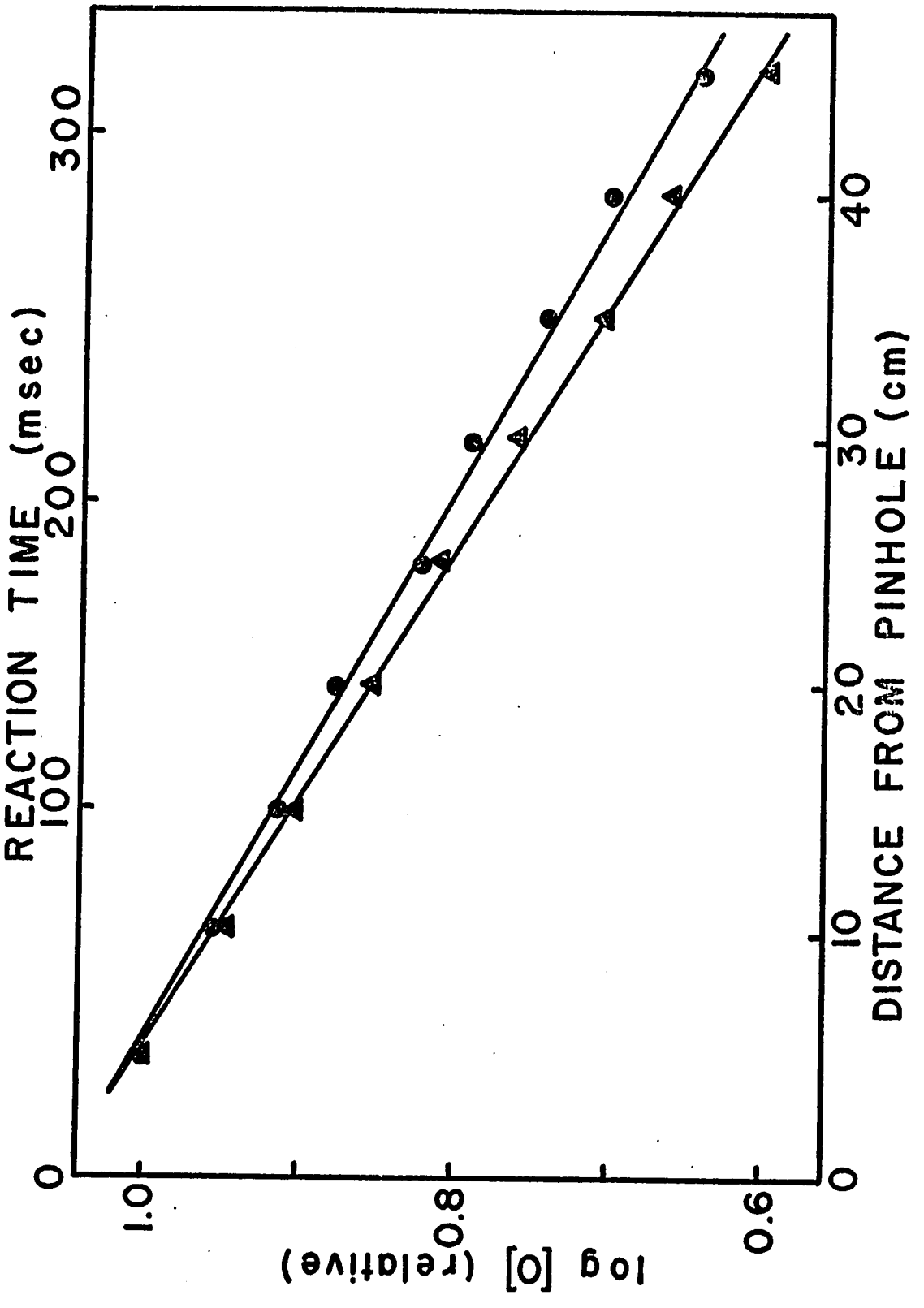

Reproduced with permission of the copyright owner. Further reproduction prohibited without permission.

Production of Atoms and Measurement of Atom Concentration

In the majority of oxygen atom experiments atoms were generated by the microwave discharge of a mixture of 5-10 percent molecular oxygen in helium. In preliminary experiments argon was used as the inert carrier; however, an unknown species produced in the discharge of "pure" argon reacted to a small extent with the stable reactant, dicyanoacetylene. This was not the case with helium and therefore the cause of switching carrier gases. An added advantage gained in using helium was that there were no interesting mass peaks (i.e., products or intermediates) near m/e = 4 (He) while there were many centered around m/e = 40 (Ar); therefore, there was less interference from background in product and intermediate surveys.

Oxygen atom concentrations were usually determined by titration with nitrogen dioxide, NO_2. The flow of atoms was taken as the measured flow of NO_2 at the endpoint of the titration since the reaction stoichiometry is one O atom consumed per NO_2 molecule consumed. Since our flow metering system measured flow in terms of total moles per second, the equilibrium

$$2NO_2 \rightleftharpoons N_2O_4$$

must be considered to determine the true flow of NO_2. In Table 7 values for the equilibrium constant

$$K_{Eq}^{T} = \frac{[N_2O_4]}{[NO_2]^2} = \exp - (\Delta G_{Rxn}/RT) \quad (atm.^{-1}) \quad (9)$$

have been calculated from the free energies of formation[26] at three

Reproduced with permission of the copyright owner. Further reproduction prohibited without permission.

Table 7: Equilibrium Constants for the reaction $2NO_2 \rightleftharpoons N_2O_4$ at Selected Temperatures Calculated from JANAF Tables[26]

$$K_{Eq}^{T} = [N_2O_4] / [NO_2]^2 \quad (atm^{-1})$$

Temperature (^oK)	ΔG_{NO_2} (kcal/m)	$\Delta G_{N_2O_4}$ (kcal/m)	ΔG_{Rxn} (kcal/m)	K_{Eq}^{T} (atm^{-1})
298	12.247	23.355	-1.139	6.73
300	12.274	23.486	-1.062	5.86
302	12.301	23.617	-0.985	5.09

Reproduced with permission of the copyright owner. Further reproduction prohibited without permission.

selected temperatures. If P is the total pressure in the flow metering system and x the partial pressure of NO_2,

$$K_{Eq}^{T} = \frac{P - x}{x^2} \qquad (10)$$

The true flow of NO_2, F, is then found from the measured flow, F', by

$$F = F'[2P - x]/P = C^{P,T}F' \qquad (11)$$

In Table 8 a number of constants, $C^{P,T}$, defined by equation 11 are listed for different total pressures of $NO_2 + N_2O_4$ in the flow metering system.

With mass spectrometric detection there were several means by which the titration may be accomplished. These will be referred to as visual, instrumental, overtitration, and molecular oxygen methods;

1.) The visual endpoint; that is, the extinction of the yellow air afterglow has been widely used and is discussed elsewhere.[1]

2.) The instrumental end point is defined as the point at which m/e = 16 (O) is reduced to background. The peak height must be measured at low (ca. < 17.5 ev) ionizing voltage to prevent fragment ion formation from O_2 or NO_2.

3.) In the overtitration technique the instrumental endpoint is passed by 10-20 percent and m/e = 46 (NO_2) is monitored while the discharge is extinguished. The percent reaction of NO_2 may then be calculated from the change in the peak height and the flow of oxygen atoms taken as that percent of the total NO_2 flow.

4.) The molecular oxygen method is somewhat unique of the four in

Reproduced with permission of the copyright owner. Further reproduction prohibited without permission.

Table 8: Correction Constants, $C^{P,T}$, for NO_2 Flows at Various Total Pressures, P, of the Flow Metering System.

P (torr)	$C^{P,298}$	$C^{P,300}$	$C^{P,302}$
150	1.431	1.407	1.383
140	1.419	1.395	1.371
130	1.406	1.382	1.358
120	1.392	1.369	1.345
110	1.377	1.354	1.330
100	1.361	1.338	1.315
95	1.353	1.329	1.306
90	1.343	1.320	1.297
80	1.324	1.301	1.279
70	1.302	1.280	1.258
60	1.277	1.256	1.235
50	1.249	1.229	1.209
40	1.217	1.198	1.180
30	1.179	1.162	1.146
20	1.133	1.120	1.107
10	1.076	1.067	1.059
5	1.041	1.036	1.031

Reproduced with permission of the copyright owner. Further reproduction prohibited without permission.

that it is not dependent on the reaction with nitrogen dioxide. If m/e = 32 (O_2) is observed while the discharge is turned off the percent dissociation may be calculated and the flow of atoms determined by multiplying the flow of oxygen, times the percent dissociation, times two.

However, as figure 13 indicates the apparent percent dissociation is clearly a function of the ionizing voltage. This effect has been observed previously,[27, 28] and is attributed to the presence of excited molecular oxygen in the $^1\Delta_g$ and possibly $^1\Sigma g^+$ states which have a lower appearance potential than ground state oxygen. Therefore at lower ionizing voltages the peak height of m/e = 32 actually increases when the discharge is struck, indicating the impossible situation of a negative degree of dissociation. Measurement of the percent change was not reproducible at lower ionizing voltages; however, if the peak height ratios were taken at 70 v, well up on the plateau of figure 13, consistent results for O-atom concentrations were obtained.

Considerable effort was spent in an attempt to determine which of these methods gave the most consistent and accurate results. Oxygen atom concentrations obtained by the four techniques varied by about 15 percent; however, were consistently in the order molecular oxygen < instrumental $\sim$ overtitration < visual. Generally less than five percent dissociation of molecular oxygen could be obtained in our system unless water or some other impurity was introduced upstream of the discharge. We chose to maintain the purity to assure that reactions with species other than O atoms were negligible. Hence O-atom concentrations determined by the molecular oxygen technique were difficult to measure and were less accurate than those of the other

Reproduced with permission of the copyright owner. Further reproduction prohibited without permission.

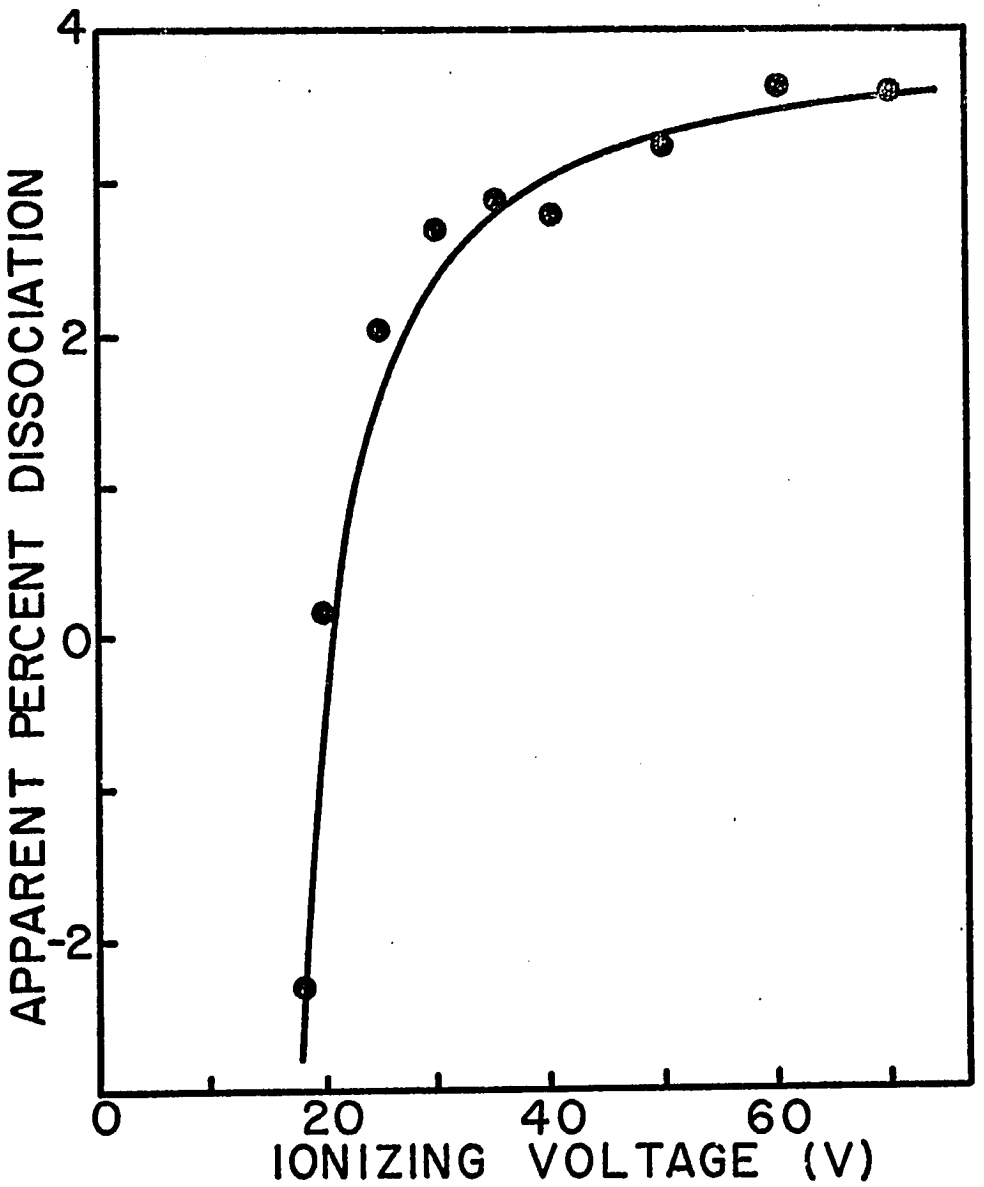

Figure 13: The apparent percent dissociation of molecular oxygen determined by monitoring m/e = 32 as a function of ionizing voltage; 298°K, 1.0 torr, 627 cm/sec linear flow velocity.

Reproduced with permission of the copyright owner. Further reproduction prohibited without permission.

methods. The accuracy of the visual method was also questionable as it relied on the sensitivity of the eye to determine the point at which the afterglow was extinguished. This could be quite subjective, particularly at total pressures below about three torr, estimates varying by ten percent among several people. We therefore chose the instrumental method to determine O-atom concentrations in all of the values reported. The four techniques were periodically checked against each other, and the results described above were always consistent.

In a number of trials oxygen atoms were generated by the nitric oxide titration of active nitrogen.[3] This procedure generates oxygen atoms relatively free of molecular oxygen, and is further discussed in Section VI. The molecular nitrogen method for atom concentration determination was not applicable here as very inaccurate results were obtained because the small percent dissociation (ca. 1 percent) of molecular nitrogen cannot be precisely determined.

In this system the visual endpoint was found to lie about 5 percent short of the instrumental, here defined as the point at which m/e = 14 (N) is reduced to background. The instrumental endpoint was used in all calculations in order to be consistent with the O-atom reaction studies.

Although no external check is available for the validity of our method the visual endpoint method appears to be incorrect. In figure 14 the relative concentrations of oxygen (m/e = 16) and nitrogen (m/e = 14) atoms are plotted as a function of added titrant. As shown not only does the nitrogen peak continue to decrease, but the oxygen peak continues to increase beyond the visual endpoint.

Active nitrogen was generated by passing a stream of pure nitrogen through a microwave discharge. Nitrogen atom concentration was

Reproduced with permission of the copyright owner. Further reproduction prohibited without permission.

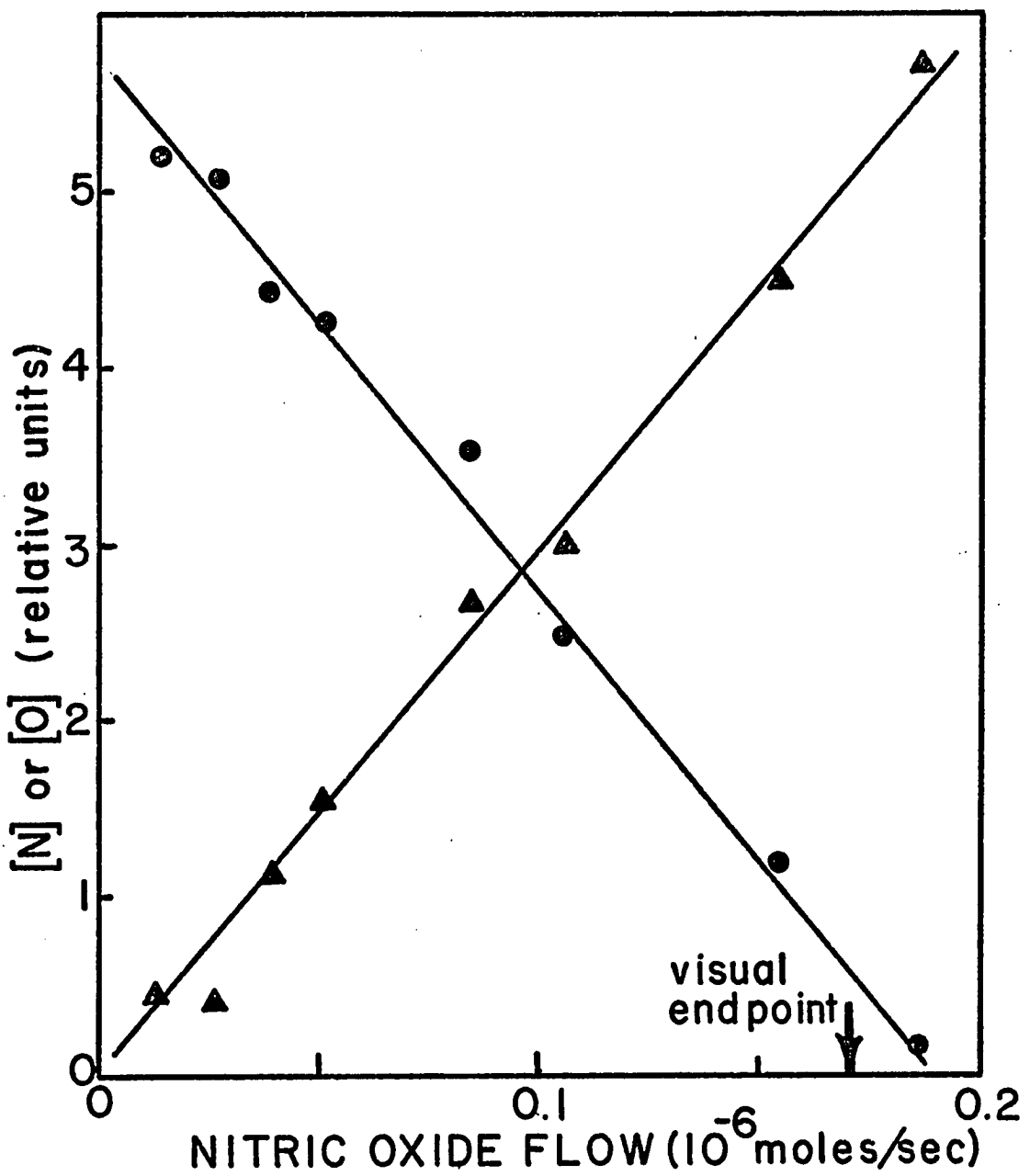

Figure 14: Relative oxygen and nitrogen atom concentrations in the nitric oxide titration of active nitrogen at 0.47 torr, 298°K and 380 cm/sec linear flow velocity: ● N-atom concentration, ▲, O-atom concentration.

Reproduced with permission of the copyright owner. Further reproduction prohibited without permission.

determined by titration with nitric oxide again using the instrumental endpoint.

A problem arose experimentally in titrations of both active nitrogen and O atoms stemming from the effect of trace impurities on the microwave discharge. Baker et al.[29] have shown that the addition of as little as 0.005 percent of impurity can increase N-atom production from a molecular nitrogen discharge by a factor of ten.

We have observed an increase in atom production upon introduction of small amounts of reactant or titrant to the flow reactor and attribute this increase to axial diffusion of small amounts of reactant or titrant against the flow into the discharge region. While this explanation at first glance appears unlikely, as the discharge is located far upstream of the reactor, the effect is more pronounced at low linear flow velocities and pressures, as would be expected for a diffusion controlled process. (See Appendix B.)

The purpose of the atom titration is to standardize the m/e = 14 (N-atom) or m/e = 16 (O-atom)peak height for concentration in the flow reactor and relies on atom production remaining constant while the titration is made. Therefore, in operation a very small amount ($< 10^{-10}$ moles/sec) of DCA was introduced to the flow system between the discharge and the flow reactor thus increasing the atom production so that when titrant was added through the probe no further enhancement could be observed. The atom peak height before the titration then corresponds to the atom flow determined by the endpoint.

Reproduced with permission of the copyright owner. Further reproduction prohibited without permission.

Wall Poisoning

Although not fully understood it is well known that surface recombination of oxygen[1] and nitrogen[2] atoms on Pyrex is greatly affected by treatment of the surface with acids, bases or other substances. Before beginning quantatitive measurements a procedure had to be developed which would give reproducible conditioning of reactor walls and thus enable us to choose either conditions or methods such that our results would not be affected by any heterogeneous recombination contribution.

The wall recombination of oxygen atoms at 1.0 torr was chosen as a reference for wall conditioning. As discussed previously k_w for:

$$O \xrightarrow{k_w} \tfrac{1}{2}O_2$$

was determined by titration of active nitrogen with nitric oxide at the probe tip. The oxygen atom concentration is then measured as a function of time, that is, distance between the pinhole and the probe, and is related by:

$$\ln \frac{[O]}{[O]_o} = -k_w t \qquad (12)$$

In every run the instrument was turned on, all flows and pressures adjusted to the desired conditions and allowed to run with the discharge on for 2 to 4 hours to allow for equilibration of pumping speeds and surface conditioning. Points were taken in random order to eliminate any systematic error from residual probe effects. Figure 15 is a typical result. The surface recombination coefficient, γ , is related to

Reproduced with permission of the copyright owner. Further reproduction prohibited without permission.

Figure 15: Rate of heterogeneous removal of O atoms; [O] versus time; 1.0 torr, 300°K, 140 cm/sec linear flow velocity; $k_{wall} = 2.0\ sec^{-1}$; reactor poisoned with 5 percent HF and rinsed with distilled water data taken after four heating cycles.

Reproduced with permission of the copyright owner. Further reproduction prohibited without permission.

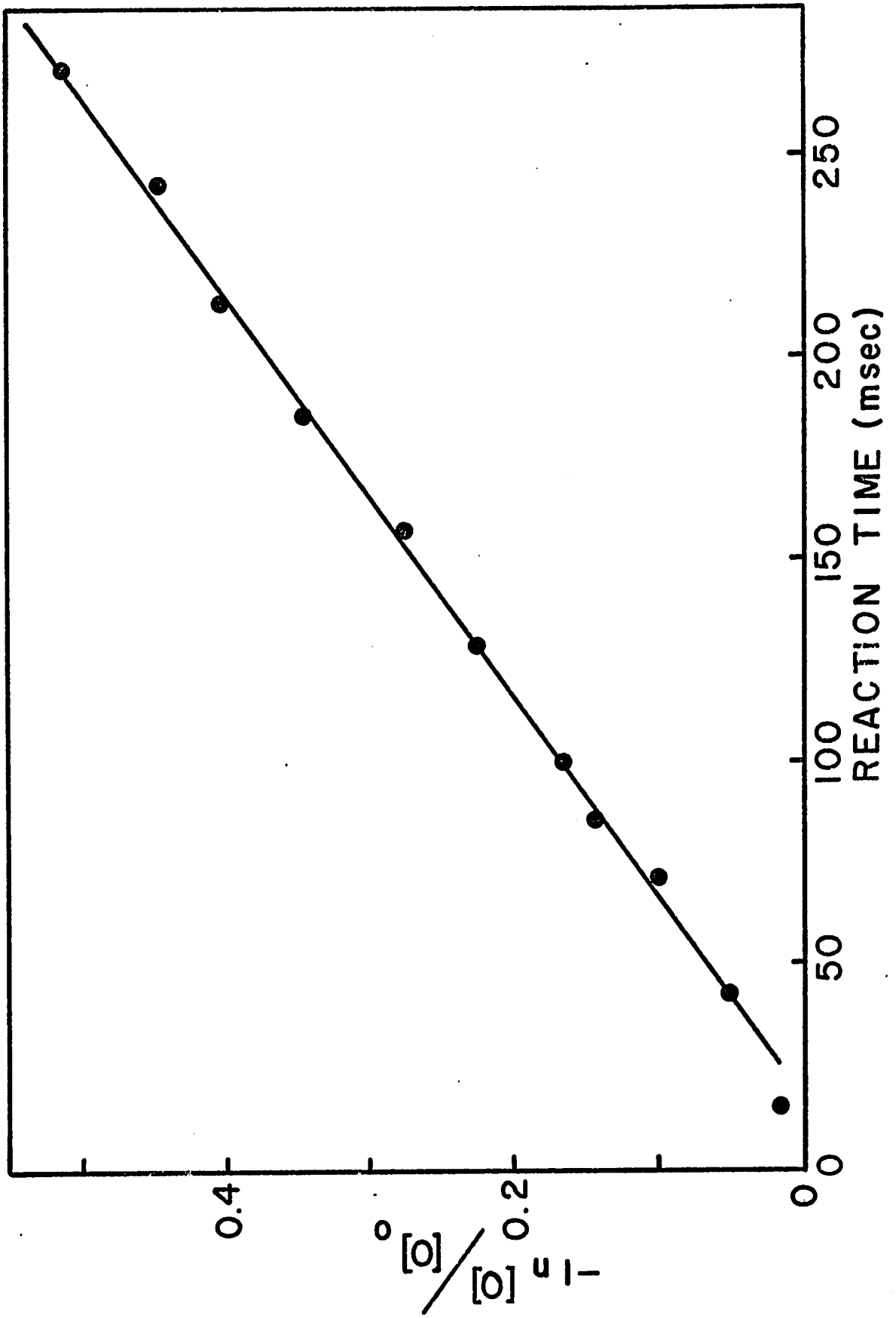

Reproduced with permission of the copyright owner. Further reproduction prohibited without permission.

k_w by:[1]

$$\gamma = \frac{2rk_w}{\bar{\nu}} \qquad (13)$$

where: r = radius of flow reactor

$\bar{\nu}$ = average speed of atoms from kinetic theory:[30]

$$\bar{\nu} = \left[\frac{8kT}{\pi m}\right]^{\frac{1}{2}}$$

Generally the recombination coefficient is lowered by treatment with strong acids and greatly increased by treatment with base. Many different poisoning agents have been used to lower γ such as:[1, 2, 31] HF, HNO_3 syrupy phosphoric acid, meta-phosphoric acid, Na_2HPO_4, $Mg_3(PO_4)_2$, H_2O and teflon; however, details as to concentrations, washings, applications, and conditioning after poisoning are generally not fully discussed in these references.

Hydrofluoric acid was used in our system as it is very effective yet simple to use. Greaves and Linnett[32] report $\gamma = 3.1 \times 10^{-5}$ for HF treated Pyrex, lower than either HNO_3 or H_3PO_4. Their data were obtained using the sidearm method for atom concentration measurements developed by Smith[33] and therefore was not expected to agree with our findings as recombination coefficients vary widely from one laboratory to another even when the same method is used. However, it provides information as to the relative efficiencies of different poisoning agents.

A number of methods were tried, a few of which are shown in Table 9. Treatment with five percent HF for 2-3 minutes was found to be sufficient

Reproduced with permission of the copyright owner. Further reproduction prohibited without permission.

Table 9: Heterogeneous O-atom Recombination Rate Constants Determined for a Number of Different Poisoning Techniques. Reactor Heated to ~ 200°C for about 4 Hours and Cooled (Continuously Pumped). All Data Obtained at 298°K; 1.0 torr Pressure and 140 cm/sec LFV, Nitrogen Carrier.

% HF	Water Rinse	Number of Heating Cycles	k_w (sec^{-1})
25	No	0	21.8
2.5	No	0	11.4
5.0	Yes	0	2.5
5.0	Yes	1	4.7
5.0	Yes	2	1.5
5.0	Yes	3	1.6
5.0	Yes	4	2.0

Reproduced with permission of the copyright owner. Further reproduction prohibited without permission.

for poisoning, requiring a brief wash with distilled water after treatment. Further conditioning was also required as evidenced by a gradual decrease in k_w measured over a period of days after the reactor had been newly poisoned. The conditioning could be accelerated by heating the reactor to about 200°C for several hours then cooling while under vacuum. Repeating this procedure 2-3 times would generally yield a $k_w < 2\ sec^{-1}$ as shown in Table 9. Linnett and Marsden,[34] again using Smith's sidearm method observed a slight decrease in γ after having flamed their reactor while pumping.

The condition of the wall was periodically checked by measurement of k_w. Typically k_w was less than $2\ sec^{-1}$ corresponding to a γ of 6×10^{-5}. The reactor was repoisoned only if k_w increased significantly above $2\ sec^{-1}$ or if the reactor had been subject to repair, cleaning or atmosphere for more than several days.

Reproduced with permission of the copyright owner. Further reproduction prohibited without permission.

III Preparation and Purification of Reagents

Matheson Ultrapure Oxygen (see Table 10), prepurified nitrogen (99.997%) and prepurified argon (99.998%) were used without further purification. The carrier gas, helium, nitrogen or argon, was passed through a Pyrex wool packed liquid nitrogen trap upstream of the discharge.

For those runs in the oxygen atom reactions in which the main objective was the identification of products and intermediates the helium carrier was purified by passage through a titanium sponge furnace at 600°C (see figure 8). The furnace was a pipet shaped quartz vessel (22 mm O.D.) 150 cm long with a perforated quartz disk at one end and was packed with about 100 g of titanium sponge (Alfa - 4 + 40). The heater consisted of a bifilar winding of nichrome wire (24 gauge) powered by a 110v variac.

Very little information could be obtained from the literature on the proper temperature for maximum purification, therefore, an experiment was conducted to determine optimum operating conditions. The furnace was heated to 1100°C and pumped on overnight then cooled to room temperature and the instrument run at 2.8 torr with only helium flowing. The mass spectrum was then taken as the temperature was increased by 200° intervals, yielding the results given in Table 11. As can be seen impurity removal is most efficient at about 600°C, which was the temperature used in all subsequent runs. Adsorbent was regenerated by pumping for 8-10 hours at 1100°C before each use.

Nitric oxide (Matheson) was purified[35] by passage through 50 percent

Reproduced with permission of the copyright owner. Further reproduction prohibited without permission.

Table 10: Gas Analysis of Matheson Ultrapure Oxygen Used in Flow Experiments.

Gas	Analysis (ppm)
CO_2	0.0
Kr	14.0
Xe	1.4
N_2	1.0
Ar	0.0
H_2O	< 2.0
CH_4	0.0

Reproduced with permission of the copyright owner. Further reproduction prohibited without permission.

Table 11: Instrument Background from Helium Carrier Measured with the Discharge on as a Function of Titanium Sponge Furnace Temperature; 2.8 torr; LFV = 50 cm/sec; All Other Peaks Were Negligible.

Furnace Temperature (±20°C)	Background Peak Height (Relative Units)			
	N_2 (m/e = 28)	NO (m/e = 30)	CO_2; N_2O (m/e = 44)	O_3 (m/e = 48)
28	.00354	.160	.0153	.0135
300	.00362	.006	.0147	.0149
400	.00284	-	.0113	.0101
600	.00238	-	.0105	.0092
800	.00248	-	.0110	.0092

Reproduced with permission of the copyright owner. Further reproduction prohibited without permission.

aqueous KOH to remove NO_2, then through anhydrous P_2O_5 and subsequent trap-to-trap distillation. Nitrogen dioxide (Matheson) was mixed with oxygen[35] to react with NO impurity then passed through P_2O_5 and distilled. Acetylene (Union Carbide) was used without purification as mass spectral analysis showed negligible impurity and cyanogen (Matheson) was purified by trap-to-trap distillation.

Dicyanoacetylene was prepared from acetylenedicarboxamide. For initial work the diamide was purchased from Eastman; however, in later experiments was prepared from the much less expensive dimethylacetylene-dicarboxylate (Aldrich) according to the procedure given by Saggiomo.[36]

An apparatus for the generation of DCA was constructed as outlined by Bloomquist and Winslow[37] but was abandoned as the yield was less than five percent. Satisfactory yields (ca. 30 percent) were obtained by modification of the procedure given by Byrd.[38] Acetylenedicarboxamide (2.5g), P_2O_5 (21g) and calcined sand (42g) were thoroughly mixed under vacuum in a 3-neck, 500 ml flask, and the temperature suddenly raised to 215°C by immersion in an oil bath. The mixture was continuously stirred and the crude product collected in a trap at - 196°C. Continuous pumping through the trap was necessary to insure fast exit of DCA from the heated flask before decomposition. Reaction was complete in about 30 minutes, indicated by a drop in pressure to less than 250μ.

One major objection still remains to our procedure. When the batch size is increased the percent yield drops due to decomposition of product before leaving the P_2O_5-sand mixture. As a result many small batches must be run, a very time consuming process as the apparatus must be cleaned between runs.

The product was purified (chief impurities: C_2N_2 and HCN) by

Reproduced with permission of the copyright owner. Further reproduction prohibited without permission.

distillation, saving the lower boiling fraction until the vapor pressure agreed with that reported by Saggiomo;[36] generally 3-4 distillations were required. Analysis by mass spectroscopy showed no impurities.

Reproduced with permission of the copyright owner. Further reproduction prohibited without permission.

IV Methods of Rate Constant Determination

All values for rate constants were obtained under pseudo-first order conditions with at least a fifteen-fold excess of one reactant. Determinations were made with each reactant in excess and although differing in method, both types measured the rate of removal of one species. For the reaction stoichiometry:

$$aA + xX \longrightarrow \text{Products}$$

the measured rate is $\frac{dA}{dt}$ or $\frac{dX}{dt}$ which are related by:

$$\frac{1}{a}\frac{dA}{dt} = \frac{1}{x}\frac{dX}{dt} \qquad (14)$$

Therefore measurement of both rates yields the ratio of the stoichiometric coefficients:

$$\frac{\frac{dA}{dt}}{\frac{dX}{dt}} = \frac{a}{x} \qquad (15)$$

This ratio is usually referred to as the stoichiometric factor.

When the stable reactant is in excess two reactions must be considered:

$$A \xrightarrow{k_w} \tfrac{1}{2}A_2$$

Reproduced with permission of the copyright owner. Further reproduction prohibited without permission.

$$A + X \xrightarrow{k_x} \text{Products}$$

where A = atom

X = stable reactant

With the reactant concentration, [X], and linear flow velocity, LFV, held constant the integrated rate expression becomes:

$$\ln \frac{[A]}{[A]_d} = -(k_w + k_x[X]) \frac{d}{LFV} \qquad (16)$$

where d = distance between reactant probe and pinhole

$[A]_d$ = atom concentration at reactant probe

[A] = atom concentration at pinhole

The atom concentration at the pinhole can then be measured at different probe positions, a plot of ln [A] versus d yielding $(k_w + k_x[X])$ from the slope.

If $k_x \sim 2 \times 10^{-15}$ cm^3/molecule sec and $[X] \sim 4 \times 10^{15}$ molecules/cm^3, values typical of our system, it is readily seen that k_w and $k_x[X]$ are of the same magnitude. Therefore in order to extract k_x from the data k_w must be measured in a separate experiment, or the quantity $k_w + k_x[X]$ determined for two [X]. These procedures are both subject to fluctuations in k_w over the span of the experiment, a quantity which we have observed to change by as much as 30 percent in consecutive determinations.

This method is also objectionable for reactions with DCA as it would require at least 0.4 g of DCA for every rate constant determination. This roughly corresponds to the batch yield discussed in the preceeding section.

These problems may be avoided by the use of what we shall refer to

Reproduced with permission of the copyright owner. Further reproduction prohibited without permission.

as the fixed probe method. With the reactant inlet probe fixed at a distance, d, from the pinhole and a constant linear flow velocity, LFV, the integrated rate expression is:

$$\ln \frac{[A]}{[A]_d} = -\frac{(k_x)(d)[X]}{LFV} - \frac{(k_w)(d)}{LFV} \qquad (17)$$

where $[A]_d$ = $[A]$ at the point of mixing, i.e., in the vicinity of the probe tip. This quantity is never measured, but as shown below its value is not required for the determination of k_x.

If $[A]_o$ is equal to $[A]$ at the mass spectrometer pinhole when $[X] = 0$,

$$\ln \frac{[A]_o}{[A]_d} = -\frac{(k_w)(d)}{LFV} \qquad (18)$$

and thus

$$\ln \frac{[A]}{[A]_o} = -\frac{(k_x)(d)[X]}{LFV} \qquad (19)$$

The slope of a plot of $\ln [A]/[A]_o$ versus $[X]$ is proportional to k_x, the second order rate constant, provided that the slope is evaluated in the pseudo-first order region of the graph. To eliminate instrumental effects such as back diffusion of atoms into the probe or stagnation at the pinhole, from which uncertainties in the effective magnitude of d arise, the slopes were determined at two different probe positions and the equations solved simultaneously for the rate constant. Typical results are shown in figures 18 and 19.

This procedure eliminates the objections previously raised as

Reproduced with permission of the copyright owner. Further reproduction prohibited without permission.

determinations may be made in roughly half the time, without altering any instrument setting other than the probe position. Thus k_w is subject to less change and far less DCA is required. Care must be taken, however, in the choice of LFV and atom concentration to yield a measurable extent of atom consumption, yet assure that the LFV is unaffected by the flow of stable reactant required to obtain pseudo-first order conditions.

With atoms in excess atom consumption will be dependent only on the heterogeneous recombination and therefore:

$$[A] = [A]_o \exp(-k_w d/LFV) \tag{20}$$

where $[A]_o = [A]$ at the reactant input, d cm from the pinhole. This expression can then be combined with the second order rate law for removal of stable species, X, and integrated:

$$\frac{d\ln[X]}{d(d)} = -\frac{k_x[A]_o}{LFV} \exp(-k_w d/LFV)$$

$$\ln\frac{[X]}{[X]_o} = \frac{k_x[A]_o}{k_w}\left[\exp(-k_w d/LFV)-1\right] \tag{21}$$

The exponential term may be evaluated in a Taylor series:[39]

$$e^x = 1 + \frac{x}{1!} + \frac{x^2}{2!} + \frac{x^3}{3!} + \cdots$$

and approximating the atom concentration by neglecting quadratic and

Reproduced with permission of the copyright owner. Further reproduction prohibited without permission.

higher terms (where $k_w d/LFV$ is small):

$$\ln \frac{[X]}{[X]_o} = -\frac{(k_x)[A]_o(d)}{LFV} \qquad (22)$$

A plot of $\ln [X]_o/[X]$ versus d will then yield a straight line, the slope of which will be proportional to k_x. If the exponential approximation is invalid the plot will be curved, which is not visually apparent from our data (see figures 16 and 17).

Bogan[40] has shown that if the exponential is used explicitly for the atom concentration the value for k_x obtained is equal, within experimental error, to that obtained in the approximate treatment. Bogan's method used a non-linear least squares analysis for evaluation of both k_x and k_w, the latter also in satisfactory agreement with the results of separate experiments.

The atom concentration was subject to change between successive data points; therefore, if $[A]_o^i$ is the atom concentration at the probe tip for the ith data point and $[A]_o$ is some arbitrary standard atom concentration (usually the mean $[A]_o^i$):

$$\ln \frac{[X]_o^i}{[X]^i} = \frac{(k_x)(d_i)[A]_o^i}{LFV} - \frac{k_x[A]_o^i}{k_w} \qquad (23)$$

$$\frac{[A]_o}{[A]_o^i} \ln \frac{[X]_o^i}{[X]^i} = \frac{(k_x)(d_i)[A]_o}{LFV} - \frac{k_x[A]_o}{k_w} \qquad (24)$$

Atom concentration was monitored mass spectrometrically for each point and the correction applied. k_x is determined from the slope, m, of equation 24 by:

Reproduced with permission of the copyright owner. Further reproduction prohibited without permission.

$$kx = \frac{(m)(LFV)}{[A]_o} \qquad (25)$$

The instrument was standardized for atom concentration by titration at the midpoint of the flow reactor both before and after each run, the experiment being discarded if atom sensitivity varied more than 10 percent. All values reported are by linear regression analysis of data, using the 95 percent confidence interval for reported errors.

Reproduced with permission of the copyright owner. Further reproduction prohibited without permission.

V The Reaction of Acetylene With Oxygen Atoms

Before beginning quantitative measurements of the DCA reaction a brief study of the reaction between acetylene and oxygen atoms was performed in order to check the accuracy of our procedures and the many calibrations. This reaction was chosen for this purpose as it is clean, relatively fast and therefore easy to measure, and has been studied in a number of laboratories by several different techniques.[12-15, 41] The literature values reported in Table 12 yield the average second order rate constant to be 1.5×10^{-13} ($\pm$ 0.4 standard deviation) cm^3/molecule sec. This is in agreement with our value, $1.0 \pm 0.3 \times 10^{-13}$ cm^3/molecule sec,* determined with atoms in excess by the movable probe technique at 1.0 torr, 302°K and in helium carrier.

Under the same conditions but with acetylene in excess and using the fixed probe technique a value of $2.0 \pm .3 \times 10^{-13}$ cm^3/molecule sec was obtained yielding a stoichiometric factor of 2.0 ± 0.4. This also is in agreement with the best literature value, 1.9 ± 0.1, calculated without the value reported by Hoyermann et al.[41] which is suspect due to its large relative magnitude.

The values which we report are merely the result of several determinations and not the best values obtainable from our system. They are meant only as a check for gross errors; the excellent agreement in such a brief survey does serve to establish the reliability of our measurements.

---

* This and all subsequent errors are the standard errors derived from first order regression analysis of data unless otherwise noted.

Reproduced with permission of the copyright owner. Further reproduction prohibited without permission.

Table 12: Literature Values for the Reaction of O-atoms with Acetylene at Room Temperature. All Determinations Used a Fast-Flow Reactor. The Stoichiometric Coefficient Is Defined as the Number of O-atoms Consumed Per Acetylene Molecule Consumed.

Rate Constant (10^{-13} cm^3/molecule sec)	Stoichiometric Coefficient	Method of Detection	Reference
1.5±0.3	>1	Mass Spectrometric	13
0.9±0.3	2.0±0.2	Mass Spectrometric	12
1.6	~4	ESR	41
1.5±0.1	1.8±0.2	ESR	14
1.5±0.1	1.9±0.1	ESR	15
2.2±0.2	--	Photometric	16
1.5±0.4	1.9±0.1	---	Best Value
1.0±0.3	2.0±0.4	Mass Spectrometric	This Work

Reproduced with permission of the copyright owner. Further reproduction prohibited without permission.

VI The Reaction of Dicyanoacetylene With Oxygen Atoms

Introduction

In the course of some preliminary experiments at about one torr on the reaction of active nitrogen with dicyanoacetylene it was observed that reaction occured at the same rate when N atoms were converted to O atoms by titration with nitric oxide. Initially this was taken as evidence that reaction was between DCA and some long lived excited molecular species present in active nitrogen (see Appendix C), since the coincidence that reaction with both oxygen and nitrogen atoms proceeded at the same rate was unlikely. At this point Meyer and Setser[42] reported investigation of the reaction with O atoms, finding the system to be chemiluminescent emitting both the ($A \rightarrow X$) and $B \rightarrow X$) bands of CN.

This created some very serious problems as if reaction occurred with O atoms, then our observations indicated that the rate was an order of magnitude slower than that reported in reference 42. We then proceeded with a detailed study of the O-atom reaction, first using atoms generated in a helium-oxygen discharge to rule out reaction with excited molecular nitrogen.

The second order rate constant was measured over the pressure range 0.75 - 5.0 torr, identifying additional intermediates and finding the overall stoichiometry to be critically dependent on the presence of molecular oxygen. The coincidence did indeed occur, as will be shown in section VII, that at pressures somewhat above one torr reaction with nitrogen or oxygen atoms occurs at the same rate; however, a rate constant invariant over the pressure range surveyed and much lower than

Reproduced with permission of the copyright owner. Further reproduction prohibited without permission.

that reported by Meyer and Setser[42] was obtained for the oxygen atom system.

Reproduced with permission of the copyright owner. Further reproduction prohibited without permission.

Results

When O atoms were in excess the concentration of DCA was measured as a function of probe position; the data were corrected for any change in atom concentration, which was monitored throughout. The instrument sensitivity for O atoms was calibrated before and after each run by O-atom titration at the midpoint of the reactor and care was taken to assure at least a 15 fold excess of O atoms over DCA. Typical results from these runs are shown in figures 16 and 17, where the rate constant is obtained from the slope, m, of the plot by:

$$k_1 = \frac{(m)\ (LFV)}{[O]} \qquad (26)$$

These figures represent the best and the worst of our results, for most runs the scatter was intermediate between these extremes.

The results are collected in Table 13. The rate constant was first determined producing oxygen atoms by the microwave discharge of 10 percent oxygen in helium carrier and with O atoms in excess the rate constant was $1.1 \pm 0.3 \times 10^{-15}$ cm^3/molecule sec, invariant over the pressure range 0.75 - 5.0 torr.

With DCA in excess the rate constant was determined by the fixed probe method as shown in Figures 18 and 19. The second-order rate constant is obtained from the slopes, m_1 and m_2, taken at the two probe positions, d_1 and d_2, to eliminate errors in the determination of the absolute reaction time by:

$$k = \frac{(m_1 - m_2)(LFV)}{(d_1 - d_2)} \qquad (27)$$

Reproduced with permission of the copyright owner. Further reproduction prohibited without permission.

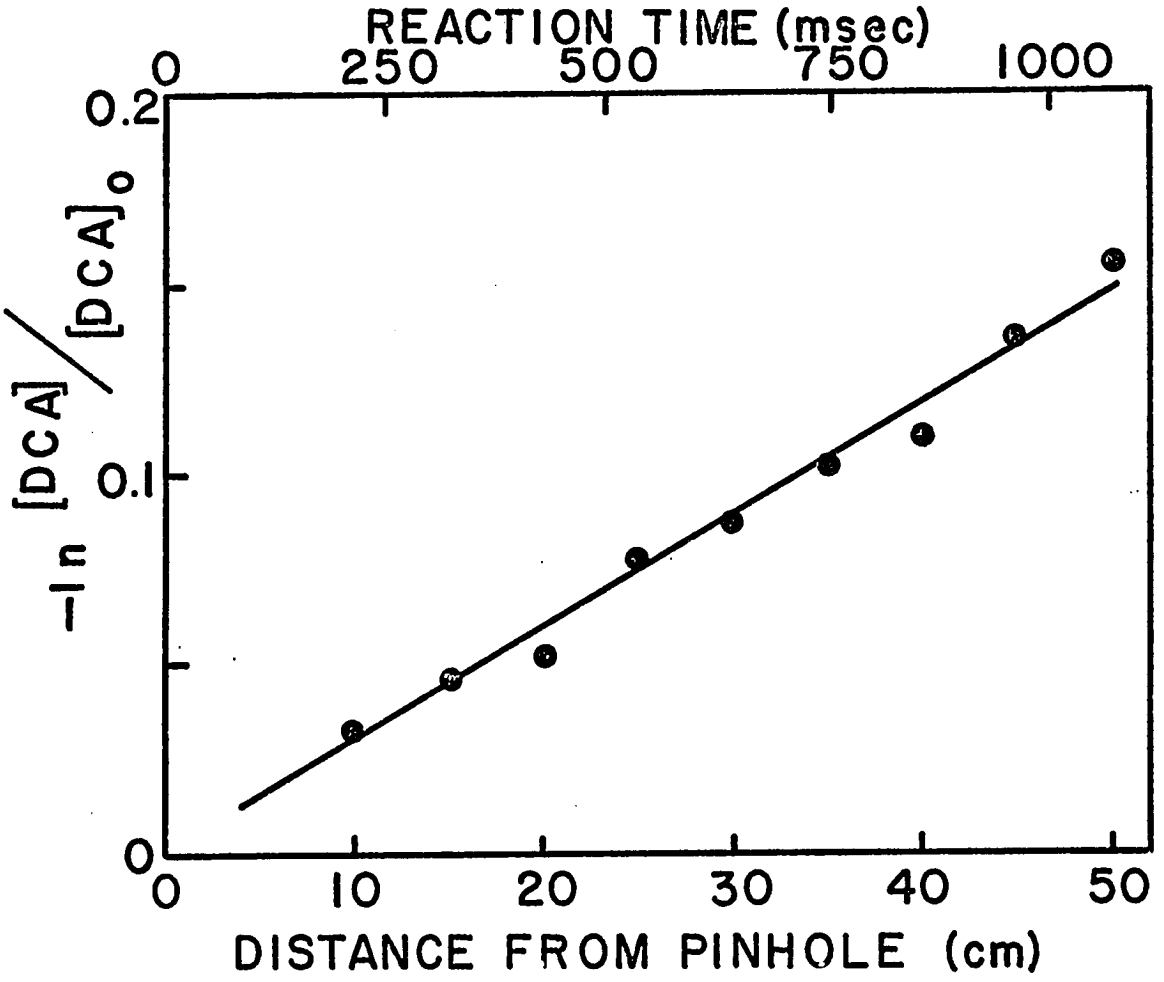

Figure 16: Rate of removal of DCA by O-atoms; [DCA] versus time; 46.7 cm/sec linear flow velocity, 4.95 torr, O_2/He discharge, [O] = 4.76 mtorr.

Reproduced with permission of the copyright owner. Further reproduction prohibited without permission.

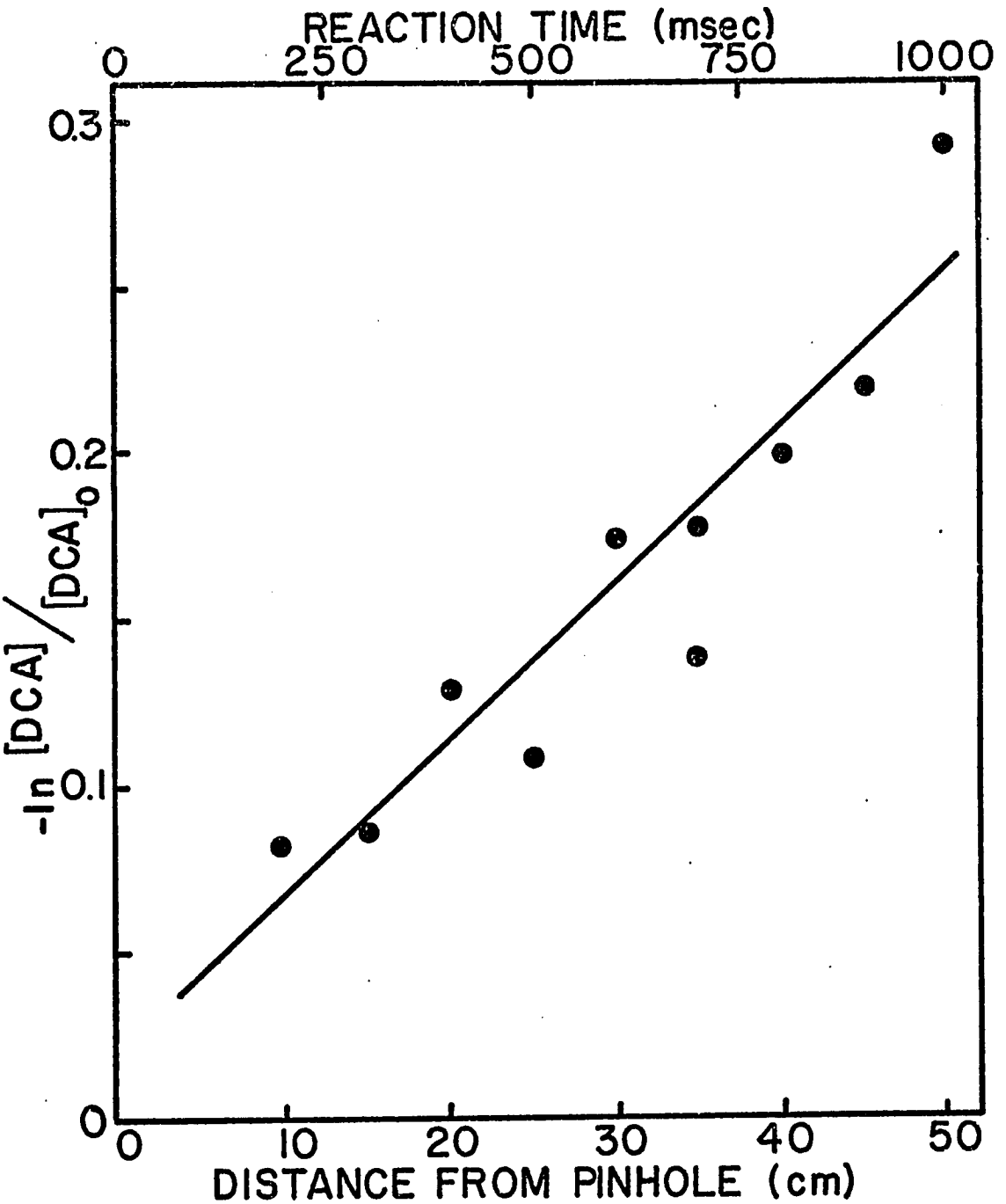

Figure 17: Rate of removal of DCA by O atoms; [DCA] versus time, 50.1 cm/sec linear flow velocity, 2.97 torr, O_2/He discharge, [O] = 5.21 mtorr.

Reproduced with permission of the copyright owner. Further reproduction prohibited without permission.

Table 13: O + DCA Second Order Rate Constants Obtained Under Various Conditions at 298-301°K; Errors Reported Are the Standard Errors Derived from First Order Regression Analysis of Data.

Pressure (torr)	Species in Excess	Pressure of Species in Excess (mtorr)	Discharged Gas	$k_1 \times 10^{15}$ (cm^3/molecule sec)
0.76	O	3.03	O_2/He	1.1±0.2
0.74	O	3.12	O_2/He	1.3±0.3
0.75	DCA	≤42.8	O_2/He	1.7±0.3
1.00	O	4.25	O_2/He	1.4±0.1
1.10	O	4.37	O_2/He	1.5±0.2
1.00	O	3.73	O_2/He	1.1±0.2
0.97	DCA	≤73.1	O_2/He	1.2±0.2
3.10	O	5.82	O_2/He	0.9±0.1
2.97	O	6.79	O_2/He	0.8±0.1
2.93	DCA	≤137.3	O_2/He	0.9±0.1
5.00	O	6.01	O_2/He	0.7±0.1
4.95	O	6.20	O_2/He	0.7±0.1
5.05	DCA	≤100.8	O_2/He	1.7±0.2
1.05	O	2.92	N_2	2.0±0.4
1.02	DCA	≤43.0	N_2	3.0±0.5
1.03	DCA	≤28.6	N_2	6.0±0.3

Reproduced with permission of the copyright owner. Further reproduction prohibited without permission.

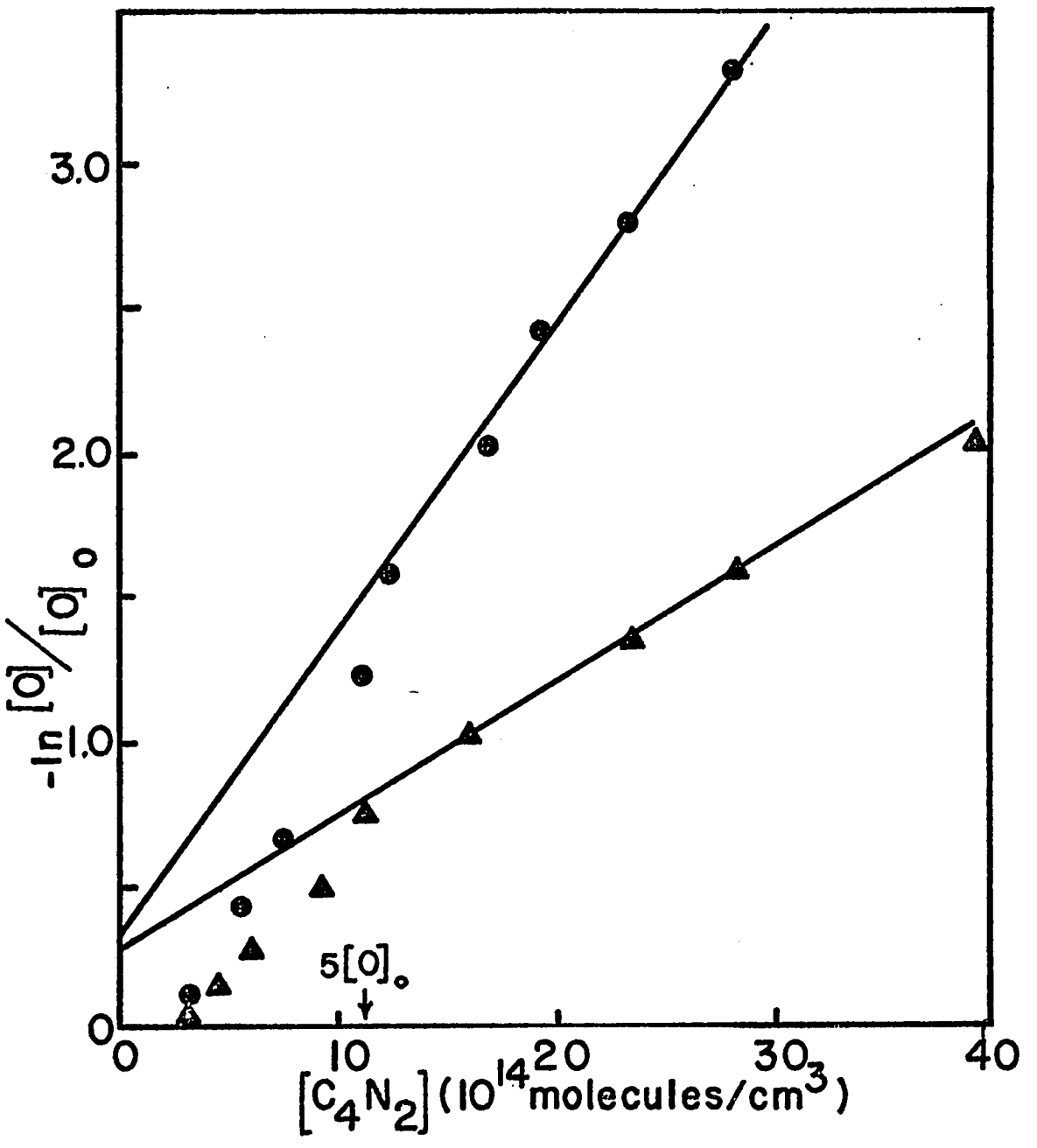

Figure 18: Fixed probe method: the rate of removal of O atoms, measured at two different probe positions, as a function of [DCA]; 5.05 torr, 298°K, 62.8 cm/sec linear flow velocity, O_2/He discharge, ● = 40 cm, ▲ = 15 cm.

Reproduced with permission of the copyright owner. Further reproduction prohibited without permission.

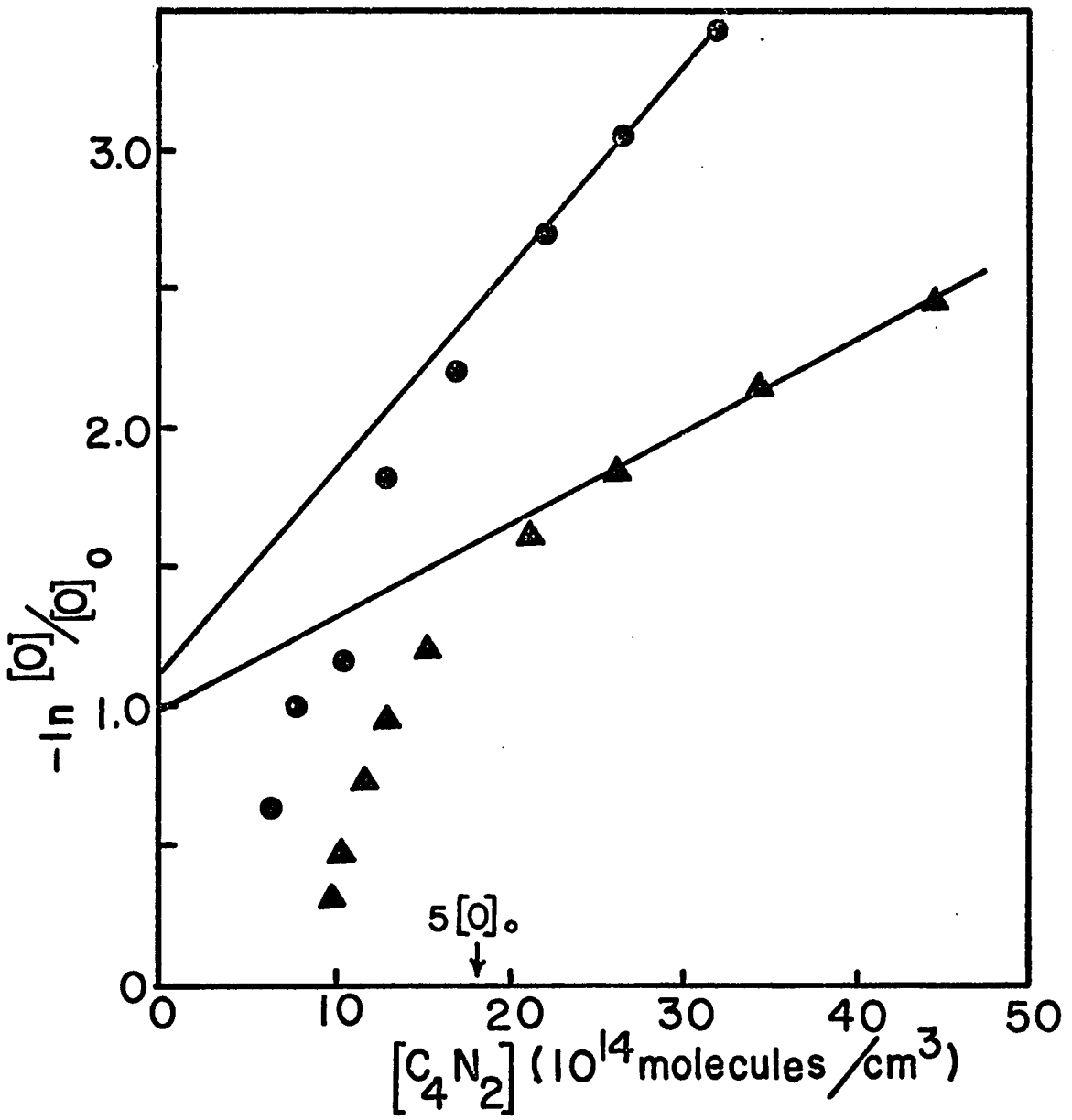

Figure 19: Fixed probe method: the rate of removal of O atoms, measured at two different probe positions, as a function of [DCA]; 2.93 torr, 299°K, 51.1 cm/sec linear flow velocity, O_2/He discharge, ● = 35 cm, ▲ = 15 cm.

Reproduced with permission of the copyright owner. Further reproduction prohibited without permission.

Here the average rate constant was $1.4 \pm 0.4 \times 10^{-15}$ cm^3/molecule sec, also invariant with respect to pressure. The stoichiometric factor, that is, the moles of O atoms consumed per mole of DCA consumed, is thereby determined as 1.2 ± 0.4. However when using "molecular oxygen free" atoms, produced by the nitric oxide titration of active nitrogen, and DCA in excess a rate constant of $3.0 - 6.0 \times 10^{-15}$ cm^3/molecule sec was obtained, giving a stoichiometric factor of 2.7 - 5.5.

In order to obtain the high flows of reactant necessary for the fixed probe method solid DCA was sublimed from an ice bath into the flow metering system with the five liter ballast volume closed (see figure 6). This maintained a constant pressure of about 35 torr, the vapor pressure at 0°C,[36] in the system yet minimized the chance of spontaneous detonation. At room temperature DCA slowly decomposes to a brown black substance visible on the walls of the storage vessel. Using the technique described above the reagent, which is normally stored over liquid nitrogen, is not allowed to stand at room temperature for any length of time and thus is less subject to decomposition. A similar method has been used to meter the flow of ozone to the flow system in other experiments, also giving satisfactory results.[43]

Reproduced with permission of the copyright owner. Further reproduction prohibited without permission.

Identification of Products and Intermediates

Dibeler et al.[44] have reported appearance potentials of fragment ions from DCA and C_2N_2, and the least of these was 17.3 v. All of our experiments were, therefore, run at an ionizing voltage of less than 16.5 v, to eliminate the possibility of incorrectly identifying as an intermediate what was actually a fragment ion from reactant or end product. Furthermore, the complete absence of ions at higher masses even when the search was made at 40 ev supports our assignment of mass peaks to parent rather than fragment ions. Peaks corresponding to CO_2, C_2N_2, NO, CO, NO_2, OC_2N and OC_2N_2 were observed in the O_2 discharge experiments. The appearance potential, A. P., of the m/e = 28 peak was determined from the data shown in figure 20. The instrument was standardized with argon (m/e = 40) and taking the spectroscopic ionization potential of argon as 15.756 v[45] the A.P. of m/e = 28 was found to be 14.2 $\pm$ 0.2 v by the extrapolated potential difference method[46] discussed by Field and Franklin.[47] This indicates the unknown product to be primarily CO (A.P. = 14.01)[47] rather than N_2 (A.P. = 15.56).[47] The major products were CO_2, CO and NO, while C_2N_2 and NO_2 were formed to a lesser extent, and OC_2N_2 and OC_2N were observable only at maximum sensitivity.

When the reaction was run in the "molecular oxygen free" system, the intermediates CN, OC_3N, and C_2N were observed in addition to OC_2N and OC_2N_2, and in comparable amounts. No conclusions can be drawn concerning CO and NO, since their contributions to the peaks at m/e = 28 and 30 would be overwhelmed by N_2 carrier and NO titrant. Cyanogen was present in a greater proportion to CO_2 than in the runs with O_2 present and NO_2, which was observed as a minor product in the O_2 discharge runs,

Reproduced with permission of the copyright owner. Further reproduction prohibited without permission.

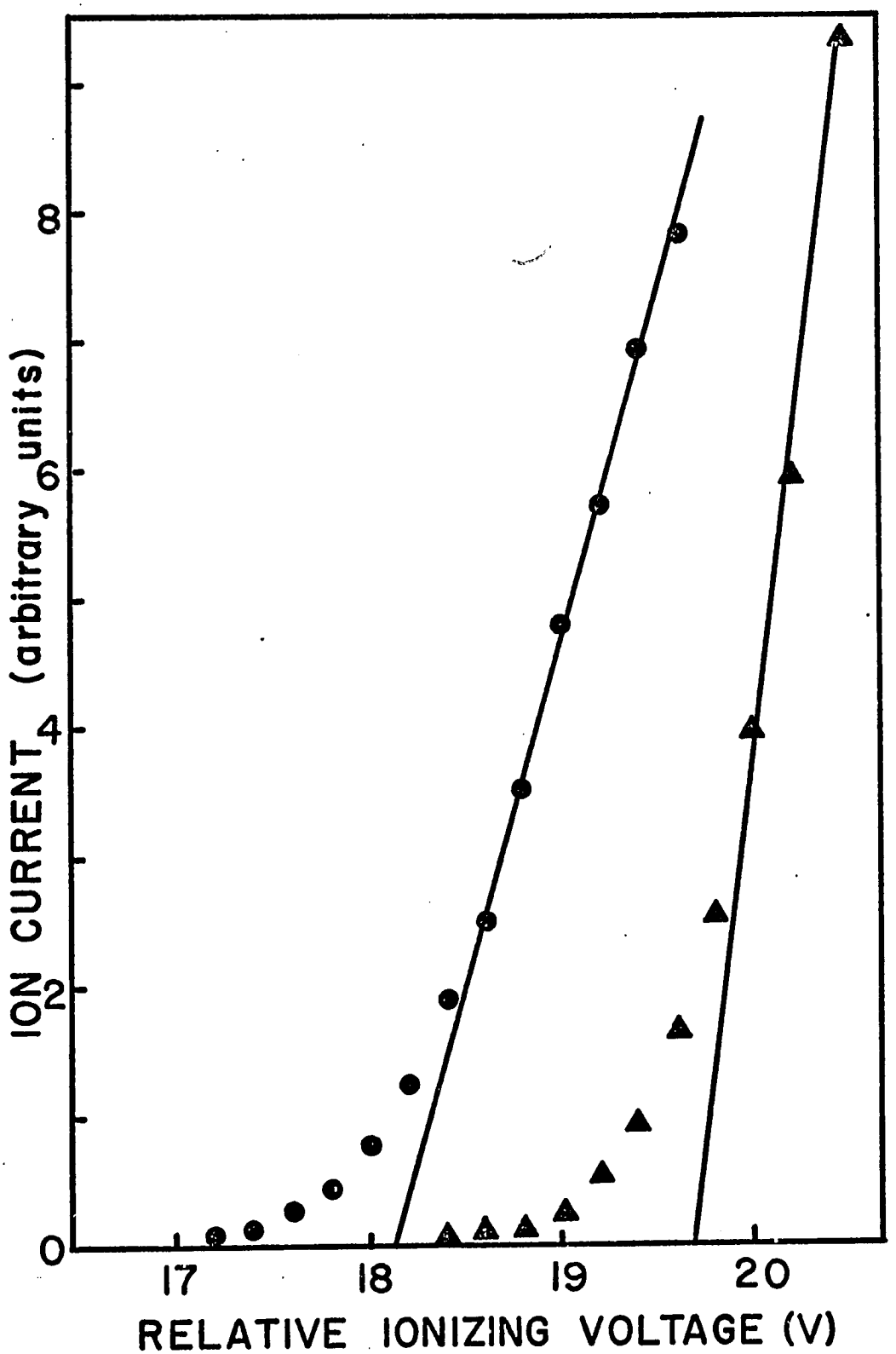

Figure 20: Appearance potential measurement of m/e = 28 peak ● ; referenced against argon, m/e = 40, ▲.

Reproduced with permission of the copyright owner. Further reproduction prohibited without permission.

was not observed. The reaction was accompanied by an intense violet chemiluminescence which was not observed in the molecular oxygen discharge system.

Reproduced with permission of the copyright owner. Further reproduction prohibited without permission.

Discussion

In the present work we have determined the room temperature rate constant for the reaction of DCA with oxygen atoms to be $1.1 \pm 0.3 \times 10^{-15}$ cm^3/molecule sec, in rather sharp contrast to the value of $3.6 \pm 0.7 \times 10^{-14}$ cm^3/molecule sec obtained by Meyer and Setser.[42] There are two possible factors contributing to this discrepancy; first, Meyer and Setser measured the reaction rate by monitoring O-atom concentration in the absence of molecular oxygen. Although their result is reported as a rate constant, it is actually the product of the rate constant and the stoichiometric factor; the true bimolecular rate constant is obtained by dividing their value by the number of O atoms consumed per DCA molecule. Our results indicate that this stoichiometric factor is critically dependent on the concentration of molecular oxygen. Apparently O_2 efficiently quenches the further consumption of atoms by secondary radicals (vide infra). This is demonstrated in the present work by a stoichiometric factor of 1.2 in the O_2 runs and a stoichiometric factor of 2.7 - 5.5 when O_2 is not present. It should be pointed out in this regard that is is virtually impossible to produce O atoms truly free of molecular oxygen. First, one must slightly overtitrate with nitric oxide to insure that N atoms are consumed, and hence oxygen can be formed via:

$$O + NO \longrightarrow NO_2 + h\nu \qquad a$$

$$O + NO + M \longrightarrow NO_2 + M \qquad b$$

$$O + NO_2 \longrightarrow NO + O_2 \qquad c$$

These reactions proceed with rate constants $k_a \cong 1 \times 10^{-17}$, $k_b \cong 5 \times 10^{-32}$ ($M = N_2$), and $k_c > 1 \times 10^{-13}$, all in molecular units.[1] At 3 torr $[N_2] \cong 10^{17}$ molecules/cm^3 giving a second-order rate constant

Reproduced with permission of the copyright owner. Further reproduction prohibited without permission.

$k_b' \cong 5 \times 10^{-15}$ cm^3/molecule sec. If the titration is deliberately stopped well short of the end point, the result will be a mixture of O and N atoms. Even in this case, the reaction system (a - c) is important near the nitric oxide input where mixing occurs and particularly important inside the injector tip due to back diffusion of nitrogen atoms into the stream of pure nitric oxide. We have tried several different injectors, the most successful being a 0.5 mm capillary tip approximately 5 mm long. Even here, however, the air afterglow extended about 2 cm past the capillary upstream into the NO supply line. Second, wall recombination of O-atoms occurs from the point of titration on, becoming more important at slower linear flow velocities. On the basis of these considerations it is not at all unlikely that the $[O_2]$ can be up to 10 percent of the [O] in the "O_2-free system". Since the stoichiometric factor for O + DCA is clearly a function of the O_2 concentration, our value of 2.7 - 5.5 should be regarded as a lower limit.

The second reason for the discrepancy in k_1 can be seen by referring to figure 17 in which the plot becomes linear only when [DCA]/[O]>6. The sharp downward break, beginning anywhere from 6 to 10 fold excess, was evident in all of our fixed probe runs. The most likely explanation of this behavior is the failure of the assumption of pseudo-first order kinetics. The value of k_1 reported by Meyer and Setser was obtained at a 3-6 fold excess; working up our data in this concentration region, assuming a first-order rate law, gives rate constants about twice that which we report in Table 13.

Reproduced with permission of the copyright owner. Further reproduction prohibited without permission.

Mechanism

The reaction O + DCA should have many points of similarity to the reaction of oxygen atoms with acetylene, for which the initial attack is believed to be:[11, 15]

$$C_2H_2 + O \longrightarrow CH_2 + CO \qquad \Delta H = -58 \text{ kcal/mole}^* \qquad A$$

$$\longrightarrow HC_2O + H \qquad B$$

$$\longrightarrow C_2O + H_2 \qquad \Delta H = -39 \text{ kcal/mole} \qquad C$$

The analogous possibilities in the O + DCA reaction are:

$$C_4N_2 + O \longrightarrow C(CN)_2 + CO \qquad \Delta H = -58 \text{ kcal/mole} \qquad 1a$$

$$\longrightarrow OC_2CN + CN \qquad 1b$$

$$\longrightarrow C_2O + C_2N_2 \qquad \Delta H = -34 \text{ kcal/mole} \qquad 1c$$

Although several reactions could account for the small quantities of OC_2N observed in all runs

$$C(CN)_2 + O_2 \longrightarrow OC_2N + NCO \qquad D$$

$$C(CN)_2 + O \longrightarrow OC_2N + CN \qquad E$$

$$C_4N_2 + O \longrightarrow OC_2N + C_2N \qquad 1d$$

we regard reaction 1d as the most important for three reasons. First, since the concentration of OC_2N is about the same with and without

---

* This and all subsequent heats of reaction have been calculated on the basis of the values given in Appendix F.

Reproduced with permission of the copyright owner. Further reproduction prohibited without permission.

molecular oxygen, reaction D is unimportant. Second, C_2N is observed in the "O_2 free" runs. Third, the stoichiometric factor was 1.2 (in the presence of O_2), while significant contribution by reaction E would require a larger stoichiometric factor.

The intermediates CN, C_2N and OC_3N were not observed with molecular O_2 present, and thus could be quenched by:

$$O_2 + CN \longrightarrow NCO + O \qquad \Delta H = -27 \text{ kcal/mole} \qquad 2$$

$$O_2 + C_2N \longrightarrow C_2O + NO \qquad \Delta H = -82 \text{ kcal/mole} \qquad 3$$

$$O_2 + OC_3N \longrightarrow CO_2 + OC_2N, \text{ etc.} \qquad 4$$

Reaction 2 is fast[6] ($k_2 = 7 \times 10^{-12}$ cm^3/molecule sec at 687°K) with very low activation energy, and in our system, where $[O_2] \cong 10^{13}$ molecules/cm^3, can easily account for removal of CN. Reaction 3 accounts for the absence of C_2N in the O_2 discharge runs, and reaction 4 could account for part of the CO_2 production as well as OC_2N.

The C_2O radical was not observed, nevertheless it has been invoked as an intermediate in the acetylene-oxygen atom system[11] and could undergo reactions 5, 6 or 7:

$$C_2O + O_2 \longrightarrow CO + CO_2 \qquad \Delta H = -198 \text{ kcal/mole} \qquad 5$$

$$C_2O + O_2 \longrightarrow 2CO + O \qquad \Delta H = -69 \text{ kcal/mole} \qquad 6$$

$$C_2O + O \longrightarrow 2CO \qquad \Delta H = -189 \text{ kcal/mole} \qquad 7$$

Reactions 5 and 6 have been shown to be important steps in the removal of C_2O in the photolysis of C_2O_3 - O_2 mixtures[48] and in the system presently under consideration could be the major steps by which CO and

Reproduced with permission of the copyright owner. Further reproduction prohibited without permission.

CO_2 are formed since CO_2 production is reduced relative to C_2N_2 in the O_2-free runs. However, if reaction 5 is sufficiently fast it would still produce appreciable amounts of CO_2, since the concentration of molecular oxygen is about 10^{13} molecule/cm^3 even in the "O_2-free" runs. It is unlikely that CO_2 could be produced to any extent by:

$$CO + O \longrightarrow CO_2 + h\nu \qquad \Delta H = -129 \text{ kcal/mole} \qquad 8$$

$$CO + O + M \longrightarrow CO_2 + M \qquad 9$$

Reaction 8 is slow[49] ($k_8 = 2 \times 10^{-20}$ cm^3/molecule sec) at room temperature, as is reaction 9. Baulch reports[49] $k_9 = 3 \times 10^{-34}$ cm^6/molecule^{2}sec and at 1 torr, where $[M] = 3 \times 10^{-16}$molecules/cm^3, $k_9' = 1 \times 10^{-17}$ cm^3/molecule sec, assuming nitrogen has an average third body efficiency.

In addition to reaction 2 several reactions can account for CN removal:

$$CN + C_2N_2 \longrightarrow N_2 + C_3N \qquad \Delta H = -78 \text{ kcal/mole} \qquad 10$$

$$CN + NO \longrightarrow CO + N_2 \qquad \Delta H = -151 \text{ kcal/mole} \qquad 11$$

$$CN + O \longrightarrow N + CO \qquad \Delta H = -75 \text{ kcal/mole} \qquad 12$$

$$CN + CN + M \longrightarrow C_2N_2 + M \qquad \Delta H = -132 \text{ kcal/mole} \qquad 13$$

Paul and Dalby have obtained a value of $k_{10} = 4 \times 10^{-15}$ cm^3/molecule sec[50] from flash photolysis experiments near room temperature, and hence reaction 10 should be of minor importance with respect to reactions 2 and 12 ($k_2 = 7 \times 10^{-12}$ cm^3/molecule sec, $k_{12} = 2 \times 10^{-12}$ cm^3/molecule sec[6]). Also, the concentrations of O and O_2 are much greater than those

Reproduced with permission of the copyright owner. Further reproduction prohibited without permission.

of the products C_2N_2 and NO, and since our measurement of the m/e = 28 appearance potential indicates that very little N_2 is formed, reaction 11 is probably negligible as well.

Several reactions can account for cyanogen production in addition to reactions 1c and 13, namely:

$$C_4N_2 + CN \longrightarrow C_2N_2 + C_3N \qquad \Delta H = -57 \text{ kcal/mole} \qquad 14$$

$$C_4N_2 + C_2N \longrightarrow C_2N_2 + C_4N \qquad \Delta H = +1 \text{ kcal/mole} \qquad 15$$

$$CN + OC_3N \longrightarrow C_2N_2 + C_2O \qquad 16$$

$$CN + OC_2N \longrightarrow C_2N_2 + CO \qquad 17$$

$$C_2N + OC_2N \longrightarrow C_2N_2 + C_2O \qquad 18$$

Setser and Thrush[5] predicted the formation of a "long lived activated adduct" in the reaction of cyanogen with oxygen atoms; we have indeed observed a peak at m/e = 68, corresponding to the species OC_2N_2. Formation could occur by three reactions in this system:

$$CN + NCO \longrightarrow OC_2N_2 \qquad 19$$

$$O + C_2N_2 \longrightarrow OC_2N_2 \qquad 20$$

$$O + C_4N_2 \longrightarrow OC_2N_2 + C_2 \qquad 21$$

Infrared absorption bands due to two distinct species have been observed in the flash photolysis of $O_3 + C_2N_2$ mixtures,[51] and attributed to the insertion and addition products of C_2N_2 with $O(^1D)$ and $O(^3P)$, respectively. In the present work $O(^3P)$ is the reacting species, thus reaction 20 would yield only the addition product; however, reaction 19 could form either of the two. It is unlikely that reaction 21 leads to

Reproduced with permission of the copyright owner. Further reproduction prohibited without permission.

appreciable formation of OC_2N_2, as the other evidence indicates that the initial attack is on the central carbons of DCA.

Several reactions can be written for NO_2 formation from NO, O, and O_2. Since their rate constants and thermochemistry are well known,[52] and as they are not associated directly with DCA + O, we do not discuss them here.

In the absence of molecular oxygen additional radical-O-atom reactions can occur resulting in the formation of stable products:

$$OC_3N + O \longrightarrow C_2O + NCO \qquad 22$$

$$NCO + O \longrightarrow CO + NO \qquad \Delta H = -78 \text{ kcal/mole} \qquad 23$$

$$OC_2N + O \longrightarrow C_2O + NO \qquad 24$$

$$C_2N + O \longrightarrow CN + CO \qquad \Delta H = -166 \text{ kcal/mole} \qquad 25$$

Reproduced with permission of the copyright owner. Further reproduction prohibited without permission.

Conclusion

The rate constant for reaction between oxygen atoms and dicyanoacetylene is $1.1 \pm 0.3 \times 10^{-15}$ cm^3/molecule sec, invariant over the pressure range 0.75 - 5.0 torr. Initial attack is believed to be at the acetylene bond, evidenced by our failure to observe NCO and our observation of the intermediates C_2N, OC_2N, OC_3N and CN. Stable end products are CO, NO, CO_2 and C_2N_2 and the presence of the intermediate C_2O is inferred. First mass spectrometric evidence of the species OC_2N_2 has been obtained.

In the presence of molecular oxygen the stoichiometric factor is 1.2, which can be accounted for if the major pathway is reactions 1b, 1c and 1d followed by reactions 2, 3, 4, 5 and 13. The stoichiometry is critically dependent on the concentration of molecular oxygen, the ratio of O atoms consumed to DCA molecules consumed increasing as the $[O_2]$ is reduced. Although this ratio did not exceed 5.5 in any of our experiments, appreciable amounts of O_2 were present at all times; the ratio could be considerably higher than 5.5 in a system truly free of molecular oxygen. The higher stoichiometric factor is explained by reactions 7, 12, 22, 23, 24 and 25 becoming more important in the O_2-free system.

The strong CN emission observed in the molecular oxygen free experiments is effectively quenched by the presence of O_2. This can be accomplished via CN removal by reaction 2 or destruction of intermediates by reactions 3, 4, 5 and 6 before CN formation.

Reproduced with permission of the copyright owner. Further reproduction prohibited without permission.

VII The Reaction of Dicyanoacetylene With Active Nitrogen

Introduction

Atom reactions with acetylene and its derivatives have been the subject of numerous investigations over the past twenty years. The reactions of active nitrogen with acetylene, methylacetylene and dimethylacetylene were first studied by Winkler and co-workers,[18, 19] who showed that the major products were HCN and C_2N_2. Although they did not report the pressure at which the experiments were conducted, an earlier reference[53] indicated that the pressure was about 0.5 torr. An extensive study of the reaction of active nitrogen with acetylene was reported in 1969 by Arrington, Bernardini and Kistiakowsky,[21] who observed a complex system with two parallel reactions; one was relatively slow and dependent upon pressure, the other was a much faster reaction proposed to be chain branching and initiated by energetic nitrogen molecules rather than nitrogen atoms.

As discussed in Section VI and reference 54, the acetylenic carbon atoms are the primary site of attack by ground state oxygen atoms, and therefore, the reaction of active nitrogen with dicyanoacetylene was investigated to determine if this was also the case with nitrogen atoms.

Reproduced with permission of the copyright owner. Further reproduction prohibited without permission.

General Features of the Reaction

There are four parameters, namely (1) total pressure (i.e., concentration of molecular nitrogen, (2) N-atom concentration, (3) initial reactant ratio, defined by $R = [DCA]_o/[N]_o$, and (4) temperature, which are, within limits, subject to independent manipulation. The visual appearance, rate, and mechanism of the reaction depend markedly on the values of these parameters, and indeed it is appropriate to consider separately three modes, or regions of reaction. At low pressure and moderate reactant ratio, a relatively slow reaction, accompanied by a uniform chemiluminescence, takes place. This we call the "slow region."

As the pressure is increased there is an abrupt increase in the intensity of the chemiluminescence, which becomes concentrated near the inlet probe; in short, a flame is generated. In addition to the changes in distribution, color and intensity of the chemiluminescence, the "flame region" is marked by a much higher rate of reaction, and by the consumption of perhaps 80 percent of the DCA.

The linear flow velocity may be increased so that the flame fills the entire reactor, or it may be decreased so that the flame is only 5-10 cm long and the slower, "post flame," region may be studied. In all three regions the reaction is chemiluminescent, and accompanied by the deposition of brown-black material on the walls of the flow reactor; deposition in the flame region is much more rapid than in the other two.

Although the onset of the flame region has been described in terms of total pressure, both the temperature and the reactant ratio, R, exert a strong influence as well. The flame must be suppressed in order to study the slow region, and the value of R required for flame suppression varies systematically with total pressure.

Reproduced with permission of the copyright owner. Further reproduction prohibited without permission.

For most of our trials the nitrogen atom concentration was about 2×10^{14} atoms/cm^3, hence the values which follow are relative to this atom concentration. For nitrogen concentrations less than about 8×10^{16} molecules/cm^3 a reactant ratio of 0.2 or less was sufficient to maintain the slow reaction at room temperature. At slightly greater nitrogen concentrations the reaction becomes increasingly sensitive to R; for example, at $[N_2] = 12 \times 10^{16}$ molecules/cm^3 R must be less than 0.08 and at $[N_2] = 20 \times 10^{16}$ molecules/cm^3 R must be less than 0.02 to maintain the slow reaction zone. This trend continues until at $[N_2] = 25 \times 10^{16}$ molecules/cm^3 a reactant ratio of only 0.005 was sufficient to produce the flame.

Reproduced with permission of the copyright owner. Further reproduction prohibited without permission.

The Slow Reaction Zone

In contrast to the flame, the reaction in the slow region is much more amenable to quantitative rate measurements; the rate constant was determined over the pressure range 0.5 - 8.0 torr, and the results are collected in Table 14* and figure 21. All values for k_{obs} were taken under pseudo-first order conditions with N-atoms in excess, the atom concentration monitored throughout and the data corrected for any change therein. For a given pressure the minimum DCA flow for flame generation was determined and the flow lowered to insure that the flame would not appear owing to small changes in atom concentration during the run.

The data of two typical runs are plotted in pseudo-first order form in figures 22 and 23; the value of k_{obs} was obtained from these and similar plots by assuming first order dependence with respect to N-atoms and dividing the slope by the N-atom concentration. That the order with respect to nitrogen atoms is in fact unity is demonstrated by the lack of systematic variation in k_{obs} among measurements made at different N-atom concentrations.

Repeated searches of the mass spectra revealed only two stable products of the reaction: cyanogen (C_2N_2) was by far the major product, with small quantities of dicyanodiacetylene (C_6N_2) being formed at pressures less than about four torr. Peaks at m/e = 26 and 38 corresponding to CN and C_2N were observed at maximum instrument sensitivity. Any other products or intermediates in the reaction had to be present at concentrations considerably less than 10^{12} particles/cm^3.

---

* The errors reported and all subsequent errors are standard errors derived from first order regression analysis of data.

Reproduced with permission of the copyright owner. Further reproduction prohibited without permission.

Table 14: Observed Pseudo First Order Rate Constants Obtained Under Various Conditions in the Slow Reaction Zone at 298-301°K. Those Results Marked by an Asterisk Were Taken in the Post-flame Zone

$[N_2]\times10^{-16}$ (molecules/cm^3)	$[N]\times10^{-14}$ (atoms/cm^3)	$[C_4N_2]/[N]$	$k_{obs}\times10^{15}$ (cm^3/molecule sec)
1.78	2.21	0.02	0.46±0.09
3.11	2.24	0.10	0.79±0.06
4.04	1.92	0.06	0.7±0.2
4.89	1.69	0.07	1.0±0.2
5.68	1.34	0.09	0.65±0.09
6.42	2.10	0.07	1.5±0.1
7.30	2.51	0.07	2.61±0.07
8.21	1.89	0.07	2.1±0.2
9.57	2.80	0.06	2.5±0.3
10.5	1.74	0.08	3.3±0.5
10.9	1.91	0.08	5.6±0.5
12.0*	1.67	0.09	7.7±1.1
12.8	2.19	0.08	9.5±0.5
13.0	2.95	0.02	10.5±0.3
14.4	2.24	0.009	11.3±1.4
15.0	2.58	0.02	15.3±0.9
15.8*	1.21	0.10	38±5
15.9	1.81	0.02	38±3
16.7	1.84	0.02	17±1

Reproduced with permission of the copyright owner. Further reproduction prohibited without permission.

$[N_2]\times10^{-16}$ (molecules/cm^3)	$[N]\times10^{-14}$ (atoms/cm^3)	$[C_4N_2]/[N]$	$k_{obs}\times10^{15}$ (cm^3/molecule sec)
17.0	1.87	0.01	24±3
17.8	1.72	0.02	82±5
18.7	2.12	0.01	58±3
20.6*	1.74	0.02	51±10
22.0	1.79	0.02	84±9
23.3	2.89	0.01	59±9
24.0	2.42	0.01	46±7

Reproduced with permission of the copyright owner. Further reproduction prohibited without permission.

Figure 21: The effect of nitrogen molecule concentration on the observed second order rate constant at 298 - 301°K. ● = slow reaction zone; ▲ = post flame zone.

Reproduced with permission of the copyright owner. Further reproduction prohibited without permission.

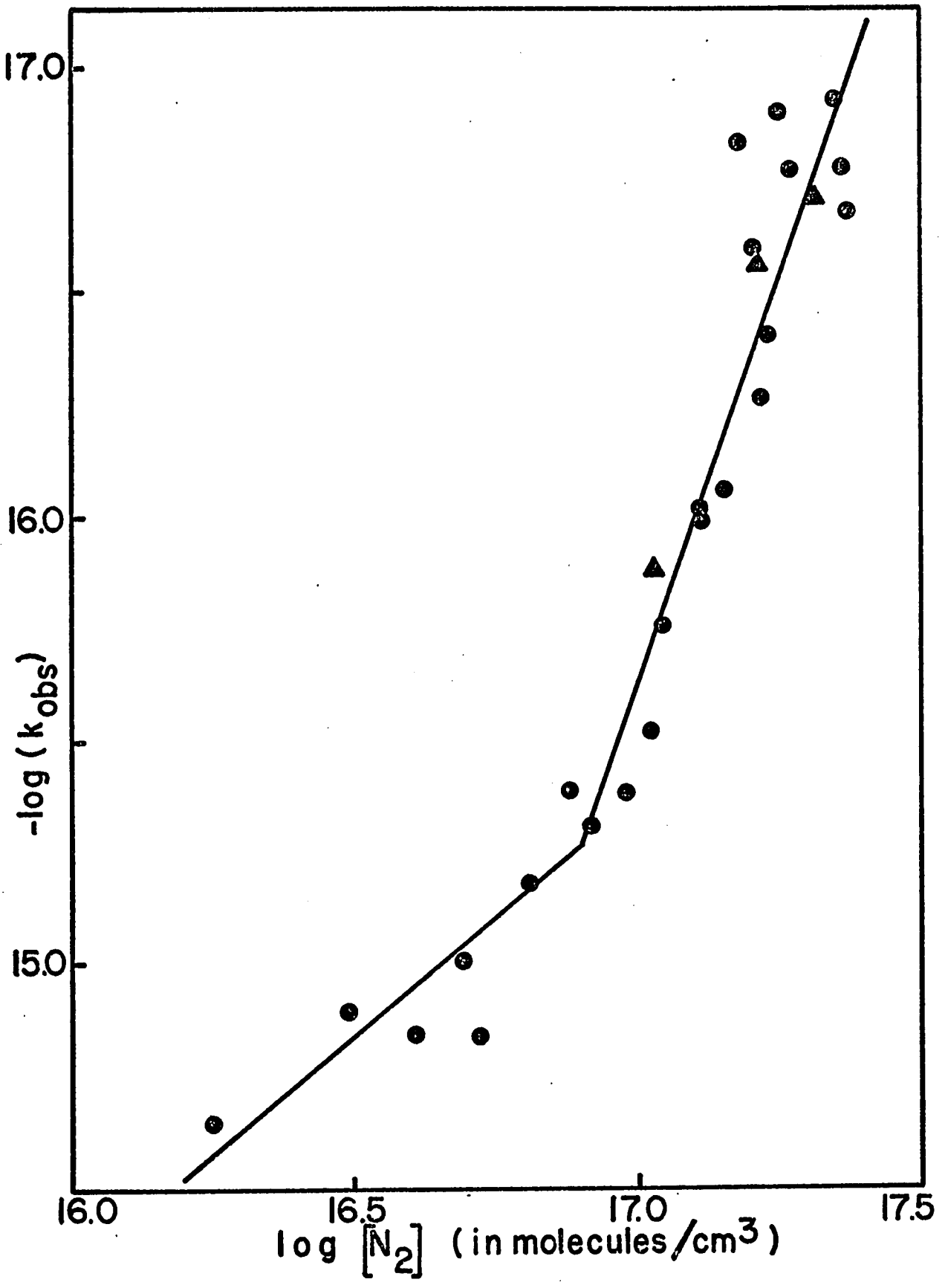

Reproduced with permission of the copyright owner. Further reproduction prohibited without permission.

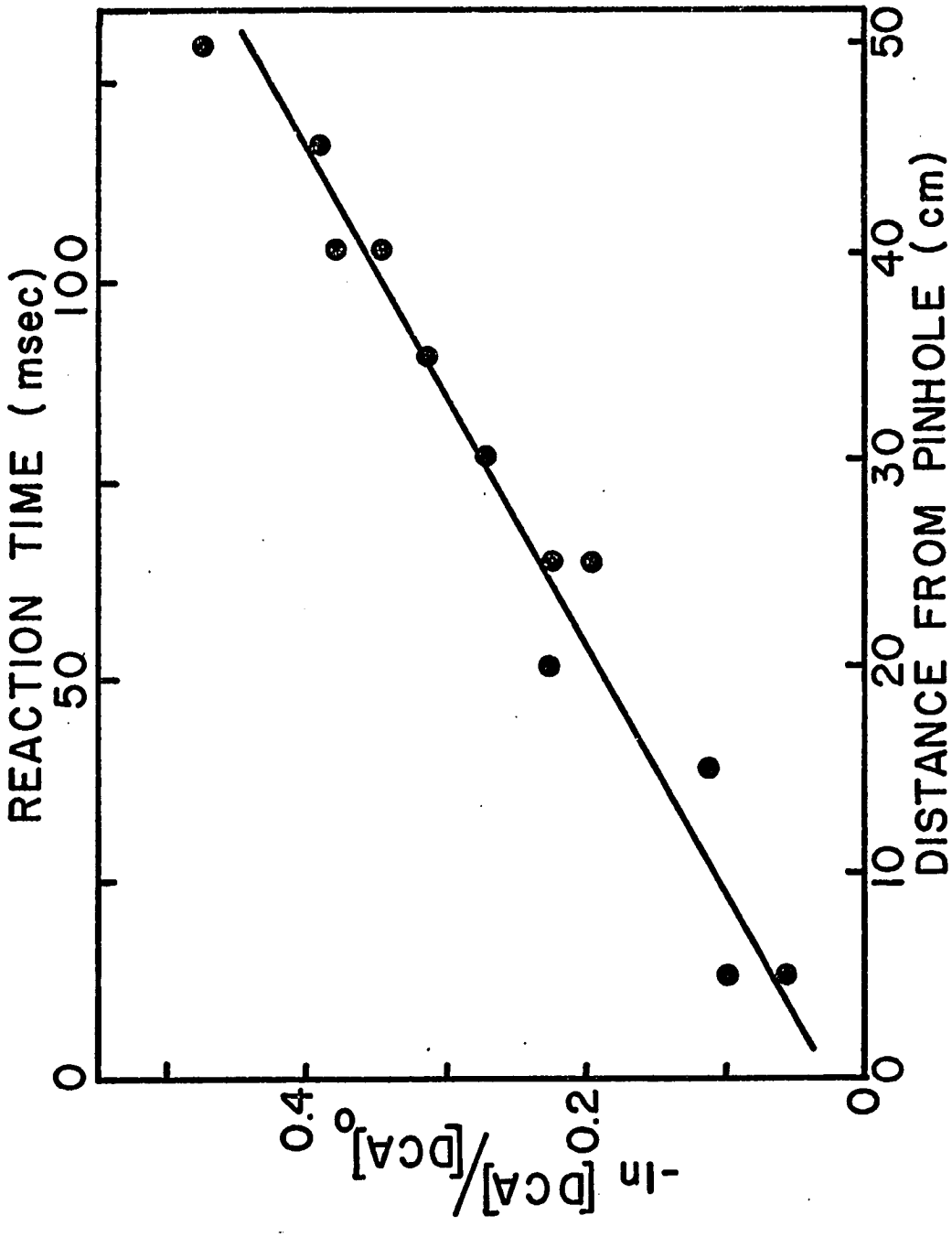

Figure 22: Rate of removal of DCA by N-atoms versus time; linear flow velocity = 386 cm/sec; total pressure = 5.20 torr; 300°K; [N] = 1.8×10^{14} atom/cm^3.

Reproduced with permission of the copyright owner. Further reproduction prohibited without permission.

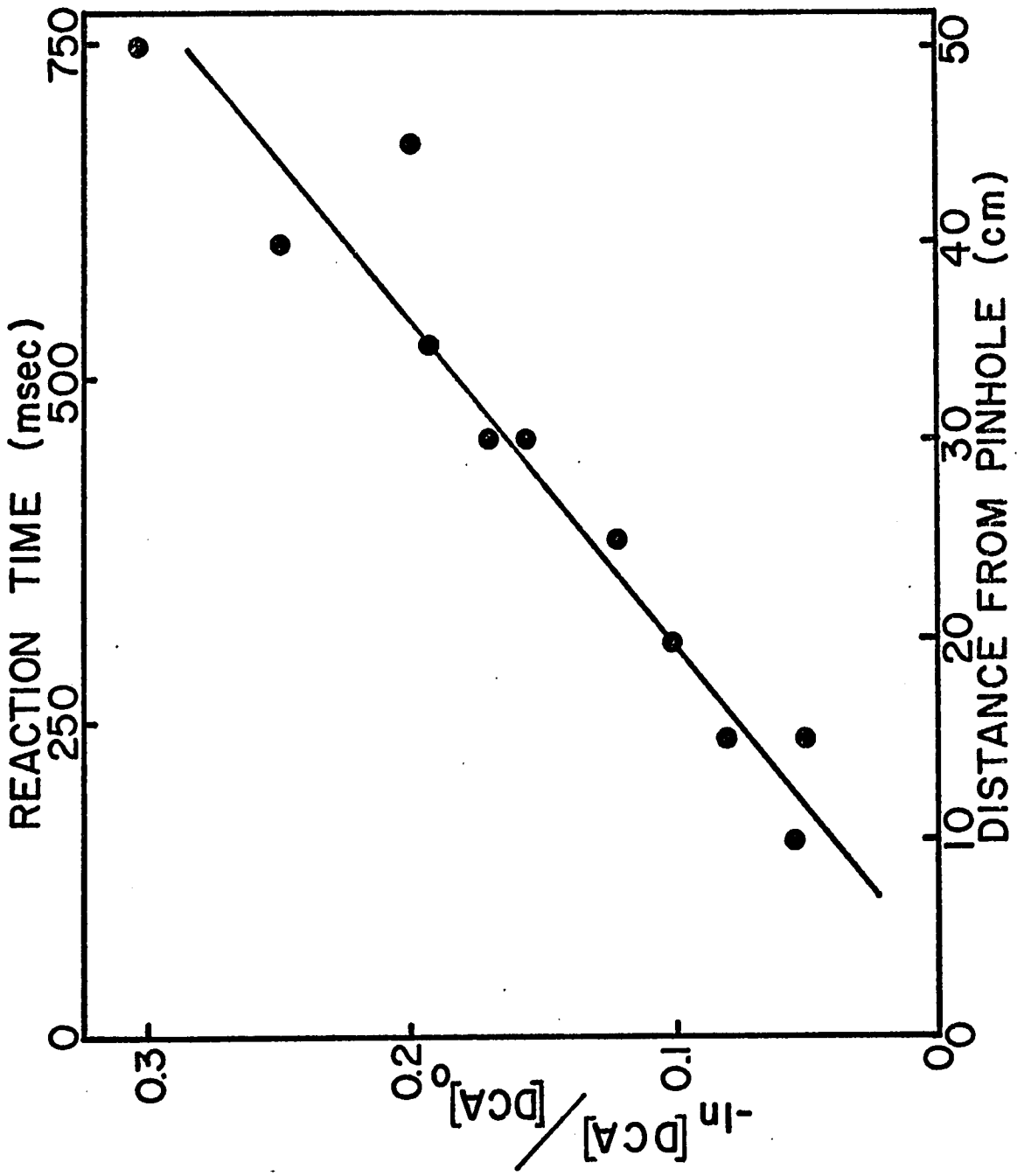

Figure 23: Rate of removal of DCA by N atoms versus time; linear flow velocity = 67.1 cm/sec; total pressure = 2.54 torr; 299°K; [N] = 1.89×10^{14} atom/cm^3

Reproduced with permission of the copyright owner. Further reproduction prohibited without permission.

The data in Table 14 are shown graphically in figure 21, where the logarithmic presentation is a matter of convenience rather than fundamental significance. The two straight lines in figure 21 are least-square fits to the two groups of rate constants, high and low pressure, and serve primarily to illustrate the most striking feature of this reaction, namely, the abrupt change in mechanism at a pressure of about 10^{17} molecules/cc. As indicated by the slopes of the lines, the pressure dependence is approximately first order at low pressures, changing to somewhat greater than third order at high pressures.

In Table 15 are collected the results of elevated temperature runs at two different total pressures, chosen so that one would be on each side of the break in figure 21. The high-pressure rate constants exhibit a significant increase as the temperature is raised, and least-squares analysis yields a value of 700 ± 450 cal/mole for the activation energy. The low-pressure data on the other hand, exhibit no significant temperature dependence; least-squares treatment gives an activation energy of -45 ± 110 cal/mole. Trials at temperatures above those reported could not be made due to onset of the flame zone.

Reproduced with permission of the copyright owner. Further reproduction prohibited without permission.

Table 15: Observed Pseudo First Order Rate Constants for Two Selected Nitrogen Concentrations at Various Temperatures. Trials Marked with an Asterisk Indicate That Values Were Obtained by Interpolation of Data from Table 14.

$[N_2]\times10^{-16}$ (molecules/cm^3)	Temperature (^oK)	$[N]\times10^{-14}$ (atoms/cm^3)	$[C_4N_2]/[N]$	$k_{obs}\times10^{15}$ (cm^3/molecule sec)
4.90	300*	****	****	1.05
4.91	380	1.65	0.04	1.2±0.2
4.90	421	1.50	0.03	1.0±0.2
4.90	471	1.69	0.03	1.0±0.5
4.91	479	0.98	0.03	1.0±0.6
14.43	300*	****	****	13.0
14.42	335	2.58	0.009	19±3
14.40	336	2.27	0.01	20±3
14.43	378	2.07	0.01	15±3
14.41	419	2.25	0.01	16±3
14.43	446	1.93	0.009	29±9

Reproduced with permission of the copyright owner. Further reproduction prohibited without permission.

Nitrogen Atom Consumption in the Flame Zone

In figure 24 several representative plots of nitrogen atom concentration versus DCA concentration are shown. These data are all obtained at 3.0 torr under which conditions the flame appears when $R \geq 0.1$; hence the catastrophic decrease in [N] shown in figure 24 is associated with the flame zone of the reaction. Although these data all refer to a fixed time (22.5 msec) after mixing, the shape of the plot does not depend strongly on reaction time. Close examination of the initial drop in N-atom concentration reveals a slight but significant downward curvature, i.e., the rate of N-atom consumption increased in a non-linear way as more DCA is added. Since a simple rate increase in a second order reaction as one reactant increases would not show this accelerated behavior, it must be concluded that what is in fact being observed is the transition from the slow region to the much faster flame region.

The shapes of the curves shown in figure 24 show a striking resemblance to those obtained by Arrington et al.[21] for the reaction of active nitrogen with acetylene; however, apart from the numerical values of the atom and reactant concentrations, there are two signicant differences, as follows.

In Table 16 are listed the various initial concentrations, that is, concentrations derived from measuring the flow rate into the reactor, of DCA which correspond to the minima in N-atom concentration. Also listed are the ratios initial [DCA]/initial [N] corresponding to the minima. This ratio has a constant value in the acetylene system,[21] that is, the minimum [N] was always reached when the acetylene flow rate was about 7 percent of the total reactant flow. Arrington et al.[21]

Reproduced with permission of the copyright owner. Further reproduction prohibited without permission.

Figure 24: Nitrogen atom concentration 22.5 msec after addition of DCA versus initial DCA concentration for three initial atom concentrations; linear flow velocity = 888 cm/sec; total pressure = 3.00 torr; 299°K.

Reproduced with permission of the copyright owner. Further reproduction prohibited without permission.

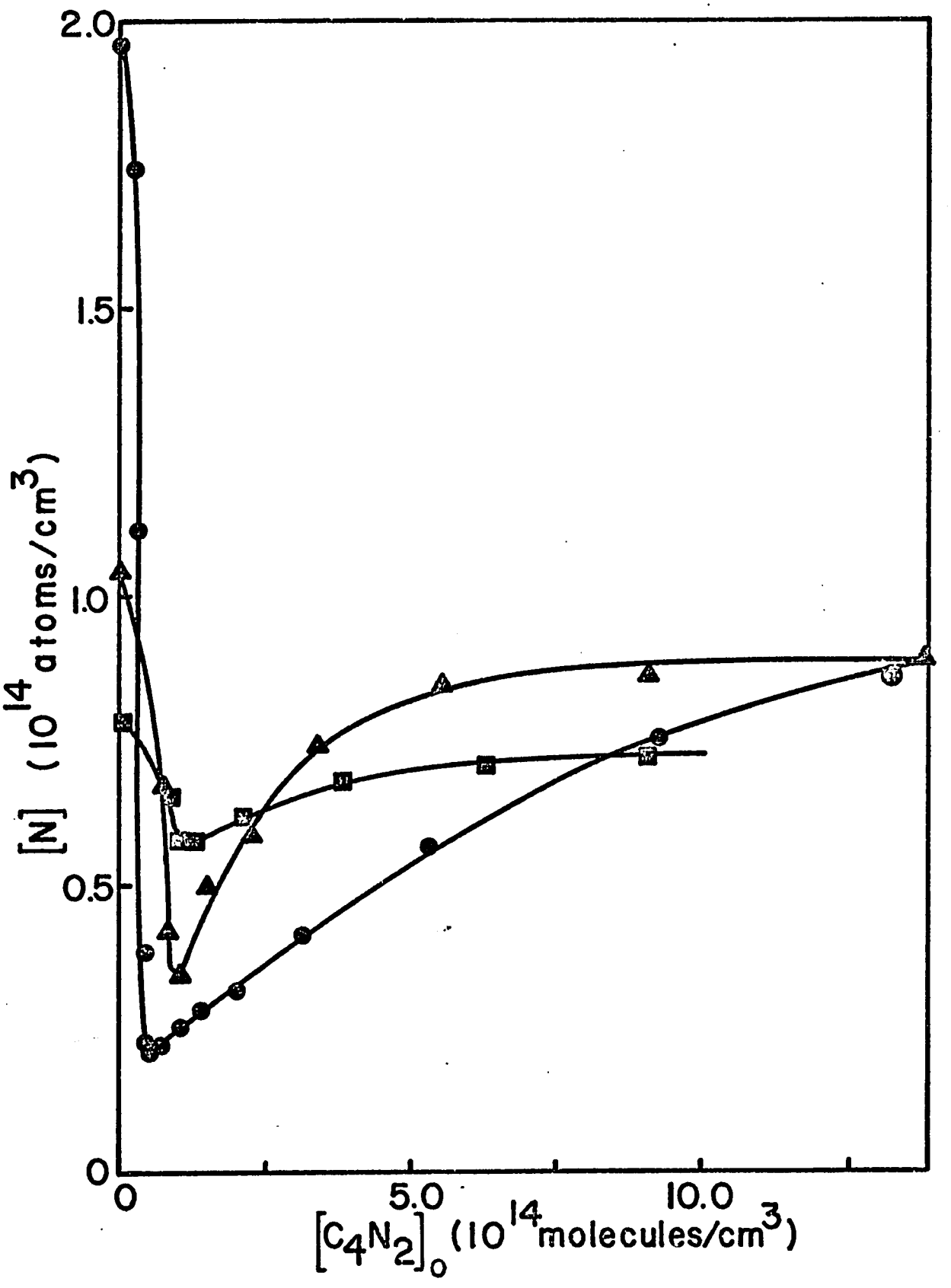

Reproduced with permission of the copyright owner. Further reproduction prohibited without permission.

Table 16: Initial Reactant Ratios, $[C_4N_2]_o/[N]_o$, Corresponding to the Minima of Figure 24.

Pressure (torr)	Reaction Time(msec)	Initial $[N]\times10^{-14}$ (atoms/cm^3)	Initial $[C_4N_2]\times10^{-14}$ (molecules/cm^3)	$[C_4N_2]_o$
2.0	30.0	0.69	1.05	1.52
2.5	19.0	1.15	1.33	1.15
2.5	19.0	1.71	1.21	0.71
3.0	22.5	0.78	1.15	1.48
3.0	22.5	1.05	0.97	0.92
3.0	22.5	1.49	0.75	0.50
3.0	22.5	1.92	0.58	0.30

Reproduced with permission of the copyright owner. Further reproduction prohibited without permission.

interpreted this behavior as being due to "a very fast recombination of nitrogen atoms occuring only at low $(C_2H_2/N)_o$ ratios." Later on in the paper they propose a mechanism for this fast reaction, a chain recombination with metastable nitrogen molecules ($A^3\Sigma_u^+$) playing the major role as chain carrier. In the DCA reaction, on the other hand, the DCA flow corresponding to the minimum in [N] depends inversely on the initial atom concentration. Secondly, whereas in the acetylene system the minimum [N] is about 5×10^{14} atoms/cm^3 regardless of the initial atom concentration, with DCA there is again an inverse dependence: minimum [N] are 2, 3.5 and 6×10^{13} atoms/cc for initial concentrations of 1.95, 1.05 and 0.8×10^{14} atoms/cc, respectively. This behavior is also strongly indicative of a chain mechanism which consumes N-atoms in the flame region, and which will be discussed (vide infra).

Results of mass balance experiments in the flame zone were not reproducible, and values for the stoichiometric factor, that is, the number of N atoms consumed/DCA molecule consumed, ranged from 2 to 12. Such non-reproducibility is also characteristic of chain reactions. The major problem in obtaining these data is that the measurements must necessarily be made in the region of figure 24 where the atom concentration is falling steeply, and hence a minor fluctuation in DCA flow rate will have disproportionately large effect on the observed mass balance.

As in the slow reaction zone the major product from the reaction was cyanogen, C_2N_2, with dicyanodiacetylene, C_6N_2, formed to a much lesser extent and observed only at pressures below 4 torr; intermediates observed were CN and a small peak at m/e = 38 corresponding to C_2N. Formation of molecular nitrogen could not be observed owing to the large

Reproduced with permission of the copyright owner. Further reproduction prohibited without permission.

background at m/e = 28.

Quantitative measurement of the rate of reaction in the flame zone was not possible, owing to extreme sensitivity to external parameters. Slight changes in reactant concentrations, wall conditioning or total pressure resulted in a variation in the rate constant over a factor of twenty in some instances. However, all the values which we obtained were at least ten times greater than those measured in either the slow reaction zone or the post-flame region at the same temperature and total pressure.

Flame emission spectra were recorded at low resolution, and bands corresponding to CN ($B^2\Sigma^+ \rightarrow X^2\Sigma^+$) and CN ($A^2\Pi \rightarrow X^2\Sigma^+$) were identified (see figure 25). Time available for emission measurements was limited by the formation of opaque deposits on the reactor wall, and high resolution spectra could not be obtained.

Reproduced with permission of the copyright owner. Further reproduction prohibited without permission.

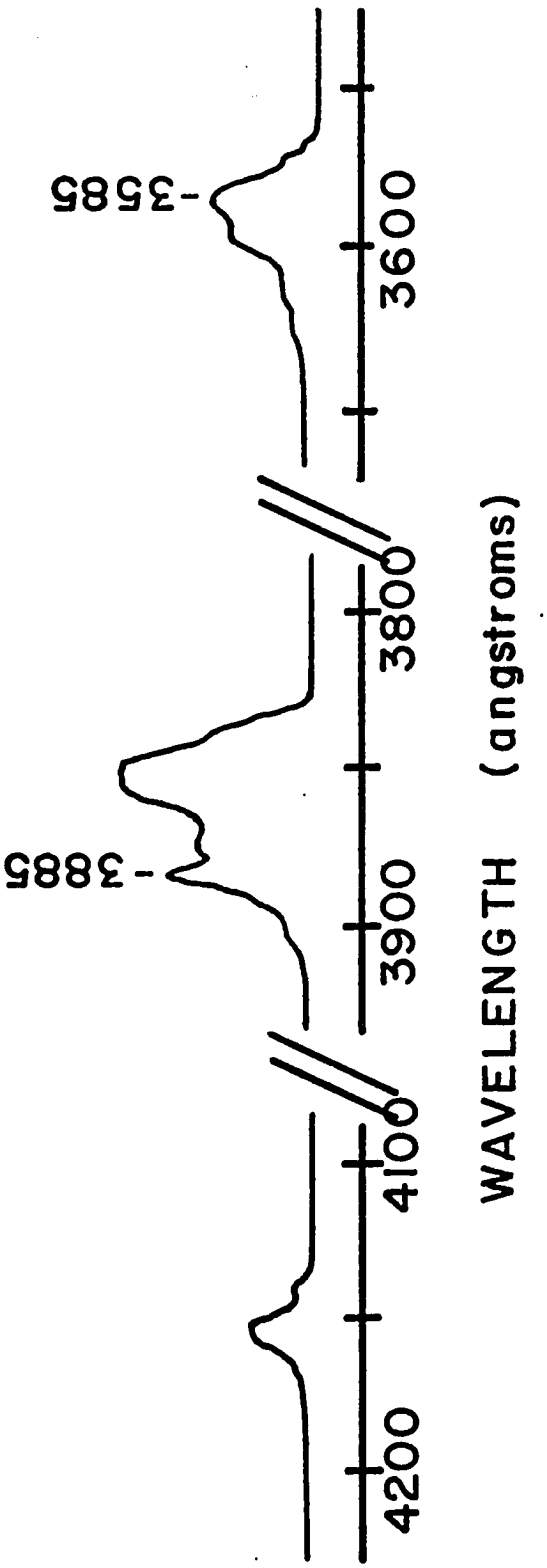

Figure 25: Emission from the reaction of N atoms with dicyanoacetylene in the flame region taken at 4.9 torr and 300°K.

Reproduced with permission of the copyright owner. Further reproduction prohibited without permission.

The Post Flame Zone

In the region beyond the flame the reaction rate decreases, and the chemiluminescence, while not entirely extinguished, is greatly reduced in intensity. This behavior is illustrated in figure 26, where the emission intensity (unfiltered) and the DCA consumption are shown as a function of time. To the eye the post-flame region looks much the same as the pre-flame, slow reaction zone, that is, the chemiluminescence is the same color and about the same intensity. Hence it is not unreasonable to suggest that the mechanism in the post-flame zone is the same as in the slow reaction region. This supposition is supported by the quantitative measurements as well, for the bimolecular rate constant can be calculated from the slope of the line in the post-flame zone of figure 26. Several such determinations yielded post-flame rate constants numerically equal to those obtained at the same total pressure, but under conditions in which only the slow reaction took place. These determinations are denoted by an asterisk in Table 14 and by ▲ in figure 21.*

---

* The data from figure 26 appear in table 14 as the entry at $[N_2]$ = 15.8×10^{16} molecules/cm^3.

Reproduced with permission of the copyright owner. Further reproduction prohibited without permission.

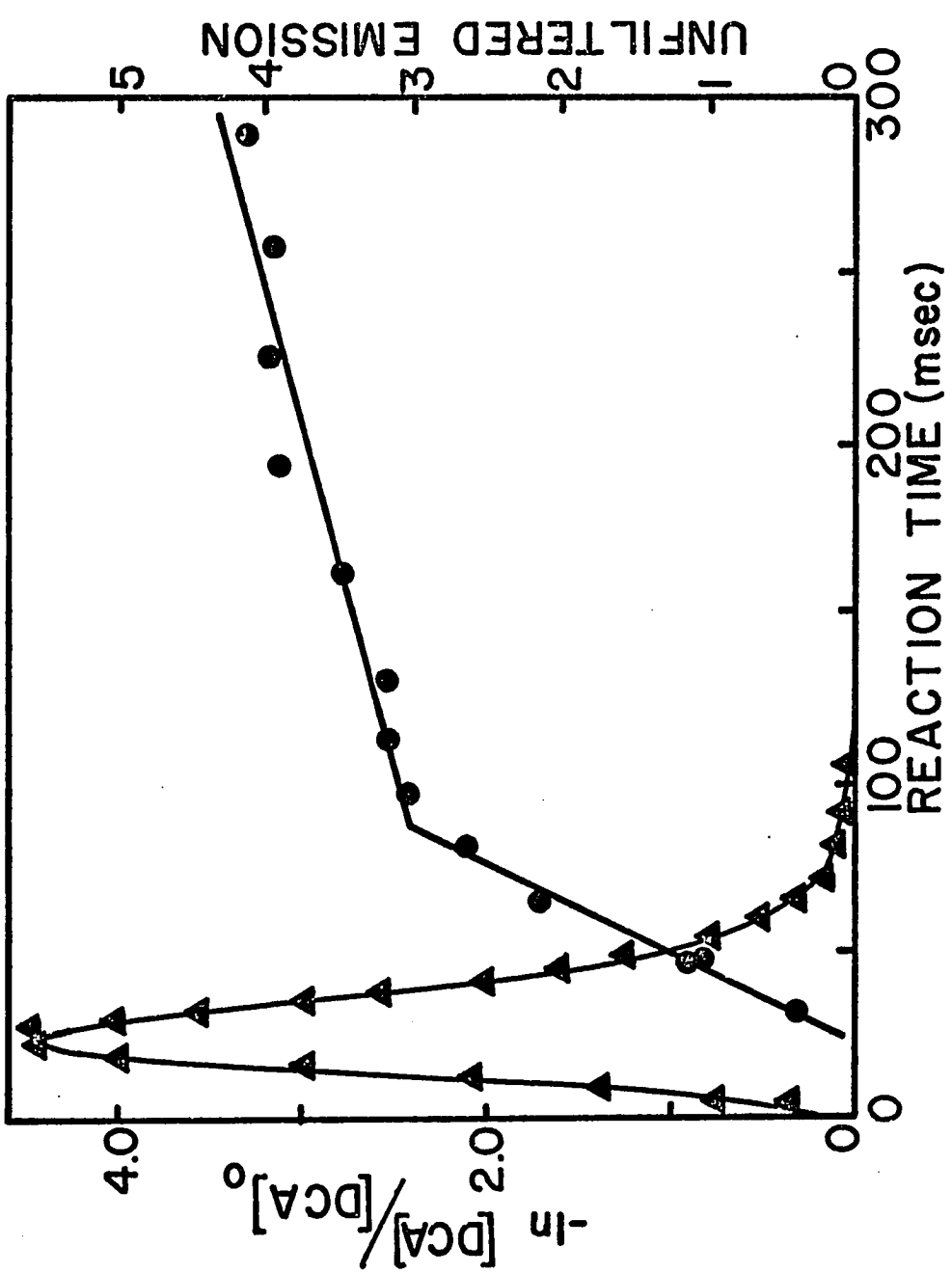

Figure 26: Rate of removal of DCA by N-atoms, ●; unfiltered emission (relative units), ▲, versus time. Linear flow velocity = 155 cm/sec; total pressure = 4.88 torr; 299°K; [N] = 1.2×10^{14} atoms/cm^3.

Reproduced with permission of the copyright owner. Further reproduction prohibited without permission.

Mechanism of the Flame Zone

Rapid recombination of N-atoms has frequently been observed in similar systems,[21, 55-57] and is believed to be due to a chain mechanism involving CN and NCN

$$NCN + N \longrightarrow CN + N_2 \qquad \Delta H = -113 \text{ kcal/mole}^* \text{ (ground state products)} \qquad 28a$$

$$CN + N + M \longrightarrow NCN + M \qquad \Delta H = -113 \text{ kcal/mole} \qquad 29a$$

or the analogous possibility with CN_2 rather than NCN

$$CN_2 + N \longrightarrow CN + N_2 \qquad \Delta H = -150 \text{ kcal/mole} \qquad 28b$$

$$CN + N + M \longrightarrow CN_2 + M \qquad \Delta H = -76 \text{ kcal/mole} \qquad 29b$$

originally presented by Bayes. A different mechanism involving carbon atoms has been proposed by Safrany and Jaster:[9]

$$CN + N \longrightarrow N_2 + C \qquad \Delta H = -45 \text{ kcal/mole}$$

$$C_2N_2 + C \longrightarrow C_2N + CN \qquad \Delta H = +42 \text{ kcal/mole}$$

$$C_2N + N \longrightarrow 2CN \qquad \Delta H = -91 \text{ kcal/mole}$$

The endothermicity of the second step precludes its importance in a system composed primarily of room temperature nitrogen, and although we did observe some C_2N we believe that it originates from subsequent

---

* This and all subsequent heats of reaction have been calculated on the basis of the values given in Appendix F.

Reproduced with permission of the copyright owner. Further reproduction prohibited without permission.

N-atom attack on cyanogen, the major product.

Several aspects of the behavior in the flame zone, as illustrated in figure 24 are sufficient to permit some definite conclusions as to the mechanism of the reaction. These are; the precipitous decrease in atom concentration attendant on the introduction of small quantities of DCA, the fact that the atom concentration reaches a minimum and then increases as more DCA is added, the fact that as the initial atom concentration is increased, less DCA is required to generate the flame, and finally that at higher initial atom concentrations the consumption of atoms is more complete. A chain mechanism is certainly operative, as indicated by the rapidity of atom consumption and the small quantities of DCA required to initiate the consumption. The chain is initiated by the bimolecular attack of N-atoms on DCA, followed by decomposition of the hot adduct to produce chain carriers:

$$N + C_4N_2 \rightleftharpoons NC_4N_2^* \qquad 26$$

$$NC_4N_2^* \longrightarrow C_3N + NCN \qquad \Delta H = -38 \text{ kcal/mole} \qquad 27a$$

The chain is then propagated by the steps

$$NCN + N \longrightarrow N_2 + CN \qquad 28a$$

$$CN + N + N_2 \longrightarrow NCN + N_2 \qquad 29a$$

(or by the analogous steps 28b and 29b). The rate of the chain recombination depends on the concentration of NCN, which increases as more DCA is added, hence the precipitous drop in figure 24. However, on further addition of DCA the N-atom concentration increases, indicating

Reproduced with permission of the copyright owner. Further reproduction prohibited without permission.

a decrease in chain length. This is due to the removal of chain carriers by

$$CN + C_4N_2 \longrightarrow C_2N_2 + C_3N \qquad \Delta H = -57 \text{ kcal/mole} \qquad 30$$

and, equally important, to a decrease in the initiation rate by the competing reaction

$$NC_4N_2^* + C_4N_2 \longrightarrow C_2N_2 + C_6N_2 + N \qquad \Delta H = +3 \text{ kcal/mole} \qquad 31$$

Reactions 30 and 31 account for the observed products, although there are no doubt other reactions which produce C_2N_2. There is no evidence to permit identification of the most important termination step(s); although the deposition of polymeric material on the reactor wall is suggestive of heterogeneous termination,

$$CN,\ NCN + \text{wall} \rightarrow \text{polymer}$$

homogeneous processes may equally well be responsible:

$$CN + CN + N_2 \longrightarrow C_2N_2 + N_2$$
$$NCN + CN + N_2 \longrightarrow C_2N_2 + N + N_2$$
$$NCN + NCN + N_2 \longrightarrow C_2N_2 + 2N_2$$

Finally, the fact that at higher initial N-atom concentration the recombination is faster and more complete requires that there be an additional initiation step, <u>second order</u> in N atoms. The only

Reproduced with permission of the copyright owner. Further reproduction prohibited without permission.

possibility is

$$C_4N_2 + N + N \longrightarrow C_2N_2 + 2CN \qquad \Delta H = -73 \text{ kcal/mole} \qquad 32$$

which may be viewed either as a termolecular step or as two bimolecular steps, reaction 26 followed by

$$NC_4N_2^* + N \longrightarrow C_2N_2 + 2CN$$

The chain recombination of N atoms thus consists of the initiation steps 26, 27a, and 32 in competition with reaction 31, the propagation steps 28a and 29a, and termination by undetermined heterogeneous and homogeneous steps as well as by reaction 30.

Reproduced with permission of the copyright owner. Further reproduction prohibited without permission.

Mechanism in the Slow Reaction Zone

For a bimolecular reaction which exhibits pressure dependence the steady state expression for observed rate constant may be written as the quotient of two polynomials in powers of the third body concentration. As discussed in Appendix E, if a single mechanism governs the slow reaction throughout the entire pressure range, it should be possible to fit the experimental data to a polynomial of the form

$$k_{obs} = \sum_{i=o} a_i[M]^i / \sum_{i=o} b_i[M]^i \qquad (28)$$

where the coefficients a_i and b_i are simple functions (sums and/or products) of the rate constants for the elementary reaction steps. Non-linear regression analysis of the data from Table 14 was carried out for polynomials as high as third order, in both numerator and denominator, and although the curves obtained followed the general shape of the observed data, it proved impossible to obtain a good fit unless one or more of the coefficients was allowed to assume a negative value (see Appendix E). However, this means one or more negative rate constants, and we conclude that a single mechanism, however complicated, cannot explain our data over the entire pressure range. We must therefore separately discuss the high and low pressure regions, with the dividing line being taken at about three torr, i.e., at the change in slope of the data in figure 21.

Reproduced with permission of the copyright owner. Further reproduction prohibited without permission.

The Low-Pressure Region

For nitrogen concentrations less than about 10^{17} molecules/cm^3 the data may be understood in terms of a mechanism similar to that reported by Arrington et al.[21] for the acetylene reaction. Experimentally we have observed a second order rate law

$$-\frac{d[DCA]}{dt} = k_{obs}[N][DCA]$$

in which the observed rate constant increases with total pressure in an approximately linear fashion. The first step must be the bimolecular combination of the reactants

$$N + C_4N_2 \rightleftharpoons NC_4N_2^* \qquad 26$$

The observed pressure dependence requires that subsequent reactions of the hot $NC_4N_2^*$ be bimolecular.*

$$NC_4N_2^* + N_2 \longrightarrow C_3N + NCN + N_2 \quad \Delta H = -38 \text{ kcal/mole} \qquad 27b$$

Reaction 28, $NCN + N \longrightarrow CN + N_2$ provides a ready source of the observed CN radical. Reaction of the hot adduct with DCA produces the observed small amounts of dicyanodiacetylene.

---

* Other products are possible in this step, such as $C_3N_2 + CN$, $\Delta H = 17$ kcal/mole, or $C_2N_2 + C_2N$, $\Delta H = 18$ kcal/mole, but these reactions are sufficiently endothermic to be relegated to a minor role. (ΔH based on formation from ground state $N + C_4N_2$.)

Reproduced with permission of the copyright owner. Further reproduction prohibited without permission.

$$C_4N_2 + NC_4N_2^* \longrightarrow C_2N_2 + C_6N_2 + N \quad \Delta H = +3 \text{ kcal/mole} \quad 31$$

Under the low-pressure conditions the radical intermediates diffuse to the wall and are destroyed there in preference to homogeneous termination steps:

$$C_3N,\ NCN,\ CN + \text{wall} \longrightarrow \text{polymer}$$

If the concentration of $NC_4N_2^*$ is assumed to be in steady state, the above reaction sequence leads to

$$-\frac{d[DCA]}{dt} = k_{obs}[N][DCA] \quad \text{where}$$

$$k_{obs} = \frac{k_{26}(k_{27b}[N_2] + 2k_{31}[DCA])}{k_{-26} + k_{27b}[N_2] + k_{31}[DCA]} \qquad (29)$$

It may further be assumed that $k_{31}[DCA] \ll k_{27b}[N_2]$, inasmuch as there is no hint of curvature in any of the data exemplified by figures 22 and 23, and therefore there can be no second-order dependence on DCA in the reaction scheme. Equation 29 may thus be written in reciprocal form

$$\frac{1}{k_{obs}} = \frac{1}{k_{26}} + \frac{k_{-26}}{k_{26}k_{27b}} \cdot \frac{1}{[N_2]} \qquad (30)$$

Reproduced with permission of the copyright owner. Further reproduction prohibited without permission.

A reciprocal plot of the low pressure data appears in figure 27, and the slope and intercept lead to the values

$$k_{26} = 5.3 \pm 4.3 \times 10^{-15} \text{ cm}^3/\text{molecule sec}$$

$$k_{-26}/k_{26}k_{27b} = 3.76 \pm .8 \times 10^{31} \text{ molecule}^2 \text{ sec/cm}^6$$

An upper limit to k_{27b} may be set equal to the collision frequency, calculated at 300°K with collision diameters of N_2 = 3.5 Å and NC_4N_2* = 8.5 Å, from which

$$k_{27b} \leq 7.2 \times 10^{-10} \text{ cm}^3/\text{molecule sec}$$

and

$$k_{-26} \leq 1.4 \pm 1.1 \times 10^{8} \text{ sec}^{-1}$$

Although the standard errors of the values of k_{obs} quoted in Table 14 are not excessive for this type of experiment, when the data are plotted in reciprocal form the errors are magnified, leading to large uncertainties in the values of k_{26} and k_{-26}. These should be regarded as order-of-magnitude estimates only.

Reproduced with permission of the copyright owner. Further reproduction prohibited without permission.

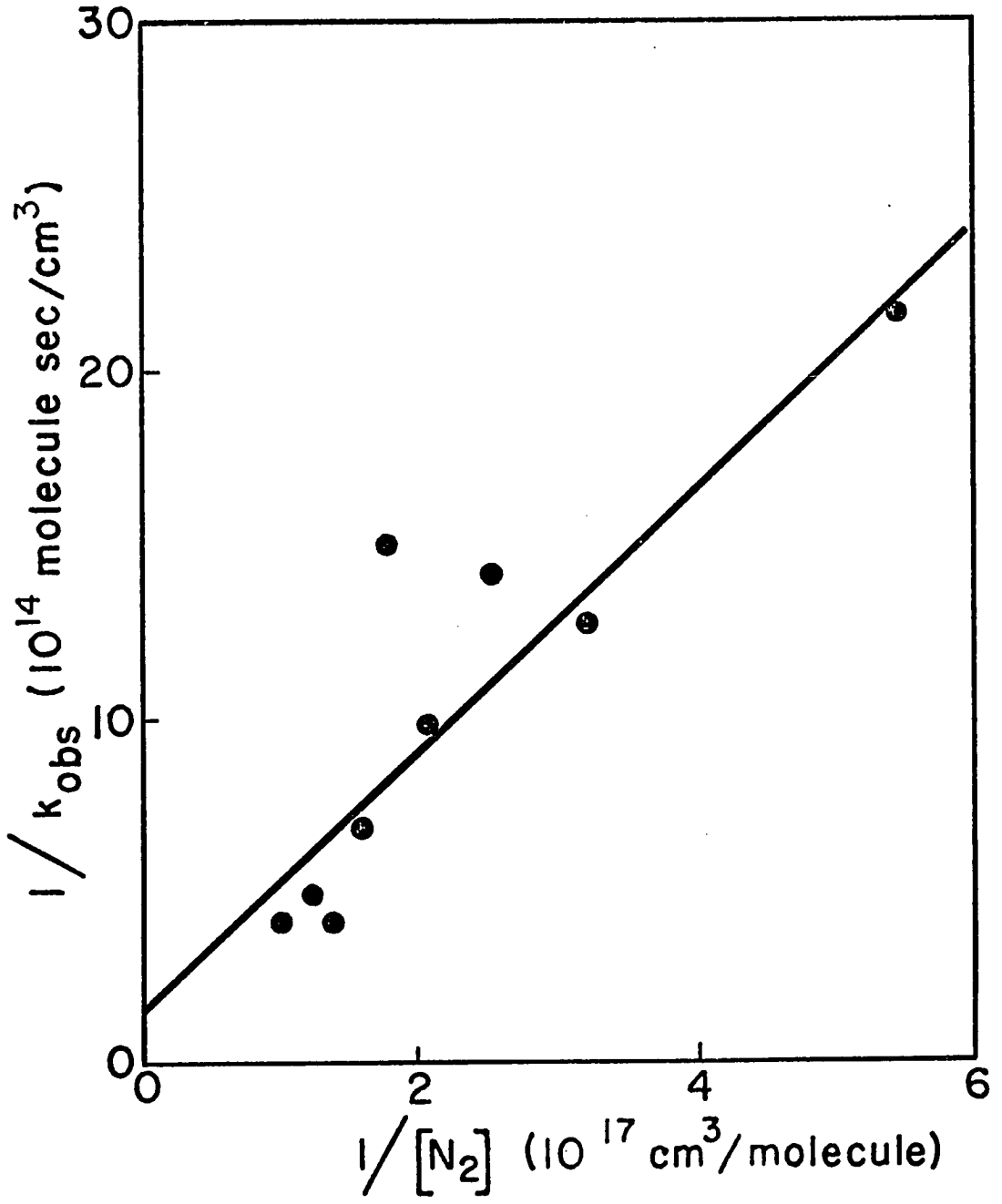

Figure 27: Reciprocal plot of low pressure data from Table 14. Slope = $3.8 \pm 0.8 \times 10^{31}$ molecule^2 sec/cm^6; intercept = $1.9 \pm 1.8 \times 10^{14}$ molecule sec/cm^3.

Reproduced with permission of the copyright owner. Further reproduction prohibited without permission.

The High Pressure Region

Initially we should inquire whether the low pressure mechanism could be amended or expanded to apply as well to the high pressure conditions. We have shown in a general way (vide supra) that this could not be done, but it is instructive to consider the specific case as well, using real reactions and a plausible (one of several such) mechanism.

One attractive possibility is the participation of excited molecular species, namely N_2 ($A^3\Sigma_u^+$) which is a well-known constituent of active nitrogen.[2] Thrush has demonstrated[20, 58] that the A state population in active nitrogen is governed by the decay scheme

$$N + N + N_2 \longrightarrow N_2(A) + N_2 \qquad F$$

$$N_2(A) \longrightarrow N_2(X) + h\nu \qquad G$$

$$N(^4S) + N_2(A) \longrightarrow N_2(X) + N \qquad H$$

from which the steady-state population is:

$$[N_2(A)]_{ss} = \frac{k_F[N]^2[N_2]}{k_H[N] + k_G} \qquad (31)$$

It has recently been shown that the radiative lifetime of $N_2(A)$ is about 2 seconds;[59-61] using this value and Wray's[62] value of $k_H = 5.4 \times 10^{-11}$ cm^3/molecule sec, it is always true in our experiments that $k_G \ll k_H[N]$. Hence

$$[N_2(A)]_{ss} = \frac{k_F[N][N_2]}{k_H} \text{ molecules/cm}^3 \qquad (32)$$

Reproduced with permission of the copyright owner. Further reproduction prohibited without permission.

The absolute intensity of emission from $N_2(A)$, the Vegard-Kaplan emission, is given by[58]

$$k_G[N_2(A)]_{ss} = I_{VK} = 5 \times 10^{-23}\,[N][N_2] \text{ photons/cm}^3 \text{ sec}$$

and therefore $[N_2(A)]_{ss} = I_{VK}/k_G$

or
$$[N_2(A)]_{ss} = 10^{-22}[N][N_2] \qquad (33)$$

From this we calculate, at the highest pressure of our experiments, a value of 5×10^9 molecules/cm^3 for the concentration of $N_2(A)$. At intermediate and lower pressures the concentration is of course less, but is is continuously repopulated by reaction F and is available for reaction with dicyanoacetylene.

$$N_2(A) + C_4N_2 \rightleftharpoons N_2C_4N_2^* \qquad 33$$

$$N_2C_4N_2^* + N_2 \longrightarrow 2C_2N_2 + N_2 \qquad \Delta H = -121 \text{ kcal/mole} \qquad 34$$

$$\longrightarrow C_3N_2 + NCN + N_2 \qquad \Delta H = -12 \text{ kcal/mole} \qquad 35$$

$$\longrightarrow CN + C_3N + 2N_2 \qquad \Delta H = -67 \text{ kcal/mole} \qquad 36$$

If reactions 33-36 are considered together with reactions F, G, and H, to govern $N_2(A)$ concentration a steady state expression may be obtained:

$$[N_2(A)]_{ss} = \frac{k_F(k_{33} + k'[N_2])[N]^2[N_2]}{(k_G + k_H[N])(k_{-33} + k'[N_2]) + k_{33}k'[C_4N_2][N_2]} \qquad (34)$$

Reproduced with permission of the copyright owner. Further reproduction prohibited without permission.

where $k' = k_{34} + k_{35} + k_{36}$

For our system the N-atom concentration is large enough so that $k_G \ll k_H[N]$, and if also $k_{33}[C_4N_2] \ll k_H[N]$ equation 34 would become identical to equation 32. The concentration of DCA was always less than 8 percent of the atom concentration, so we may use the known value of k_H[62] to obtain the condition $k_{33} \ll 6 \times 10^{-10}$ cm^3/molecule sec. This is almost certainly true, since 6×10^{-10} cm^3/molecule sec is the gas kinetic collision frequency expressed as a rate constant; thus we conclude that the steady state concentration of $N_2(A^3\Sigma_u^+)$ is unaffected by reaction with DCA. We may then apply the steady state hypothesis to the concentration of $NC_4N_2^*$, $N_2C_4N_2^*$, CN, and NCN in the system of reactions 26-36, and, using the same approximation as before, $k_{31}[DCA] \ll k_{27}[N_2]$, the expression is obtained

$$k_{obs} = 3K_{32}[N] + \frac{k_{26}(k_{27a} + k_{27b}[N_2]}{k_{-26} + k_{27b}[N_2]} + \frac{(k' + k_{35} + k_{36})\, k_{33} 10^{-22}[N_2]^2}{k_{-33} + k'[N_2]} \qquad (35)$$

where k_{obs} is the second order rate constant for the disappearance of DCA in an excess of N-atoms.

This expression could account for a quadratic pressure dependence, which comes about through the two steps

$$N_2(A) + C_4N_2 \longrightarrow N_2C_4N_2^*$$

$$N_2C_4N_2^* + N_2 \longrightarrow C_3N_2 + NCN + N_2$$

Reproduced with permission of the copyright owner. Further reproduction prohibited without permission.

each of which is first order in total pressure. It is simple enough to escalate the pressure dependence to cubic or even quartic by requiring further collisions with N_2, for instance

$$C_3N_2 + N_2 \longrightarrow \text{Reactive species}$$

but our only justification for doing so would be that the observed pressure dependence cannot be accounted for by any simpler mechanism. Far more serious, however, is that there is no set of numerical values of rate constants which will cause equation 35, or any other steady state expression derived from a reasonable mechanism, to simultaneously fit the high and low-pressure data. The conclusion, once again, is that a new and different mechanism becomes operative as the pressure is raised beyond about 3 torr.

We therefore conclude that at higher pressures DCA is consumed in a chain reaction, and that the rapid increase in our reported second order rate constant is a consequence of increased chain length. In the mechanism which follows, we omit the several reactions involving $N_2(A^3\Sigma_u^+)$ since there is no evidence for the participation of excited molecular species in the DCA consumption scheme (see Appendix D). Also, in the interest of keeping the proposed mechanism within reasonable bounds, we omit the reactions of C_2N_2, the major product, although these reactions certainly occur. The reaction of cyanogen with active nitrogen has been the subject of several studies,[2, 7-10] and the reactive species CN, NCN and C_2N are certainly involved. One might therefore argue that the reaction of active nitrogen with DCA is an auto-accelerated one, and that therein lies the explanation for the increase

Reproduced with permission of the copyright owner. Further reproduction prohibited without permission.

in rate constant at higher pressures. The evidence does not, however, support this view: were the reactions auto-accelerated there would be an upward curvature of the plots exemplified by figures 22 and 23, and no such curvature was ever observed. Secondly, even supposing a slight upward curvature to be lost in the scatter of points, in the auto-accelerated case we would expect a correlation between observed rate constant and extent of reaction: no such correlation is apparent from our data.

The chain decomposition of DCA is mediated by the chain carrier NCN, produced in the initiation steps

$$N + C_4N_2 \rightleftharpoons NC_4N_2^* \qquad 26$$

$$NC_4N_2^* \longrightarrow NCN + C_3N \qquad \Delta H = -38 \text{ kcal/mole} \qquad 27a$$

which are the same as in the low pressure mechanism. The propagation steps are

$$NCN + C_4N_2 \longrightarrow C_2N_2 + C_3N_2 \qquad \Delta H = +2 \text{ kcal/mole} \qquad 37$$

$$C_3N_2 + N \longrightarrow C_2N_2 + CN \qquad \Delta H = -90 \text{ kcal/mole} \qquad 38$$

$$CN + N + M \longrightarrow NCN + M \qquad \Delta H = -150 \text{ kcal/mole} \qquad 29a$$

and chain termination occurs by a variety of heterogeneous and homogeneous reactions, just as in the flame zone.

Our observations may be explained in terms of this mechanism as follows. As the pressure rises, the rate of DCA consumption (and hence k_{obs}) increases owing to the suppression of the diffusion-controlled

Reproduced with permission of the copyright owner. Further reproduction prohibited without permission.

heterogeneous termination steps. A more important cause for the increase in k_{obs}, however, is the fact that one of the propagation steps, reaction 29a, is termolecular, a feature not usually found in radical chain mechanisms. It is this feature which explains as well the relative unimportance of the chain in the low-pressure region. In support of the identification of reaction 29a as the major rate-determining step is our observation of the intermediate CN, whereas NCN was below our limit of detectability. The implication is that reactions 37 and 38 proceed much more rapidly than reaction 29a.

The stable product dicyanodiacetylene, C_6N_2, is observed only at low pressure as a consequence of reaction 31, since it is not produced by the chain mechanism operative at high pressure.

Finally, the observation of trace quantities of C_2N is to be expected from subsequent reactions of the major product C_2N_2, for example,

$$C_2N_2 + N \longrightarrow C_2N + N_2 \qquad \Delta H = -3 \text{ kcal/mole}$$

which has been postulated as being of primary importance in the reaction of active nitrogen with cyanogen.[9, 10]

Reproduced with permission of the copyright owner. Further reproduction prohibited without permission.

Appendix A The Heat Equation: Application to the Fast Flow Reactor

The design requirements for the fast flow reactor as discussed in Section I are: 1) Approximately 20 mm diameter flow tube; 2) Axial reactant inlet; 3) 0-50 msec reaction time at 10 m/s flow rate; 4) Operating pressures of 1-10 torr (carrier gas); 5) Operating temperatures of 300-500°K; 6) Provision for temperature measurement within the reactor; 7) Flexibility as to choice of reactant.

We consider the problem of temperature control and ask specifically what length of furnace is required to bring the flowing gas up to reaction temperature. To a good approximation this is equivalent to the question, "How long does it take to heat a stationary gas to the desired reaction temperature?"

Reproduced with permission of the copyright owner. Further reproduction prohibited without permission.

The Exact Solution

The system can be looked at as a circular plug of radius 1, moving along the reactor at the desired flow rate. The region inside the plug is initially at room temperature and the perimeter at the desired final temperature. Instead we solve the problem of temperature history in an infinite cylinder of stationary gas. Margeneau and Murphy[63] developes an exact solution of the heat equation, which is:

$$\frac{K}{\rho s}\nabla^2 U - \frac{\delta U}{\delta t} = 0 \qquad (A1)$$

where U = temperature

ρ = density

s = specific heat

K = thermal conductivity

by defining new functions such that

$$U(x,y,z,t) = S(x,y,z) \cdot T(t); \quad K/\rho s = a^2$$

substituting and separating variables:

$$\frac{\nabla^2 S}{S} = \frac{\dot{T}}{a^2 T}$$

Since the two sides are independent, they must be equal to the same constant. Setting this constant equal to $-k^2$ and treating the space and time parts separately:

Reproduced with permission of the copyright owner. Further reproduction prohibited without permission.

$$\frac{\dot{T}}{T} = -a^2k^2 \qquad (A2)$$

with solutions of the form: $T_k = C_k e^{-a^2k^2t}$

$$\nabla^2 S + k^2 S = 0 \qquad (A3)$$

Converting equation A3 to cylindrical polar coordinates and recognizing that $\frac{\delta S}{\delta z} = 0$ by initial specification of the problem (infinite cylinder), we obtain:

$$\frac{\delta^2 S}{\delta r^2} + \frac{1}{r}\frac{\delta S}{\delta r} + \frac{1}{r^2}\frac{\delta^2 S}{\delta \theta^2} + k^2 S = 0 \qquad (A4)$$

further separation is then accomplished by substituting:

$$S(r,\theta) = R(r) \cdot \Theta(\theta)$$

and multiplication by $\frac{r^2}{S} = \frac{r^2}{R \cdot \Theta}$

therefore: $$\frac{r^2}{R}\frac{\delta^2 R}{\delta r^2} + \frac{r}{R}\frac{\delta R}{\delta r} + r^2k^2 = -\frac{1}{\Theta}\frac{\delta^2 \Theta}{\delta \theta^2} \qquad (A5)$$

Again, both sides are independent, hence equal to the same constant, say m^2. Treating each part separately we obtain:

$$\frac{1}{\Theta}\frac{\delta^2 \Theta}{\delta \theta^2} = -m^2 \qquad (A6)$$

Reproduced with permission of the copyright owner. Further reproduction prohibited without permission.

with solutions of the form: $\Theta_m = C_m e^{\pm im\theta}$

$$r^2\frac{\delta^2 R}{\delta r^2} + r\frac{\delta R}{\delta r} + (r^2k^2 - m^2)R = 0 \qquad (A7)$$

This is Bessel's Equation with the solution

$$R_k = J_m(kr)$$

where J(kr) is the Bessel Function of the independent variable, kr. The complete solution is:

$$U = R \cdot \Theta T; \text{ or}$$

$$U = \sum_{n=o}^{\infty} a_n J_m(kr) e^{\pm im\theta} e^{-a^2k^2t} \qquad (A8)$$

where: $a_n = C_k \cdot C_m$

Since radial symmetry implies Θ_m = constant; m = 0

$$U = \sum_{n=o}^{\infty} a_n J_o(kr) e^{-a^2k^2t}$$

Our interest is in the case with the gas initially at room temperature, 300°K, and the final desired temperature, 500°K.

Defining conditions and transforming:

Reproduced with permission of the copyright owner. Further reproduction prohibited without permission.

$U(l,t) = 500°K = H$

$U(o,o) = 300°K = A$

$V = U - H$

$V(l,t) = O$

$V(o,o) = A - H$

$V(r,o) = g(r) - H$

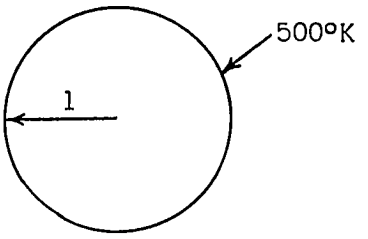

where: $g(r)$ is the initial temperature distribution inside the cylinder.

The values for the constant, k, may now be found since:

$$V(l,t) = O = \sum_{n=o}^{\infty} a_n J_o(kl) e^{-a^2k^2t} - H, \text{ for finite } t$$

implies: $J_o(kl) = O$

Bessel Functions are oscillatory, hence $J_m(\gamma)$ has an infinite number of real zeros. It also tends to zero as $\gamma \to \infty$. Values of the independent variable, γ, denoted here as α_n, at the zeros are tabulated.[64] Table A1 is a listing of α_n at the first twenty zeros of the zeroth order Bessel Function, $J_o(\alpha_n)$.

$$\alpha_n = kl$$

$$k = l/\alpha_n$$

The final solution is given by:

$$V(r,t) = \sum_{n=o}^{\infty} a_n J_o\left(\frac{l}{\alpha_n} r\right) e^{-a^2 l^2 t/\alpha_n^2}$$

Reproduced with permission of the copyright owner. Further reproduction prohibited without permission.

The coefficients, a_n may be found at t = o:

$$\int_o^a xJ_n(\beta x)J_n(\alpha x)dx = \begin{cases} 0 \text{ if } \alpha = \beta = 0 \\ \frac{1}{2}J^2_{n+1}(\alpha_s) \text{ if } \alpha = \beta = \alpha_s \end{cases}$$

substituting $V(r,o) = g(r) - H$, and multiplying by:

$$\frac{1}{\alpha_n} rJ_o(\frac{1}{\alpha_n}r)d(\frac{1}{\alpha_n}r) \qquad \text{followed by integration}$$

$$\int_o^1 (g(r)-H)\frac{1}{\alpha_n} rJ_o(\frac{1}{\alpha_n}r)d(\frac{1}{\alpha_n}r) = \sum_n^\infty \int_o^1 a_n J_o(\frac{1}{\alpha_n}r)\frac{1}{\alpha_n}rJ_o(\frac{1}{\alpha_n}r)d(\frac{1}{\alpha_n}r)$$

$$= \sum_{n=1}^\infty \tfrac{1}{2}a_n\frac{1}{\alpha_n}J_1^2(\frac{1}{\alpha_n})$$

$$\text{therefore } a_n = \sum_{n=1}^\infty \frac{2\alpha_n}{1J_1^2(\frac{1}{\alpha_n})} \int_o^1 (g(r)-H)\frac{1}{\alpha_n} rJ_o(\frac{1}{\alpha_n}r)\, d(\frac{1}{\alpha_n}r)$$

Note that for this case the temperature distribution, g(r), is a constant.

Reproduced with permission of the copyright owner. Further reproduction prohibited without permission.

Table A1: $J_v(z)$ for $V \geq 0$; nth zero denoted by α_n^{64}

n	α_n
1	2.4048255577
2	5.5200781103
3	8.6537279129
4	11.7915344391
5	14.9309177086
6	18.0710639679
7	21.2116366299
8	24. 3524715308
9	27.4934791320
10	30.6346064684
11	33.7758202136
12	36.9170983537
13	40.0584257646
14	43.1997917132
15	46.3411883717
16	49.4826098974
17	52.6240518411
18	55.7655107550
19	58.9069839261
20	62.0484691902

Reproduced with permission of the copyright owner. Further reproduction prohibited without permission.

Infinite Uniform Gaseous Plate

Computations using the exact solution though accurate, are difficult and lengthy. An approximate solution was used where the reactor was modeled by a gaseous plate of uniform thickness, L, the surfaces being held at the high temperature.

Schneider[65] derives the solution from the heat equation

$$\frac{K}{\rho s}\frac{\delta^2 T}{\delta x^2} = \frac{\delta T}{\delta t}$$

where: T = Temperature Difference
K = Thermal Conductivity
ρ = Density
s = Specific Heat

set: $T(x,t) = X(x)\cdot\Upsilon(t)$; $K/\rho s = \alpha$

Substituting and separating variables:

$$\frac{1}{X}\frac{d^2X}{dx^2} = \frac{\dot{\Upsilon}}{\alpha\Upsilon}$$

The two sides are independent. Taking the constant to be $-\lambda^2$ and treating each part separately:

$$\frac{\dot{\Upsilon}}{\Upsilon} = -\lambda^2\alpha \qquad (A9)$$

with solutions of the form:

$$\Upsilon_\lambda = C_\lambda e^{-\lambda^2\alpha t}$$

Reproduced with permission of the copyright owner. Further reproduction prohibited without permission.

$$\frac{1}{X}\frac{d^2X}{dx^2} = -\lambda^2 \qquad (A10)$$

with solutions of the form:

$$X_\lambda = C_{1\lambda}\cos\lambda x + C_{2\lambda}\sin\lambda x$$

The general solution is then given by a sum of terms of the form:

$$T_\lambda = \tau_\lambda \cdot X_\lambda = C_\lambda e^{-\lambda^2\alpha t}(C_{1\lambda}\cos\lambda x + C_{2\lambda}\sin\lambda x) \qquad (A11)$$

Defining coniditions:

$T(L,t) = T(0,t) = 0$

$T(x,0) = T_i \quad 0 \leq x \leq L$

$T = b - b_1$

$T_i = b_i - b_1$

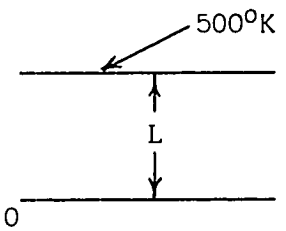

where: b_1 = 500°K (wall)

b_i = 300°K (initial)

b = Temperature at L/2

$T(0,t) = 0$ for all $t > 0$ implying:

$$C_{1\lambda} = 0$$

Also $T(L,t) = 0$ for all $t > 0$ implying:

$$\sin(\lambda L) = 0$$

$$\lambda = n\pi/L \qquad n = 0,1,2,3,4,\cdots$$

Reproduced with permission of the copyright owner. Further reproduction prohibited without permission.

$$T = \sum_{n=o}^{\infty} B_n e^{-(n\pi/L)^2 \alpha t} \sin(n\pi x/L) \qquad (A12)$$

where:

$$B_n = C_\lambda C_{2\lambda}$$

but $\sin(n\pi x/L) = 0$ at $n = 0$ for all x. Equation A12 can be written:

$$T = \sum_{n=1}^{\infty} B_n e^{-(n\pi/L)^2 \alpha t} \sin(n\pi x/L) \qquad (A13)$$

Choose the arbitrary constants, B_n, such that the series:

$$\sum_{n=1}^{\infty} B_n \sin(n\pi x/L)$$

is uniformly convergent (i.e. a Fourier Series) in which case:

$$B_n = \frac{2T_i}{L} \int_o^L \sin(n\pi x/L)dx$$

$$B_n = \frac{4T_i}{n\pi} \qquad (n = \text{odd})$$

hence the solution is:

$$T = \frac{4T_i}{\pi} \sum_{n=1}^{\infty} \frac{\sin(n\pi x/L)}{n} e^{-(n\pi/L)^2 \alpha t} \qquad (n = \text{odd}) \quad (A14)$$

Reproduced with permission of the copyright owner. Further reproduction prohibited without permission.

Calculations

We can now use the solution of the infinite uniform gaseous plate approximation to find the temperature at the center of the plate at various times. Calculations are to be made for times ranging from 10 μsec to 50 msec, assuming the gas to be helium at each of two pressures: 1 and 10 torr. Defining constants:

$K = 3.8 \times 10^{-4}$ cal°/sec cm^3 — Assume to be constant over temperature range. This value at 100°C.[25]

$S = C_p = 4.97$ cal/°m — Assume to be constant over temperature range.

$\rho = 4.01 \times 10^{-8}$ m/cm^3 @ 1 torr
$\rho = 4.01 \times 10^{-7}$ m/cm^3 @ 10 torr
} Assume to be constant over temperature range. Values given are at 400°K.

$T_i = -200°$ — As before $T_i = b_i - b_l$; the initial gas temperature minus the wall temperature.

$L = 2.0$ cm

$x = L/2 = 1.0$ cm

Calculations were carried out by computer. Summation was terminated at $n = i$ where the ith term was ≤ 1°K. Values obtained are reported in Tables A2 and A3.

Reproduced with permission of the copyright owner. Further reproduction prohibited without permission.

Table A2: Temperature at Center of Gaseous Plate at 1.0 Torr Pressure

Time (sec)	Number of Terms Calculated	Temperature Difference Between Wall and Center of Plate (°C)	Actual Temperature at Center of Plate (°K)
1×10^{-5}	9	- 200	300
3×10^{-5}	7	- 199	301
5×10^{-5}	5	- 191	309
7×10^{-5}	5	- 179	321
9×10^{-5}	5	- 165	335
1×10^{-4}	5	- 158	342
3×10^{-4}	3	- 62	438
5×10^{-4}	3	- 24	476
7×10^{-4}	3	- 9	491
9×10^{-4}	3	- 4	496
1×10^{-3}	3	- 2	498
3×10^{-3}	1	0	500
5×10^{-3}	1	0	500

Reproduced with permission of the copyright owner. Further reproduction prohibited without permission.

Table A3: Temperature at Center of Gaseous Plate at 10.0 Torr Pressure

Time (sec)	Number of Terms Calculated	Temperature Difference Between Wall and Center of Plate (°C)	Actual Temperature at Center of Plate (°K)
1×10^{-4}	9	- 200	300
3×10^{-4}	7	- 199	301
5×10^{-4}	5	- 191	309
7×10^{-4}	5	- 179	321
9×10^{-4}	5	- 165	335
1×10^{-3}	5	- 158	342
3×10^{-3}	3	- 62	438
5×10^{-3}	3	- 24	476
7×10^{-3}	3	- 9	491
9×10^{-3}	3	- 4	496
1×10^{-2}	3	- 2	498
3×10^{-2}	1	0	500
5×10^{-2}	1	0	500

Reproduced with permission of the copyright owner. Further reproduction prohibited without permission.

Discussion

Results from the exact solution should show that the infinite cylinder heats faster than the infinite gaseous plate approximation. The approximation considers heat flow from two directions while the exact case takes heat flow as radially symmetric. It is advantageous to have some quantitative measure of this difference. Calculations may be done using a Fourier Modulus, Θ, defined by Schneider.[65]

$$\Theta = \frac{\alpha}{\delta_1^2} t = \frac{Kt}{\delta_1^2 \rho_s}$$

Where: t = time

K = thermal conductivity

ρ = density

s = specific heat

δ_1 = semithickness or surface radius

Using the values from page 138 we may calculate values of the Fourier Modulus at various conditions. (See Table A4).

The parameters $P(\Theta)$ (infinite plate) and $C(\Theta)$ (infinite cylinder) are defined by:[65]

$$P(\Theta), C(\Theta) = \frac{t - t_1}{t_i - t_1}$$

Where: t = central temperature

t_1 = wall temperature

t_i = initial internal temperature

The central temperature, as reported in Tables A2 and A3, is given by:

$$T = 500 - (t_i - t_1) P(\Theta), C(\Theta)$$

$$T = 500 - 200\, P(\Theta), C(\Theta)$$

Reproduced with permission of the copyright owner. Further reproduction prohibited without permission.

Table A4: Values of the Fourier Modulus, Θ, Under Various Conditions

Pressure (torr)	Time (sec)	Θ
10.0	1×10^{-3}	0.191
10.0	5×10^{-3}	0.955
10.0	1×10^{-2}	1.91
1.0	1×10^{-4}	0.191
1.0	5×10^{-4}	0.955
1.0	1×10^{-3}	1.91

Reproduced with permission of the copyright owner. Further reproduction prohibited without permission.

Values of $P(\Theta)$ and $C(\Theta)$ are tabulated in Table A5.[65] As can be seen thermal equlibrium is reached much faster in the infinite cylinder as compared to the infinite gaseous plate approximation. In Figures A1 and A2 the data of Tables A2 and A3 are shown. These data are used in the final design to add a safety factor to the heating apparatus.

Reproduced with permission of the copyright owner. Further reproduction prohibited without permission.

Table A5: Central Temperatures for Exact Solution and Gaseous Plate Approximation[65]

Pressure (Torr)	Time (sec)	P (Θ)	C (Θ)	T (Plate)	T (Cylinder)
10.0	$1x10^{-3}$	0.78866	0.52737	-158	-106
10.0	$5x10^{-3}$	0.1207	0.00643	-24	-1
10.0	$1x10^{-2}$	0.0113	0.00000	-2	0
1.0	$1x10^{-4}$	0.78866	0.52737	-158	-106
1.0	$5x10^{-4}$	0.1207	0.00643	-24	-1
1.0	$1x10^{-3}$	0.0113	0.00000	-2	0

Reproduced with permission of the copyright owner. Further reproduction prohibited without permission.

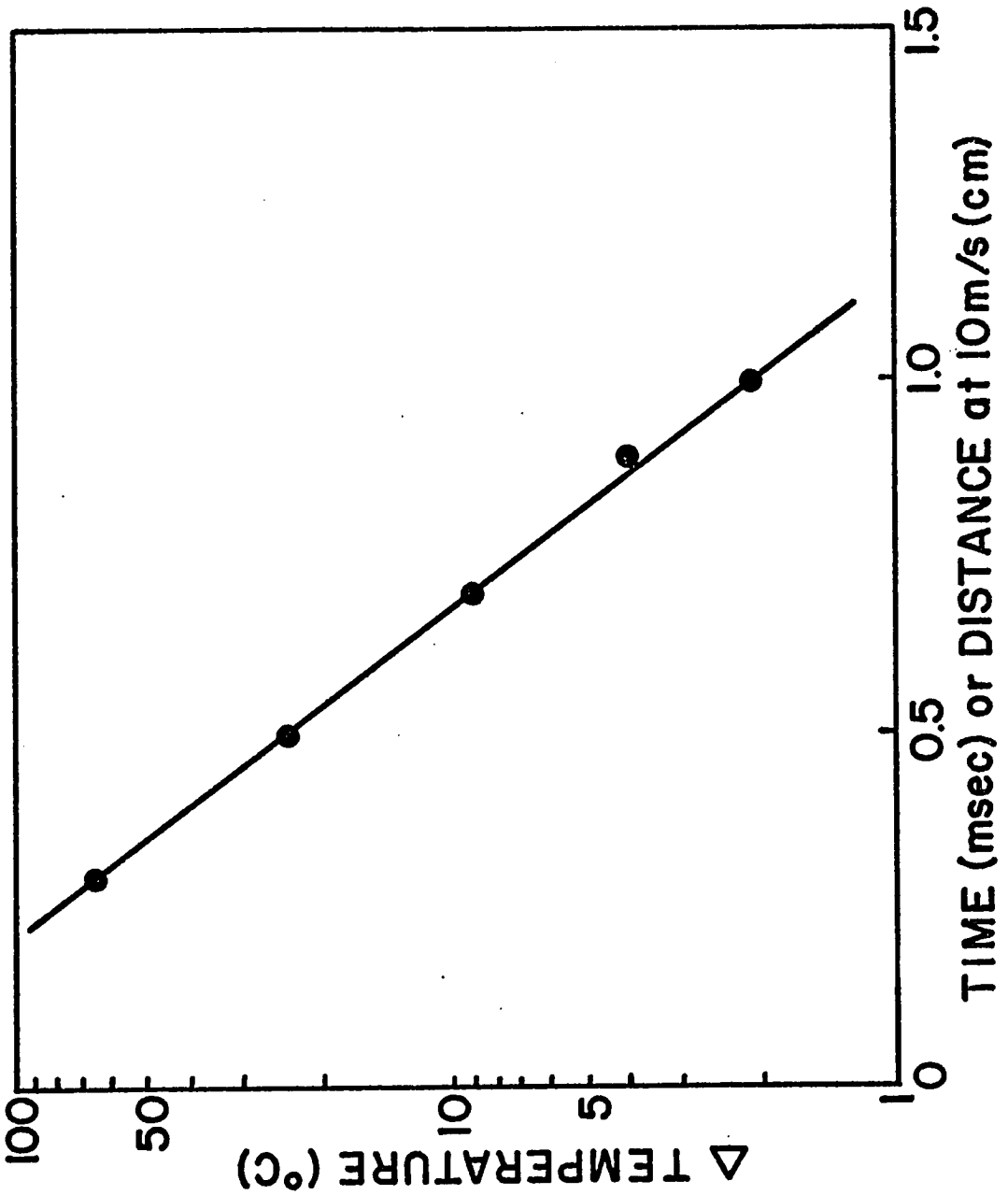

Figure A1: Δ Temperature versus time for the infinite gaseous plate at 1.0 torr where Δ Temperature is the temperature difference in centigrade degrees between the wall and center of the plate (see Table A2).

Reproduced with permission of the copyright owner. Further reproduction prohibited without permission.

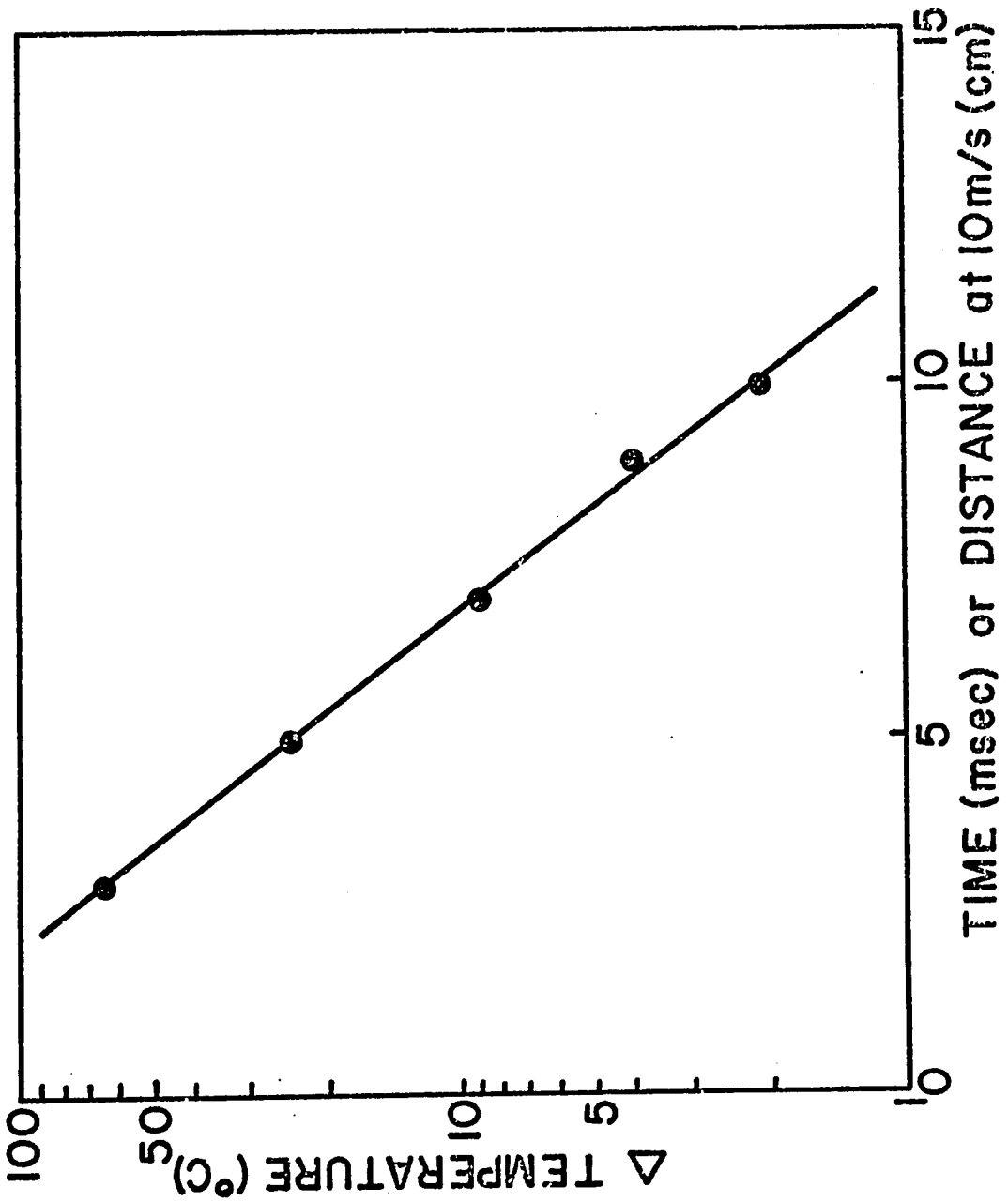

Figure A2: ΔTemperature versus time for the infinite gaseous plate at 10.0 torr where ΔTemperature is the temperature difference in centigrade degrees between the wall and center of the plate (see Table A3).

Reproduced with permission of the copyright owner. Further reproduction prohibited without permission.

Appendix B: Correction of the Rate Constant for Axial Diffusion

According to Kaufman[1] slow linear flow velocities are desirable because of their negligible pressure drop and rapid radial diffusion along the reactor; however, slow flows give rise to axial diffusion of reactants throughout the length of the reactor. Consider a flowing gaseous system with a volume element between x and x + dx where reactants are input at x = 0.

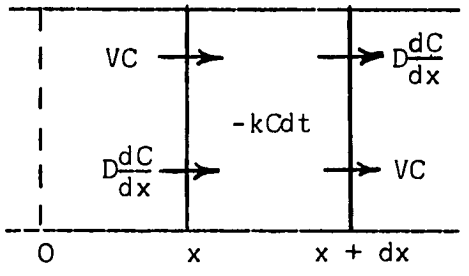

V = Average linear gas velocity

D = Diffusion coefficient of atoms

C = Atom concentration

-kC = Homogeneous and heterogeneous first order atom decay

Since the flow of atoms into the volume element is equal to the flow out:

$$-D\frac{dC}{dx}(x)dt + VC(x)dt = -D\frac{dC}{dx}(x + dx)dt + VC(x + dx)dt + kCdxdt \qquad (B1)$$

which reduces to:

$$\frac{d^2C}{dx^2} - \frac{V}{D}\frac{dC}{dx} - \frac{kC}{D} = 0 \qquad (B2)$$

The solutions are $C = Ae^{r_+x} + Be^{r_-x}$ (B3)

Reproduced with permission of the copyright owner. Further reproduction prohibited without permission.

where $$r_{\pm} = \frac{\frac{-V}{D} \pm \sqrt{\frac{V^2}{D^2} + \frac{4k}{D}}}{2}$$

Applying the boundary conditions:

1) $C = C_o$ at $x = 0$; therefore $C_o = A + B$

2) $C \longrightarrow 0$ as $x \longrightarrow \infty$; therefore $A = 0$

Equation B3 then becomes:

$$C = C_o \exp - \left[\frac{V/D + \sqrt{V^2/D^2 + 4k/D}}{2}\right] x \qquad (B4)$$

Although the discussion thus far, for simplicity, has been with respect to first order removal of atoms the same arguments hold for a pseudo-first order removal of stable reactant, here neglecting heterogeneous recombination, by redefining:

$$- kCdt = - k[O][DCA]dt$$

With atoms in excess the measured rate constant will be $k[O]$; therefore, at zero atom concentration:

$$C = C_o \exp (- Vx/D) \qquad (B5)$$

Experimentally we measure the ratio, R, of the DCA concentration with and without atoms present. From equations B4 and B5 this ratio is then found to be:

$$R = \frac{C_o \exp(r_- x)}{C_o \exp (-Vx/D)} = \exp (Vx/D + r_- x) \qquad (B6)$$

Reproduced with permission of the copyright owner. Further reproduction prohibited without permission.

The observed pseudo first order rate constant, k' is related to R by the integrated rate expression

$$k' = -\frac{V d\ln h}{dx} = -V\left[\frac{V}{2D} - \tfrac{1}{2}\left(\frac{V^2}{D^2} + \frac{4k}{D}\right)^{\frac{1}{2}}\right] \qquad (B7)$$

which reduces to:

$$k = k'[1 + Dk'/V^2] \qquad (B8)$$

The contribution from axial diffusion may then be ignored if $Dk'/V^2 << 1$. For this system the coefficient of mutual diffusion, D, will be greatest at low pressures as demonstrated in equation B9[30]

$$D = \frac{3}{8}\left[\frac{\pi kT}{2\mu}\right]^{\frac{1}{2}} \frac{1}{n\pi d_{12}^2} \qquad (B9)$$

where $\mu = m_1 m_2/(m_1 + m_2)$ is the reduced mass, n is the total molecular density and $d_{12} = (d_1 + d_2)/2$ with d_1 and d_2 the molecular diameters.

In Table B1 are collected the results of calculations at one torr and room temperature for several pertinent cases. The corrections are negligible for most cases; however, the correction must be used to avoid systematic errors in those systems where axial diffusion is appreciable.

Reproduced with permission of the copyright owner. Further reproduction prohibited without permission.

Table B1: Contribution to the Measured First Order Rate Constant From Axial Diffusion at One Torr and 300°K Assuming Diameters of 2.3, 2.5, 3.5 and 8.5 x 10^{-8} cm for O, He, N_2, and DCA, Respectively

Diffusing System	D (cm/sec)	Average k Measured (sec^{-1})	Average LFV (cm/sec)	Contribution to k from Diffusion
O - N_2	720	3.0	150	3.6%
DCA - N_2	50	0.2	100	0.1%
O - He	760	3.0	75	44 %
DCA - He	139	0.3	100	0.4%

Reproduced with permission of the copyright owner. Further reproduction prohibited without permission.

Appendix C: Species Present in Active Nitrogen

The major reactive component in active nitrogen is nitrogen atom, N (^4S); however, a number of excited molecular states are available via the rapid pre-equilibrium:

$$2N(^4S) + M \rightleftharpoons N_2(^5\Sigma_g^+) + M \qquad C1$$

$$N_2(^5\Sigma_g^+) \rightleftharpoons N_2[B(^3\Pi_g)]^* \qquad C2$$

where * refers to vibrational exitation.

The probability of curve crossing (reaction C2) has been estimated[66] to be between 10^{-1} and 10^{-2} per collision which means that from 1 to 10 percent of the $N_2(^5\Sigma_g^+)$ formed in reaction C1 will predissociate into the B state, formation occuring at the twelfth vibrational level.

Benson[67] has shown that if the lifetime of $N_2(^5\Sigma_g^+)$ is taken as $10^{-12.3}$ seconds at room temperature and a value of 10^{-2} is used for the transition probability for reaction C2, then the lifetime of the rotationally hot $(^3\Pi_g)^*$ is about $10^{-11.5}$ seconds. This is at least $10^{3.5}$ shorter than the collision frequency even at 20 torr; therefore, the metastable $N_2(^3\Pi_g)^*$ is in pseudoequilibrium with nitrogen atoms with the equilibrium constant[67]

$$K = \frac{[N_2(B)^*]}{[N]^2} = 10^{-22.9} \text{ cm}^3/\text{particle}$$

In our system the N-atom concentration was generally 2×10^{14}

Reproduced with permission of the copyright owner. Further reproduction prohibited without permission.

atoms/cm^3; we therefore had a $N_2(B)^*$ concentration of about 5 x 10^5 molecules/cm^3. The radiative lifetime of the B state is about 10^{-5} sec which is longer than collision frequencies even at 0.1 torr. Therefore the species will relax rotationally and vibrationally by collision.

The $B^3\Pi_g$ species may then undergo radiative transition to the A state

$$N_2(^3\Pi_g) \longrightarrow N_2[A(^3\Sigma_u^+)] + h\nu \qquad C3$$

The A state population is limited by reactions C4 and C5:

$$N(^4S) + N_2(A) \longrightarrow N_2[X(^1\Sigma_g^+)] + N \qquad C4$$

$$N_2(A) \longrightarrow N_2(X) + h\nu \qquad C5$$

Reactions C3-C5 define a steady state concentration of $N_2(A)$ which is discussed further in Section VII. The concentrations of these excited molecular species are small as compared to the atom concentration; however, they are quite reactive as demonstrated in Appendix D for $N_2(A)$. In any study of active nitrogen their contribution to the overall reaction must be considered and where possible measured in an independent experiment, (see Appendix D).

Reproduced with permission of the copyright owner. Further reproduction prohibited without permission.

Appendix D: Production of $N_2[A(^3\Sigma_u^+)]$ in the Absence of Nitrogen Atoms

Setser and Stedman[68, 69] have recently developed a technique for the production of $N_2[A(^3\Sigma_u^+)]$ in the absence of other active species. The system consists basically of passage of pure, dry argon through a low power hollow cathode discharge, generating metastable argon atoms ($^3P_2$, $^3P_0$). Nitrogen is introduced immediately downstream from the discharge resulting in the production of $N_2(A)$ by collision with an excited argon atom. A similar technique has been used to produce[70] and observe the reaction[71] of metastable krypton and xenon metastables.

Discovery of this system in which $N_2(A)$ is present, clean of any other excited molecular or atomic species, was of great importance to active nitrogen chemistry as the A state has frequently been postulated to account for unusual behavior in nitrogen atom reactions. The quenching rate constants, that is, rate constants for $N_2(A) + X \longrightarrow N_2(X^1\Sigma)$, determined by Setser et al.[59, 72-74] are reported in Table D1. As can be seen the rates are quite fast in most instances; therefore, even though the A state concentration is much lower than the atom concentration in active nitrogen, the A state contribution to the overall reaction could be quite significant especially at higher pressures, as shown in Section VII.

It is reported[75] that microwave excitation of argon for the purpose of $N_2(A)$ generation is undesirable, as high energy electrons are produced even at low power, from which arises the possibility of nitrogen excitation by electron impact. Therefore a dc discharge flow lamp was constructed similar to that reported in reference 75, the final design

Reproduced with permission of the copyright owner. Further reproduction prohibited without permission.

Table D1: Reported Quenching Rate Constants for the Reaction of $N_2[A(^3\Sigma_u^+)]$ with Various Small Molecules.

Quenching Molecule	Rate Constant (cm^3/molecule sec)	Reference
cis-butene-2	2.2×10^{-10}	59
Propene	2.8×10^{-10}	59
Ethene	1.6×10^{-10}	59
1,3-Butadiene	3.5×10^{-10}	59
Benzene	1.6×10^{-10}	59
Cyclopropane	no quenching	59
Methane	$\ll 1 \times 10^{-14}$	72
Ethane	$< 1 \times 10^{-14}$	72
Nitric oxide	1.1×10^{-10}	72
Nitrous oxide	1.4×10^{-11}	59
Ammonia	1.6×10^{-10}	59
Oxygen	3.3×10^{-12}	73
Sulfur dioxide	4.8×10^{-11}	59
Carbon monoxide	2.2×10^{-11}	59
Carbon dioxide	$< 1 \times 10^{-14}$	72
Hydrogen	$< 1 \times 10^{-14}$	72
Duterium	$< 1 \times 10^{-14}$	72
Methanol	6×10^{-11}	73
Acetylene	2.5×10^{-10}	59

Reproduced with permission of the copyright owner. Further reproduction prohibited without permission.

Quenching Molecule	Rate Constant (cm^3/molecule sec)	Reference
Cyanogen	5.7×10^{-11}	59
Acetonitrile	2.0×10^{-11}	73
Hydrogen cyanide	$\sim 2 \times 10^{-10}$	74
Propylnitrile	$\sim 2 \times 10^{-12}$	74

Reproduced with permission of the copyright owner. Further reproduction prohibited without permission.

is shown in figure D1. The system uses two cylindrical platinimum foil electrodes (10mm long, 2.5 mm i.d.) positioned 1.5 cm apart in a 5mm Pyrex tube. The discharge was operated typically at 300 v and 1-2 mA current; higher currents resulted in a decrease in the discharge intensity, the discharge extinguished at 15-20 mA current. Nitrogen was added to the system 0.1 - 1.0 msec downstream of the discharge giving a characteristic violet flame up to 7 cm long.

It should be pointed out that initial designs for the argon discharge lamp failed to produce excited nitrogen molecules because the residence time between the second electrode and the nitrogen input was greater than 5 msec. The present design was adopted primarily because it enabled the short lived Ar ($^3P_2$, $^3P_0$) to mix with nitrogen molecule as quickly as possible once it has left the discharge region.

An attempt was made to observe the reaction of $N_2(A)$ with DCA. The A state nitrogen in argon carrier was flowed into the reactor via the atom input, while the DCA was introduced at the probe tip which was positioned 50 cm from the time-of-flight sampling pinhole. The argon flow and pressure required to produce maximum intensity at the nitrogen-argon mixing port resulted in a linear flow velocity of 810 cm/sec and total pressure of 1.10 torr in the flow reactor giving a 62 msec contact time between reactant mixing and sampling.

We were not equipped to measure the concentration of $N_2(A)$; however, Stedman and Setser[69] have estimated that the concentration of $N_2(A)$ was about 3×10^{14} molecules/cm^3 for a similar apparatus; the dicyanoactylene concentration was about 1×10^{12} molecules/cm^3 establishing (hopefully) pseudo-first order conditions.

No change in the DCA concentration was observed over the length

Reproduced with permission of the copyright owner. Further reproduction prohibited without permission.

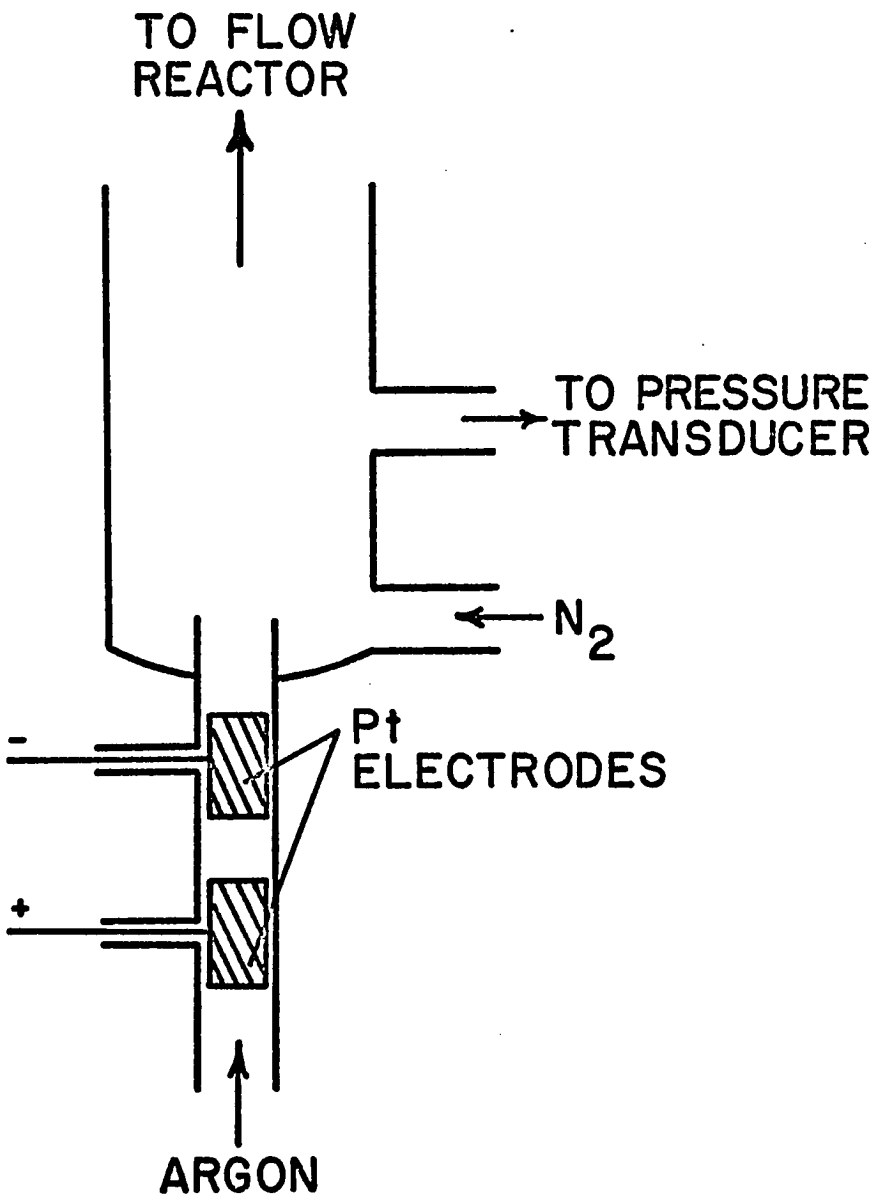

Figure D1: Final Design: Direct current argon discharge flow reactor for production of A state nitrogen.

Reproduced with permission of the copyright owner. Further reproduction prohibited without permission.

of the reactor when the argon discharge was extinguished. If we assume that the smallest detectable change corresponds to about five percent under these conditions and use as a safety factor $[N_2(A)] = 3 \times 10^{13}$ molecules/cm^3, an order of magnitude less than that reported in reference[69] due to our lack of experience in A state generation, then we may establish an upper limit for the reaction

$$C_4N_2 + N_2(A) \longrightarrow \text{Products}$$

since

$$k_{obs} = \frac{\ln([DCA]_o/[DCA])}{[N_2(A)] \cdot t_{Rxn}}$$

therefore

$$k_{obs} <\sim 2.7 \times 10^{-14} \text{ cm}^3/\text{molecule sec}$$

This is much lower than expected by comparison of the quenching rate constants from Table D1 for acetylene and cyanogen; however, our experiment must be considered marginal as we did not know the true A state concentration.

Reproduced with permission of the copyright owner. Further reproduction prohibited without permission.

Appendix E: Third Body Effects

For a bimolecular reaction exhibiting a third body, that is a pressure, dependence many generalized mechanism can be written such as step-wise deactivation:

$$A + B \longrightarrow AB'$$

$$AB' + M \longrightarrow AB'' + M$$

$$AB'' \longrightarrow \text{Products}$$

$$AB'' + M \longrightarrow AB''' + M$$

$$\vdots$$

where A, B = reactants

M = third body

AB', AB" = intermediates

or step-wise deactivation with one (or two) reactant(s) dependent on the third body concentration:

$$X + M \longrightarrow A + M$$

$$A \longrightarrow \text{Products}$$

$$A + B \longrightarrow AB'$$

$$AB' + M \longrightarrow AB'' + M$$

$$AB' \longrightarrow \text{Products}$$

where X, A, B = reactants

M = third body

AB', AB" = intermediates

Reproduced with permission of the copyright owner. Further reproduction prohibited without permission.

In each case a steady state treatment of these mechanisms results in an expression for the observed rate constant which is the quotient of two polynomials, and therefore is equal to a simple polynomial in powers of the third body concentration

$$k_{obs} = \frac{\sum_{i=o}^{n} a_i [M]^i}{\sum_{i=o}^{r} b_i [M]^i} = \sum_{i=o}^{s} c_i [M]^i \qquad (E1)$$

where a_i, b_i, and c_i are rate constants or sums and products of rate constants of the individual steps. It is then possible to fit the experimental data for the observed rate constant as a function of third body concentration to a simple polynomial to obtain the coefficients, c_i. Equation E1 may be written

$$\sum_{i=o}^{n} a_i [M]^i = \sum_{i=o}^{r} b_i [M]^i \sum_{i=o}^{s} c_i [M]^i \qquad (E2)$$

and equating coefficients in powers of [M] gives n equations with 2n unknowns:

$$a_o = b_o c_o$$
$$a_1 = b_o c_1 + b_1 c_o$$
$$a_2 = b_o c_2 + b_1 c_1 + b_2 c_o$$

It is then conceptually possible to obtain n relationships such as rate constant ratios or collision frequencies and solve the entire system. This treatment requires full knowledge of the mechanism, which

Reproduced with permission of the copyright owner. Further reproduction prohibited without permission.

is seldom the case; however, a polynomial fit of the observed rate constant (equation E1) should serve as a test to determine if the experimental results can be explained in terms of third body dependence.

This treatment was applied to the observed rate constants determined in the slow reaction region for the reaction of DCA with active nitrogen discussed in Section VII. A set of "best values" for k_{obs} were found by interpolation of all experimental data (see Table 14, Section VII), these values are reported in Table E1.

The best values were fitted to an equation of the form

$$Y(x) = C_0 + C_1x + C_2x^2 + \cdots + C_ix^i \qquad (E3)$$

where $Y(x) = k_{obs}$; $x = [N_2]$

Calculations were carried out by computer using a polynomial least squares treatment assuming Y(x) to be subject to random error while the x values were assumed to be exact. For simplicity k_{obs} and $[N_2]$ were multiplied by 10^{15} and 10^{-16}, respectively, before beginning calculations.

In Table E2 the results are collected for polynomials up to eighth order. Although the sum of deviations decreases as the order of the fit is raised several inflections are present in the calculated curve arising from sign alternation of the coefficients. This is shown graphically in figure E1 where both the best values for k_{obs} and the calculated values for a fourth order fit are plotted versus third body concentration, $[N_2]$.

For the real case all the coefficients, C_i, must be positive since a negative coefficient would require a negative rate constant in the

Reproduced with permission of the copyright owner. Further reproduction prohibited without permission.

Table E1: Best Values of the Observed Rate Constant for the Reaction of DCA with Active Nitrogen as a Function of Nitrogen Molecule Concentration Obtained by Interpolation of Experimental Data from Table 14.

$[N_2]$ (10^{16} molecules/cm^3)	k_{obs} (10^{-15} cm^3/atom sec)
0.0	0.00
1.0	0.27
2.0	0.47
3.0	0.67
4.0	0.88
5.0	1.09
6.0	1.29
7.0	1.53
8.0	1.82
9.0	2.32
10.0	3.30
11.0	4.93
12.0	6.88
13.0	9.14
14.0	11.75
15.0	15.0
16.0	23.0

Reproduced with permission of the copyright owner. Further reproduction prohibited without permission.

$[N_2]$ (10^{16} molecules/cm^3)	k_{obs} (10^{-15} cm^3/atom sec)
17.0	36.5
18.0	52.5
19.0	61.0
20.0	64.5
21.0	66.5
22.0	66.5
23.0	67.0

Reproduced with permission of the copyright owner. Further reproduction prohibited without permission.

Table E2: Polynomial Fit of the Data from Table E1 to the Equation

$$Y(x) = C_0 + C_1x + C_2x^2 + \cdots + C_ix^i$$

Where: $Y(x) = k_{obs}x10^{15}$; $x = [N_2]x10^{-16}$; x Is Exact.

i	3	4	5	6	7	8
Sum of Residuals	1568	668	284	283	169	79
C_0	5.29	-5.36	1.54	1.43	-1.90	0.74
C_1	-3.02	7.18	-3.39	-3.13	8.15	-4.72
C_2	3.05	-1.74	1.61	1.49	-5.71	5.21
C_3	-1.4E-3	0.14	-0.26	-0.24	1.57	-2.08
C_4		-3.0E-3	1.6E-2	1.5E-2	-0.20	0.40
C_5			-3.4E-4	-2.7E-4	1.4E-2	-4.2E-2
C_6				-9.7E-7	-4.4E-4	2.4E-3
C_7					5.4E-6	-7.1E-5
C_8						8.3E-7

Reproduced with permission of the copyright owner. Further reproduction prohibited without permission.

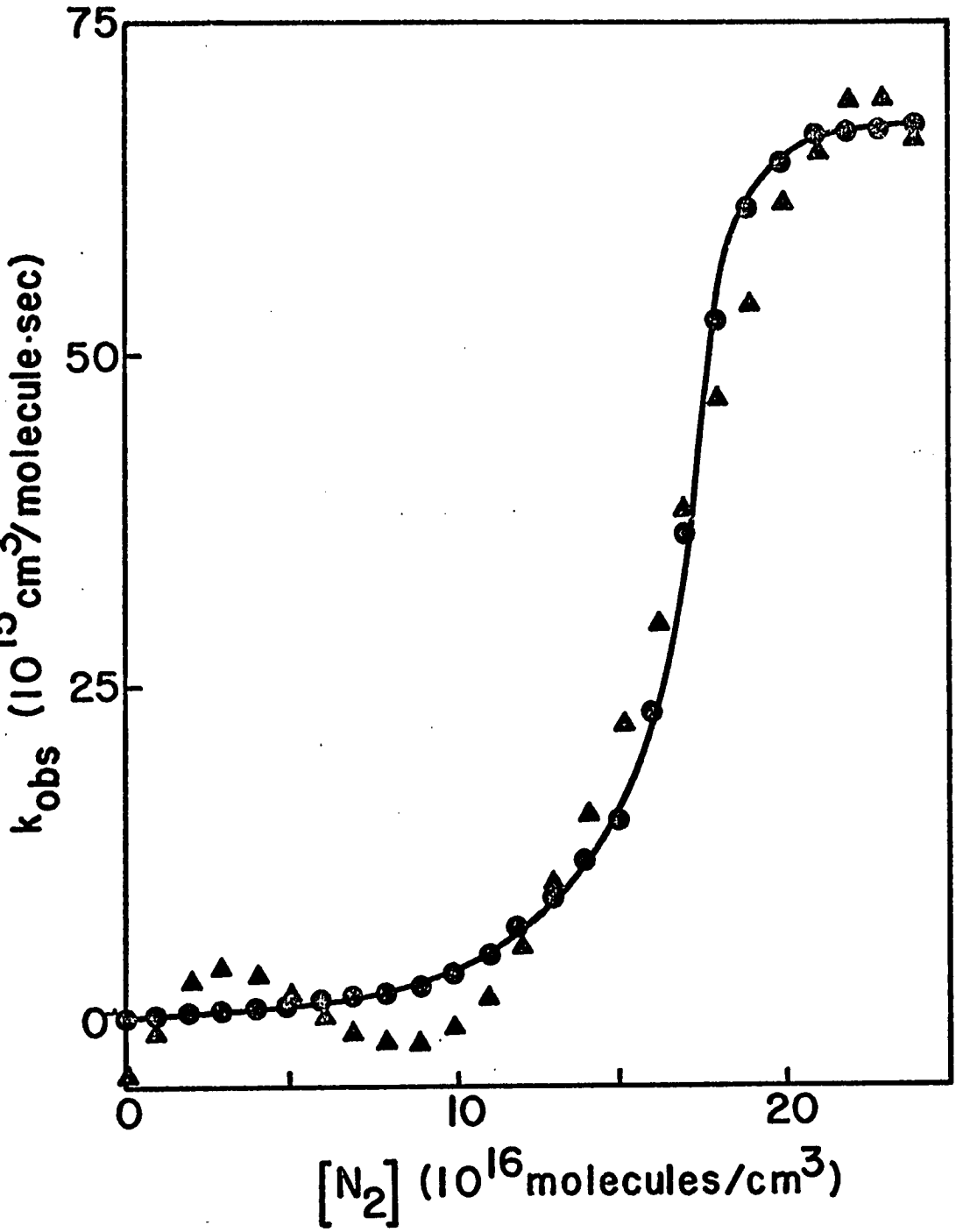

Figure E1: Fourth order polynomial fit of "best values" from Table E1; ● = best experimental values, ▲ = fourth order polynomial fit.

Reproduced with permission of the copyright owner. Further reproduction prohibited without permission.

steady state expression. We therefore conclude that a fit of this form where all coefficients are restricted to be greater than zero is impossible for our data. The negative coefficients arise from the nearly linear dependence of k_{obs} over an order of magnitude before the sharp change in apparent order with respect to third body concentration.

Reproduced with permission of the copyright owner. Further reproduction prohibited without permission.

Appendix F: Selected Heats of Formation

Substance	ΔH_f° (kcal/mole)	Reference
O	60	26
N	113	26
$N_2(A^3\Sigma_u^+)$	$\leq$142	59
NO	23	9
NO_2	8	26
C_2H_2	58	9
C_2N_2	74	26
C_4N_2	127	42
C_6N_2	183	44
CO	-25	9
CO_2	-94	26
NCO	16	5
C_2O	79	42
C	171	26
CN	$\leq$103	76
C_2N	184	42
C_3N	$<$99	42
C_4N	238	77*
C_3N_2	154	9
CN_2	140	26
NCN	103	26
CH_2	24	9

* ΔH_f° (C_4N) estimated by taking $D(NC_4{\equiv}N)$ equal to $D(HC{\equiv}N)$.

Reproduced with permission of the copyright owner. Further reproduction prohibited without permission.

References

1. F. Kaufman, "Reactions of Oxygen Atoms," Progress in Reaction Kinetics, Pergamon Press (1961).

2. A. N. Wright and C. A. Winkler, Active Nitrogen, Academic Press (1968).

3. R. Brown and C. A. Winkler, Angewandte Chemie, 9, 181 (1970).

4. H. G. Wagner and J. Wolfrum, Angew. Chem. Internat. Edit., 10, 604 (1971).

5. D. W. Setser and B. A. Thrush, Proc. Roy. Soc., A288, 275 (1965).

6. J. C. Boden and B. A. Thrush, Proc. Roy. Soc., A305, 107 (1968).

7. C. Haggart and C. A. Winkler, Can. J. Chem., 38, 329 (1960).

8. D. W. Setser and B. A. Thrush, Proc. Roy. Soc., A288, 256 (1965).

9. D. R. Safrany and W. Jaster, J. Phys. Chem., 72, 3305 (1968).

10. D. R. Safrany and W. Jaster, J. Phys. Chem., 72, 3318 (1968).

11. D. G. Williamson and K. D. Bayes, J. Phys. Chem., 73, 1232 (1969).

12. C. A. Arrington, W. Brennen, G. P. Glass, J. V. Michael, and H. Niki, J. Chem. Phys., 43, 525 (1965).

13. J. O. Sullivan and P. Warneck, J. Phys. Chem., 69, 1749 (1965).

14. J. M. Brown and B. A. Thrush, Trans. Farad. Soc., 63, 630 (1967).

15. A. A. Westenberg and N. deHaas, J. Phys. Chem., 73, 1181 (1969).

16. G. S. James and G. P. Glass, J. Chem. Phys., 50, 2268 (1969).

17. L. I. Avramenko and V. M. Krasne'kov, Acad. Sci. U.S.S.R., Div. Chem. Sci., 770 (1964).

18. J. Versteeg and C. A. Winkler, Can. J. Chem., 31, 129 (1953).

19. A. Schavo and C. A. Winkler, Can. J. Chem., 37, 655 (1959).

20. J. C. Boden and B. A. Thrush, Proc. Roy. Soc., A305, 93 (1968).

21. C. A. Arrington, O. O. Bernardini, and G. B. Kistiakowsky, Proc. Roy. Soc., A310, 161 (1969).

Reproduced with permission of the copyright owner. Further reproduction prohibited without permission.

22. H. Niki, D. Daby and B. Weinstock, 12th Symposium on Combustion, P. 277 (1969).

23. B. A. Thrush, J. Chem. Ed., 41, 429 (1964).

24. J. R. Barker, D. G. Keil, J. V. Michael and D. T. Osborn, J. Chem. Phys., 42, 2079 (1970).

25. Handbook of Chemistry and Physics, C.R.C. (1967).

26. JANAF Thermochemical Tables, Second Edition, NSRDS-NBS37 (1971).

27. W. L. Fite and R. T. Brackmann, 6th International Conference on Ionization Phenomina of Gases, (Paris), 21 (1963).

28. S. N. Foner and R. L. Hudson, J. Chem. Phys., 37, 1662 (1962).

29. R. R. Baker, A. Jacob and C. A. Winkler, Can. J. Chem., 49, 1671 (1971).

30. R. D. Present, Kinetic Theory of Gases, McGraw-Hill (1958).

31. W. Brennen and E. C. Shane, J. Phys. Chem., 75, 1552 (1971).

32. J. C. Greaves and J. W. Linnett, Trans. Farad. Soc., 55, 1345 (1959).

33. W. V. Smith, J. Chem. Phys., 11, 110 (1943).

34. J. W. Linnett and G. H. Marsden, Proc. Roy. Soc., (London), A234, 489 (1956).

35. H. Melville and B. G. Gowenlock, Experimental Methods in Gas Reactions, MacMillan (1964).

36. A. J. Saggiomo, J. Org. Chem., 22, 1171 (1957).

37. A. T. Blomquist and E. C. Winslow, J. Org. Chem., 10, 149 (1945).

38. N. R. Byrd, NASA Corp. Report, N6420601 (1964).

39. Standard Mathematical Tables, 14 Edition, C.R.C. (1965).

40. Private communication from D. J. Bogan; to be published in Ph.D. dissertation, Carnegie-Mellon Univ. (1972).

41. K. Hoyermann, H. G. Wagner, and J. Wolfrum, Z. Phys. Chem. (Frankfurt), 55, 72 (1967).

42. J. A. Meyer and D. W. Setser, J. Phys. Chem., 74, 3452 (1970).

43. D. J. Bogan, C. W. Hand and R. H. Obenauf, Rev. Sci. Inst., 43, 348 (1972).

Reproduced with permission of the copyright owner. Further reproduction prohibited without permission.

44. V. H. Dibeler, R. M. Reese, and J. L. Franklin, J. Amer. Chem. Soc., 83, 1813 (1961).

45. G. Herzberg, Atomic Spectra and Atomic Structure, Dover, N. Y., (1944).

46. a) A. W. Warren, Nature, 165, 810 (1950); b) J. W. Warren and C. A. McDowell, Discuss. Farad. Soc., 10, 53 (1951).

47. F. H. Field and J. L. Franklin, Electron Impact Phenomena and the Properties of Gaseous Ions, Pure and Applied Physics Series, Vol. 1, Academic Press (1957).

48. D. G. Williamson and K. D. Bayes, J. Amer. Chem. Soc., 89, 3390 (1967).

49. D. L. Baulch, D. D. Drysdale, and A. C. Lloyd, High Temperature Reaction Rate Data, 1, The University at Leeds (1968).

50. D. E. Paul and F. W. Dalby, J. Chem. Phys., 37, 592 (1962). The value reported was simply for the disappearance of reactants, with the nature of the products unspecified.

51. C. W. Hand and R. M. Hexter, J. Amer. Chem. Soc., 92, 1828 (1970).

52. D. L. Baulch, D. D. Drysdale and A. C. Lloyd, High Temperature Reaction Rate Data, 5, The University at Leeds (1970).

53. J. H. Greenblatt and C. A. Winkler, Can. J. Res., B27, 721 (1949).

54. C. W. Hand and R. H. Obenauf, Jr., J. Phys. Chem., 76, 269 (1972).

55. K. D. Bayes, Can. J. Chem., 39, 1074 (1961).

56. R. L. Brown and H. P. Broida, J. Chem. Phys., 41, 2053 (1964).

57. I. M. Cambell and B. A. Thrush, J. Chem. Soc., 410 (1964).

58. B. A. Thrush, J. Chem. Phys., 47, 3691 (1967).

59. J. A. Meyer, D. H. Klosterboer and D. W. Setser, J. Chem. Phys., 55, 2084 (1971).

60. D. E. Shemansky and N. P. Carleton, J. Chem. Phys., 51, 682 (1969).

61. D. E. Shemansky, J. Chem. Phys., 51, 689 (1969).

62. K. L. Wray, J. Chem. Phys., 44, 623 (1966).

63. H. Margeneau and G. M. Murphy, Mathematics of Physics and Chemistry, D. Van Nostrand (1964).

64. Handbook of Mathematical Functions, U.S. Dept. of Commerce, AMS55.

Reproduced with permission of the copyright owner. Further reproduction prohibited without permission.

65. P. J. Schneider, Conduction Heat Transfer, Addison Wesley Inc., Reading, Mass.

66. D. R. Bates, Atomic and Molecular Processes, Academic Press Inc., (1962).

67. S. W. Bensen, J. Chem. Phys., 48, 1765 (1968).

68. D. W. Setser and D. H. Stedman, J. Chem. Phys., 53, 1004 (1970).

69. D. H. Stedman and D. W. Setser, Chem. Phys. Let., 2, 542 (1968).

70. D. H. Stedman and D. W. Setser, J. Chem. Phys., 52, 3957 (1970).

71. D. H. Stedman, J. Chem. Phys., 52, 3966 (1970).

72. G. W. Taylor and D. W. Setser, J. Amer. Chem. Soc., 93, 4930 (1971).

73. J. A. Meyer, D. W. Setser and W. G. Clark, J. Phys. Chem., 76, 1 (1972).

74. D. W. Setser, Chemistry Dept., Kansas State Univ., Manhattan, Kansas 66502, Private Communication, 1971.

75. J. F. Prince, C. B. Collins and W. W. Robertson, J. Chem. Phys., 40, 2619 (1964).

76. a) D. W. Setser and D. H. Stedman, J. Chem. Phys., 49, 467 (1968); b) V. H. Dibeler and S. K. Liston, ibid., 47, 4548 (1967).

77. G. Herzberg, Molecular Spectra and Molecular Structure, 3, Van Nostrand, New York, 1966.

Reproduced with permission of the copyright owner. Further reproduction prohibited without permission.